

Biomolecular characterization of PCNA interacting proteins

Inés Martín Barros

Doctoral Thesis

2020

Biomolecular characterization of PCNA interacting proteins

Inés Martín Barros

Doctoral Thesis 2020

Directors: Dr. Francisco J. Blanco & Dr. Miren Edurne Berra Ramírez

Doctorate Program: Molecular Biology and Biomedicine

Department: Biochemistry and Molecular Biology

University of the Basque Country (UPV/EHU)

This work has been performed at the Centre for Cooperative Research in Biosciences (CIC bioGUNE) supported by the CIC bioGUNE and the Spanish Government (BFU2016-76872-R & CTQ2017-83810R)

Table of Contents

Abbreviations	13
Abstract	15
Resumen	17
Introduction	19
1. Proliferating Cell Nuclear Antigen (PCNA).....	21
1.1 Discovery of PCNA.....	21
1.2 Structure.....	21
1.3 Regulation	23
1.4 Functionality	31
Hypothesis and Aims	39
Material and Methods	43
1. Materials	45
2. Methods	45
2.1 Molecular biology	45
2.2 Cell Biology	49
2.3 Biochemistry.....	52
2.4 Structural biology and biophysics	59
Results	65
1. Characterization of the interaction between USP29 and PCNA.....	67
1.1 Validation of mass spectrometry data.....	67
1.2 The role of USP29 as a DUB for PCNA.....	68
1.3 USP29's PIP box sequences and interactions with PCNA.....	73
1.4 USP29PH mediates USP29 and PCNA interaction	83
2. USP29 regulation	84
2.1 USP29 dimer/oligomerization.....	84
2.2 Characterization of the potential PH dimerization interface by mutagenesis.....	87
2.3 USP29PH acts as a dominant negative for USP29	89
3. Structural analysis of USP29	92
3.1 USP29 and USP29PH proteins expression and purification	92
3.2 Homology based model of USP29's structure	107
4. Characterization of the interaction between p125 and PCNA	110
4.1 Binding reaction studied by calorimetry.....	111

4.2 Binding site mapping by NMR	112
Discussion	115
1. Characterization of the interaction between USP29 and PCNA.....	117
2. USP29 regulation	119
3. Structural analysis of USP29	122
4. Characterization of the interaction between p125 and PCNA	124
Conclusions	127
Bibliography	131
Appendix: Posters presented during the thesis	151

Abbreviations

53BP1: p53 binding protein 1	DUB: deubiquitinating enzymes
AIMP2: Aminoacyl tRNA synthase complex-interacting multifunctional protein 2	<i>E.coli:</i> <i>Escherichia coli</i>
AP endonuclease 1: DNA- (apurinic or apyrimidinic site) lyase	ECRs: evolutionary conserved regions
APIM: AlkB homologue 2 PCNA-interacting motif	EDTA: Ethylenediaminetetraacetic acid
ATPase: adenosine triphosphatase	EGF: epidermal growth receptor
ATR: Serine/threonine-protein kinase ATR	EM: electron microscopy
BER: base excision repair	EZH2: Histone-lysine N-methyltransferase EZH2
Cdc45: Cell division control protein 45 homologue	FEN1: flap endonuclease 1
Cdc6: cell division control protein 6 homologue	FUBP1: DNA-binding regulator FUSE binding protein 1
Cdc7: Cell division cycle 7-related protein kinase	GINS: DNA replication complex GINS protein SLD5
CDK: cyclin-dependent kinases	H2A: Histone 2A
CDK9: cyclin-dependent kinase 9	HEK293: human embryonic kidney cells
Cdt1: DNA replication factor Cdt1	HEK293FT: human embryonic kidney fast growing SV40 T antigen cells
CHAPS: (3-((3-cholamidopropyl) dimethylammonio)-1-propanesulfonate)	hELG1: enhanced level of genomic instability 1
CHK1: Serine/threonine-protein kinase Chk1	HIF-α: Hypoxia Inducible Factor α subunit
CHX: Cycloheximide	HR: homologous recombination
CMG helicase: Cdc45-Mcm2-7-GINS helicase complex	HRE: Hypoxia Responsive Elements
CPT: Camptothecin	HSQC: Heteronuclear Single Quantum Coherence
CSP: Chemical Shifts Perturbation	HTLF: Helicase-like transcription factor
CTD: C-terminal domain	HU: hidroxyurea
C-terminal: carboxyl terminal	ICR: imprinting control region
DDK: DBF4-dependent kinases	IDCL: Inter Domain Connecting Loop
DDM: n-Dodecyl-beta-Maltoside	IDP: intrinsically disordered proteins
DDR: DNA Damage Response	IDR: intrinsically disordered region
D-loop: displacement loop	IPTG: Isopropyl β -D-1-thiogalactopyranoside
DMR: differentially methylated region	ISG15: interferon-stimulated gene 15
DNA: Deoxyribonucleic acid	ITC: Isothermal titration calorimetry
DNA: double nucleic acids?	JAMM: Ab1/Mov34/Mpr1 Pad1 N-terminal+ (MPN+)
DSB: Double Strand Breaks	JNK: c-Jun N-terminal kinase
DSS: 4,4-dimethyl-4-silapentane-1-sulfonic acid	
DTT: Dithiothreitol	
DTT: DNA Damage Tolerance	

LB: Luria-Bertani broth
LC3: Microtubule-associated proteins 1A/1B light chain 3B
LIG1: DNA ligase I
Mcm2-7: minichromosome maintenance proteins 2-7
MINDY: Motif Interacting with Ub-containing Novel DUB family
MIP: Mlh1 interacting protein
MJD: Machado-Josephin Domain proteases
MMC: 3-Methylmethcathinone
MMR: mismatch repair
MMS: methyl methanesulfonate
Mono-Ub: mono-Ubiquitinated mRNAs: messenger RNA
MS: MassSpec
MSH2: DNA mismatch repair protein Msh2
MSH3: DNA mismatch repair protein Msh3
MSH6: DNA mismatch repair protein Msh6
MTH2: MutT homolog 2
NER: nucleotide excision repair
NHEJ: non-homologous end joining
NMR: Nuclear Magnetic Resonance
N-terminal: amino terminal
ORC: Origin Recognition Complex
ORF: Open Reading Frame
ori: origin of replication
OTU: ovarian tumour proteases
PARI: PCNA-associated recombination inhibitor
PBS: Phosphate-buffered Saline
PCNA: Proliferating Cell Nuclear Antigen
PEG3: paternally expressed 3
PH: Pleckstrin Homology
PHDs: Prolyl hydroxylases
PIP-box: PCNA interacting protein box
PKA: Protein kinase A
Poly-Ub: poly-Ubiquitinated
pre-RC: pre-replicative complex
PRR: Post-replication Repair
PTM: Post-translational modifications
RFC: Replication Factor C
RIR: Rev1 interacting region
RNF168: E3 ubiquitin-protein ligase RNF168
RNF8: E3 ubiquitin-protein ligase RNF8
RPA: Replication Protein A
SDS: Sodium Dodecyl Sulphate
SDS-PAGE: Sodium dodecyl sulphate polyacrylamide gel electrophoresis
SETD8: N-lysine methyltransferase KMT5A
SHPRH: SNF2 histone linker PHD RING helicase
shRNAs: small hairpin RNAs
SIAH: E3 ubiquitin-protein ligases Seven in Absentia Homolog
siRNA: Small interference RNA
SLiMs: short linear motifs
ssDNA: single stranded DNA
SUMO1: small ubiquitin-related modifier 1
TEV: Tobacco Etch Virus
Thr: threonine
TLS: Translesion synthesis
tRNAs: transfer RNA
TROSY: Transverse relaxation-optimized spectroscopy
TS: template switching
UAF1: USP1-associated factor 1
Ub: ubiquitin
UBM: ubiquitin-binding motifs
UCH: ubiquitin C-terminal hydrolases
UIMs: ubiquitin interacting motifs
USP: ubiquitin specific protease
UV: ultraviolet
VHL: Von Hippel-Lindau
XPG: DNA repair protein complementing XP-G cells
XRCC1: DNA repair protein XRCC1
ZUP1: Zinc finger-containing Ubiquitin Peptidase 1

Abstract

Proliferating Cell Nuclear Antigen (PCNA) is the human DNA sliding clamp necessary for the DNA replication and damage response. PCNA interacts with numerous partners through a conserved sequence known as PIP motif. We found PCNA as one of the top 10 interacting proteins of the deubiquitinating enzyme USP29 and we have discovered that USP29 expression decreases PCNA poly-Ubiquitination under genotoxic stress and that this de-poly-Ubiquitination depends on the catalytic activity of USP29.

Different attempts to purify the USP29 protein were done with no success. Using model peptides, we have determined that the interaction with PCNA does not occur through a number of PIP boxes in the USP29 sequence. In contrast, co-immunoprecipitation assays showed that the N-terminal Pleckstrin Homology domain of USP29 interacts with PCNA, although it does not have a PIP sequence motif. Purification of the isolated PH domain was unsuccessful. We found that USP29 forms dimers/oligomers through the PH domain to be active as a DUB since the expression of USP29PH acts as a dominant negative mutant.

DNA polymerase δ replicates the lagging strand while bound to PCNA. PCNA interacts with all subunits of Pol δ (p125, p50, p68 and p12), but only the interaction with p68 and p12 has been structurally characterized. In this thesis, solution NMR- and isothermal calorimetry-based analyses of the p125–PCNA interaction have identified that the C-terminal fragment of the catalytic subunit of the human polymerase δ (p125⁹⁹⁶⁻¹⁰⁰⁹) binds PCNA through a non-canonical PIP box motif with a dissociation constant of $103 \pm 14 \mu\text{M}$ at 37 °C. This affinity is lower than the affinity of PCNA for the subunits p12 and p68 of human polymerase δ .

Resumen

PCNA (por sus siglas en inglés, *Proliferating Cellular Nuclear Antigen*) es la abrazadera que es desliza sobre el ADN necesaria para la replicación del ADN y la respuesta al daño. PCNA interactúa con numerosas proteínas a través de una secuencia conservada y conocida como motivo PIP. Resultados del laboratorio identificaron PCNA como una de las 10 principales proteínas que interactúan con la enzima desubiquitinasa (DUB) USP29 y hemos descubierto que la expresión de USP29 disminuye la poli-ubiquitinación de PCNA en respuesta a un estrés genotóxico y que esta des-poli-ubiquitinación depende de la actividad catalítica de USP29.

Los diferentes intentos realizados para purificar la proteína USP29 resultaron infructuosos. Usando péptidos sintéticos como modelo, hemos determinado que la interacción con PCNA no ocurre a través de ninguno de los motivos PIP identificados en la secuencia USP29. En cambio, los ensayos de co-inmunoprecipitación mostraron que el dominio PH (*Pleckstrin Homology*) del extremo N-terminal de USP29 interactúa con PCNA, aunque no tiene un motivo PIP. La purificación del dominio PH no tuvo éxito. Descubrimos que USP29 forma dímeros/oligómeros a través del dominio PH y dicha dimerización es necesaria para la actividad de USP29 como DUB ya que la expresión de USP29PH actúa como un dominante negativo.

La ADN polimerasa δ es la encargada de replicar la cadena rezagada del ADN a través de su unión con PCNA. PCNA interactúa con todas las subunidades de Pol δ (p125, p50, p68 y p12), pero solo la interacción con p68 y p12 se ha caracterizado estructuralmente. En esta tesis, los análisis basados en RMN y calorimetría isotérmica de la interacción p125-PCNA han identificado que el fragmento C-terminal de la subunidad catalítica de la polimerasa humana δ (p125⁹⁹⁶⁻¹⁰⁰⁹) se une a PCNA a través de un motivo PIP no canónico, con una constante de disociación de $103 \pm 14 \mu\text{M}$ at 37°C . Esta afinidad es menor que la afinidad de PCNA por las subunidades p12 y p68 de la polimerasa humana δ .

Introduction

1. Proliferating Cell Nuclear Antigen (PCNA)

1.1 *Discovery of PCNA*

PCNA was discovered 42 years ago in the serum of patients with systemic lupus erythematosus (Miyachi et al., 1978). Two years later, a protein named cyclin, which was differentially expressed in the S-phase of the cell cycle, was identified by an independent group (Bravo & Celis, 1980). Subsequent experiments showed that they were the same protein (Mathews et al., 1984).

1.2 *Structure*

The first structure of human PCNA was determined by crystallography together with the C-terminal region of the cell-cycle checkpoint protein p21^(WAF1/CIP1) (PDB: 1AXC; at 2.6 Å resolution) (Gulbis et al., 1996) (Figure I1). The crystal structure of the isolated PCNA homotrimer was later solved in two different spatial groups (PDB: 1VYM and 1W60) (Kontopidis et al., 2005). Like all the sliding-clamps, PCNA has a ring-shaped structure to encircle the double-strand DNA (De March et al., 2017). Human PCNA is a homotrimeric protein of 87 kDa. Each protomer contains two domains linked through the IDCLs (Inter Domain Connecting Loops). Next to the IDCL, the protomers show a hydrophobic pocket on the front face of the ring where PCNA-interacting proteins bind (Figure I1).

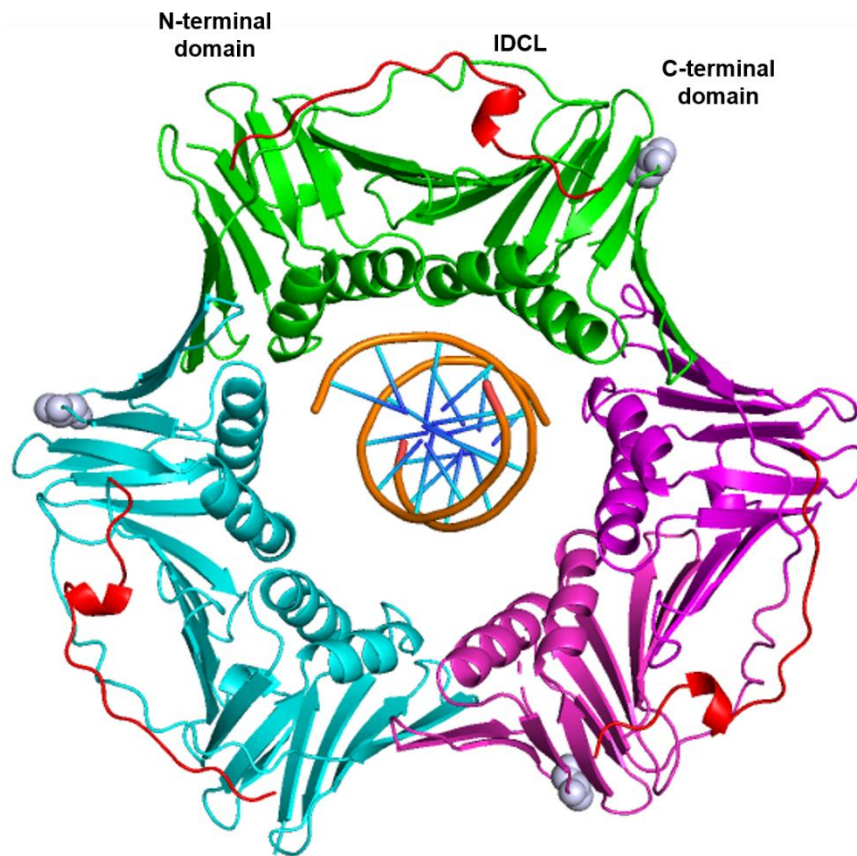


Figure I1: Crystal structure and schematic representation of the domains of PCNA. (A) Front view of the structure of human PCNA bound to DNA (PDB: 6GIS) and to the C-terminal fragment of p21, shown in red (PDB: 1AXC). Each protomer is represented in a different colour (green, cyan and pink). The two domains (N-terminal and C-terminal) and the IDCL are labelled in one of the protomers. The K164 residues, where ubiquitin is attached to PCNA, are depicted in grey spheres.

In 2007, the NMR (Nuclear Magnetic Resonance) spectrum of PCNA was assigned (Figure I2) (Sánchez et al., 2007) and the structural features measured in solution correlated well with the structure determined by crystallography (de Biasio et al., 2011).

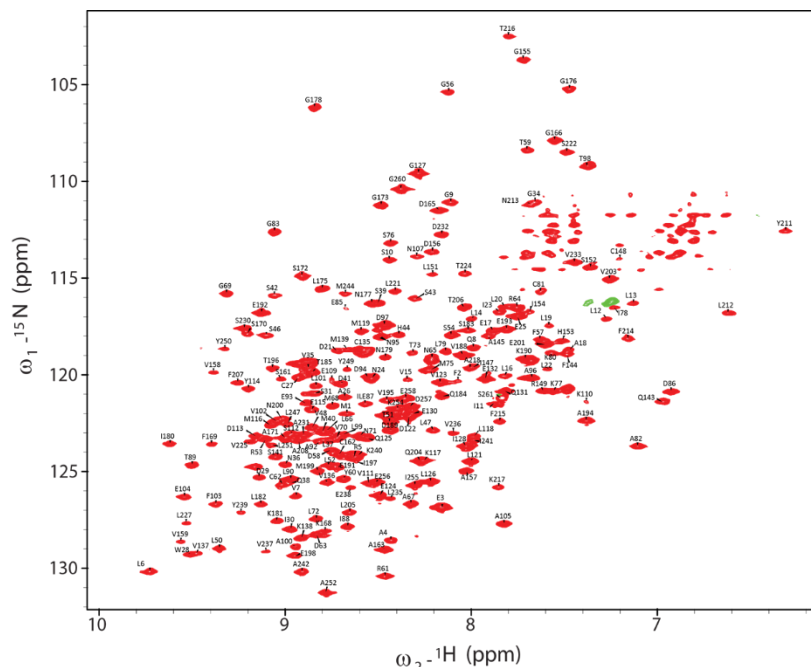


Figure I2: ^1H - ^{15}N TROSY fingerprint spectrum of perdeuterated human PCNA (recorded at 35°C and 800 MHz). Out of the 251 backbone amides (the number of amino acids excluding the first residue and the 8 prolines) only 12 remain unassigned (Sánchez et al., 2007). The signals in the spectrum without labels correspond to the side chains of Asn, Gln and Arg residues. Green signals are folded in the indirect dimension (arginine side chains).

The structure of DNA sliding clamps is highly conserved from viruses to humans although the sequence is not. For instance, *E. coli* and *S. cerevisiae* only have a ~10% sequence identity (Krishna et al., 1994). Human PCNA is less stable (as seen by chemical and thermal denaturation) and is more dynamic than yeast PCNA, indicating an evolutionary advantage to interact with a larger number of diverse partners (De Biasio et al., 2011).

1.3 Regulation

1.3.1 PCNA interacting proteins and the PIP box

PCNA provides a molecular platform that coordinates a wide range of processes involved in maintenance, duplication and transmission of the genome (Moldovan et al., 2007). Although this plethora of proteins that bind to PCNA have

disparate structures, most of them have IDRs (intrinsically disordered region) or they are IDPs (intrinsically disordered proteins) (Hubert Li et al., 2017). IDPs and IDRs bind to other partners through short linear motifs (SLiMs) (Prestel et al., 2019a). In the case of PCNA-binding proteins the SLiM is called PIP box or an extended version named PIP degron (Havens & Walter, 2009). The canonical PIP-box was first described by Warbrick and colleagues in 1998 (Warbrick et al., 1998). The PIP-box sequence follows the pattern of QXXhXXaa, where *h* is an aliphatic hydrophobic residue, *a* is an aromatic hydrophobic one (F, W, or Y), and *X* is any amino acid (De Biasio & Blanco, 2013). The PIP degron serves to target PCNA for degradation and contains a basic residue (K or R) four amino acids after the second aromatic residue as well as a TD motif (threonine and aspartic) just before the aromatic residues within the PIP-box (Havens & Walter, 2009).

The first structural characterization of a PIP-box-PCNA interface corresponded to a fragment from p21 bound to human PCNA (PDB: 1AXC) (Gulbis et al., 1996) (Figure I1). A similar mode of binding has been later described for several PIP-box fragments of different proteins. The PIP box forms a 3_{10} helix of four residues, an extended N-terminal region, and a C-terminal region that interacts with the IDCL and sometimes displays a β -strand secondary structure (Figure I1). The helix is inserted into a hydrophobic pocket on the front side of PCNA while the glutamine sits in the Q-pocket establishing hydrogen bonds with the backbone of PCNA (Bruning & Shamoo, 2004; Gulbis et al., 1996). The interaction of several PIP-box containing peptides with PCNA have also been characterized in solution (De Biasio et al., 2012). NMR and Isothermal titration calorimetry (ITC) demonstrate that three peptides can simultaneously bind to the three identical protomers of PCNA with no evidence of cooperativity (De Biasio et al., 2015).

Not all the proteins that interact with PCNA have a canonical PIP-box motif. Some of the Y-family DNA polymerases (Pol η , Pol ι and Pol κ) bind to PCNA through non-canonical PIP-boxes, in which the first glutamine at position 4 and the aromatic residue at position 8 is not conserved (Hishiki et al., 2009; Masuda et al., 2015). Furthermore, the PIP-motif has similarities with the RIR (Rev1 interacting region), the MIP (Mlh1 interacting proteins), and the APIM (AlkB homologue 2 PCNA-interacting motif) motifs (Boehm & Washington, 2016).

These observations suggest that a broader definition of the PIP-box motif should be considered. even if the rules that define the differential affinity of these ligands are unknown.

1.3.2 PTM: Ubiquitination and USP29

The interaction of PCNA with its partners is modulated by different post-translational modifications (PTMs) (De Biasio & Blanco, 2013). PCNA can be modified by ubiquitination, SUMOylation, ISGylation, NEDDylation, ADP-ribosylation, acetylation, phosphorylation, and methylation (González-Magaña & Blanco, 2020).

Ubiquitin conjugation is one of the most common post-translational protein modifications, involved in many biological processes (Swatek & Komander, 2016).

Ubiquitin (Ub) is a highly conserved 76 amino acid protein that is expressed in all human cell types (McClellan et al., 2019). Ubiquitination consists on the covalent Ub conjugation to a target protein through a three-step enzymatic reaction (Hershko et al., 1983). Thus, Ub is attached to a cysteine within the active site of an E1 ubiquitin-activating enzyme, which transfers ubiquitin to an E2 ubiquitin-conjugating enzyme and finally, a specific E3 ubiquitin-ligase attaches the ubiquitin to a lysine residue of its target substrate through the Ub C-terminal di-glycine (Gly-Gly) motif (Pickart, 2001).

Ub can be attached to one or multiple lysine residues of the target protein resulting in mono-ubiquitination or multi-mono-ubiquitination, respectively (Petroski & Deshaies, 2005). The Ub itself has seven internal lysine residues (K6, K11, K27, K29, K33, K48 or K63) that can be ubiquitin-acceptors and build poly-Ub chains (Pickart & Fushman, 2004). These chains can be homo- or heterotypic poly-Ub chains which can be formed by branched Ub or mixed chains of Ub attached to different lysine residues (Guzzo & Matunis, 2013).

Each type of ubiquitin chain corresponds to a type of biological signal to modulate cellular processes. Mono-ubiquitination has been shown to regulate processes such as endocytosis, histone regulation or the budding of retroviruses from the plasma membrane (Hicke, 2001). Multi-mono-ubiquitination has been

reported to mark cell-surface receptors to trigger their internalization and subsequent lysosomal degradation (Haglund et al., 2003). Poly-ubiquitination has been long related to be the principal signal to target proteins for proteasomal degradation. However, is the type of Ub chain that decides the fate of the protein. K48- and K11-linked poly-Ub are indeed the main signal for protein degradation (Chau et al., 1989; Matsumoto et al., 2010). K6- and K27-chains have been related to mitophagy, nuclear translocation and DNA damage responses (Akutsu et al., 2016). K11-, K29- and K33-Ub chains have been linked to cell cycle regulation, WNT/ β -catenin signalling, and cellular trafficking and kinase signalling, respectively (Akutsu et al., 2016). Finally, K63-chains allow fast and reversible formation of signalling complexes (Wong & Cuervo, 2010; Yau & Rape, 2016).

As most post-translational modifications, ubiquitination is a reversible process. Deubiquitinating enzymes or DUBs play the antagonistic roles of E3 Ub-ligases. DUBs are responsible for cleaving Ub or Ub-like proteins from target proteins (Clague et al., 2013) by catalysing the hydrolysis of the isopeptide bond between Ub and the target protein or between Ub moieties in the context of poly-Ub chains. Based on the architecture of their catalytic centre, DUBs are classified into seven different groups: Ubiquitin-Specific Protease (USPs), Ubiquitin C-terminal Hydrolases (UCHs), Ovarian Tumour Proteases (OTUs), Machado-Josephin Domain proteases (MJDs) (also known as Josephins), Motif Interacting with Ub-containing Novel DUB family (MINDYs) and Zinc finger-containing Ubiquitin Peptidase 1 (ZUP1) are cysteine proteases, whereas the seventh family, the JAMM (Ab1/Mov34/Mpr1 Pad1 N-terminal+ (MPN+)) domain (also known as MPN), are zinc-dependent metalloproteases (Clague et al., 2019).

1.3.2.1 Ubiquitin-specific protease 29 (USP29)

Usp29 is a maternally imprinted gene (He et al., 2016). The murine gene of ubiquitin-specific processing protease 29 (*Usp29*) was first discovered within the imprinted region around the *Peg3* (paternally expressed 3) gene at mouse chromosome 7 (Kim et al., 2000). It was named based on the homology with a yeast ubiquitin hydroxylase. The 7 genes at the *Peg3* imprinted domain share functionalities such as the control of foetal-growth rates and maternal-caring

behaviours, as well as their transcriptional regulation and imprinting. The Peg3 domain is associated with differentially methylated regions (DMR) known to control imprinting control regions (ICR). There are around 20 evolutionary conserved regions (ECRs) (Figure I3), which are responsible for controlling the transcription and imprinting of the Peg3 domain (Thiaville et al., 2013). The human gene *USP29* was also found next to the human *PEG3* gene (chromosome 19q13.4) and in contrast to the murine expression (in brain and testis), the human gene was mostly detected in testis (Kim et al., 2000).

Until now, *USP29* is the only DUB and the second protein in the ubiquitination pathway, together with the gene of the ubiquitin ligase *Ube3a* (Rougeulle, Cardoso, Fontés, Colleaux & Lalande, 1998) shown to be regulated through genomic imprinting.

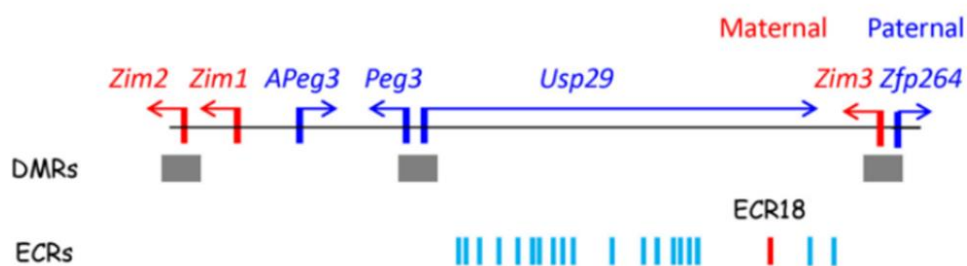


Figure I3: Organization of the human Peg3 domain. Schematic representation of the Peg3 domain, which consists of 7 genes: 3 maternally expressed (red) and 4 paternally expressed (blue). The 20 evolutionary conserved regions (ECR) are in the central non-coding region of the Peg3 domain and control the imprinting and transcription of it (He & Kim, 2014).

The transcription of *USP29* is activated by the DNA-binding regulator FUSE binding protein 1 (FUBP1). Moreover, FUBP1 interacts with p38 (also known as JTV1 or AIMP2) to upregulate the transcription of *USP29* under oxidative stress (Liu et al., 2011). This upregulation by AIMP2 (Aminoacyl tRNA synthase complex-interacting multifunctional protein 2) has also been linked to Parkinson’s disease pathogenesis (Jo et al., 2020).

The human gene of *USP29* encodes a 922 amino acid protein and shares 42.5 % amino acid sequence identity with its murine homologue (Kim et al., 2000). *USP29* protein is mostly located in the nucleus of the cells and strongly expressed in testis (Kim et al., 2000). Like all the DUBs from the USP family, *USP29* harbours a split catalytic domain, called USP domain, with the classic

catalytic core formed by the triad of cysteine, histidine and asparagine residues. (Clague et al., 2013) (Figure I4). The USP domain is shaped resembling an open hand exposing its thumb (Cys), palm (His/Asp) and fingers (Hu et al., 2002). Most USP domains cleave the isopeptide linkage between two ubiquitin molecules, and hence contain two ubiquitin-binding sites. The Ub molecules bind USP over the fingers (distal Ub), and the thumb (proximal Ub) (Ye et al., 2009) (Figure I4).

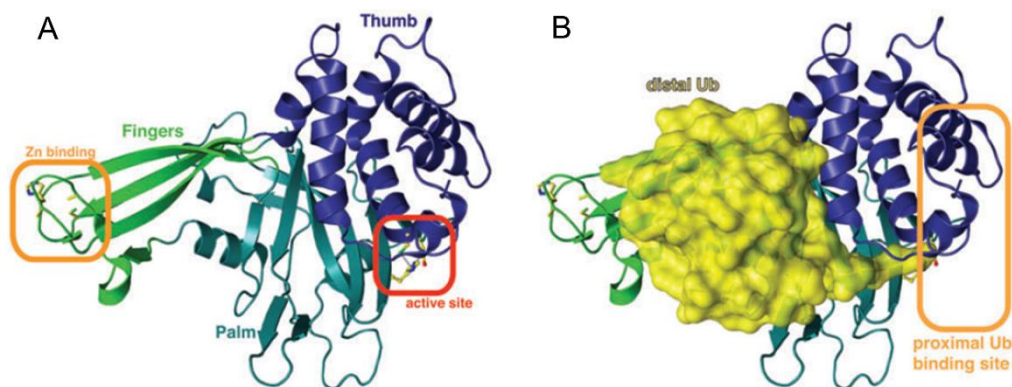


Figure I4: 3D USP domain structure. A) The USP domain structure of USP7 where Fingers (in green), Thumb (in blue) and Palm (light blue) are indicated along with the active site position. **B)** The Ub location on USP domain where proximal Ub can be observed located near the USP active site (Figure from Ye et al, 2009).

USP29 has been described to cleave K48 Ub chains to protect its substrates from proteasomal degradation (Liu et al., 2011; Martín et al., 2015).

In the phylogenetic tree of the USPs, USP29 clusters within USP26 and USP37 (Clague et al., 2013). Interestingly, these three proteins are the only DUBs which contain a Pleckstrin Homology (PH) domain. The PH domain of USP37 is the only one that has been confirmed and structurally characterised (PDB 3U12), the other two being predicted by sequence homology. Many PH structures have been determined and they are similar in structure, which consists of two perpendicular anti-parallel beta-sheets, followed by a C-terminal amphipathic helix (Macias et al., 1994; Yoon et al., 1994). However, PH domains are difficult to detect in protein sequences due to the different lengths of their beta-strand connecting loops.

PH domains span around 120 amino acids (aa 1-104 in the case of USP29) and are present in a wide variety of proteins. The PH domains bind phosphatidylinositol lipids within biological membranes (such

as phosphatidylinositol (3,4,5)-trisphosphate and phosphatidylinositol (4,5)-bisphosphate) (Wang & Shaw, 1995) and have been reported to play also a role in protein-protein interactions recruiting other proteins to different membranes or cellular compartments. They bind proteins such as the $\beta\gamma$ -subunits of heterotrimeric G proteins (Deng Shun Wang et al., 1994) or protein kinase C (Drugan et al., 2000; Yao et al., 1994).

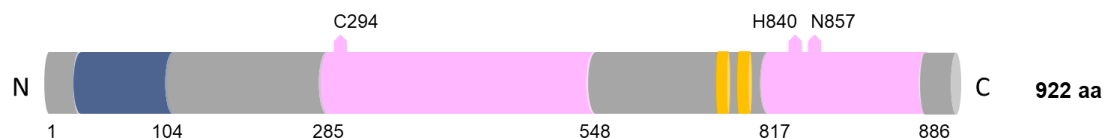


Figure I5: Schematic representation of USP29. Domain structure of the ubiquitin carboxyl-terminase 29 (USP29). The following domains are shown from N-terminal (N) to C-terminal (C): PH domain (blue), bipartite catalytic domain (pink), and two ubiquitin interacting motifs (orange). Along with the disordered predicted regions (grey). The residues forming the catalytic triad of USP29 are also marked (C294, H840 and N857).

USP29 together with USP25, USP26, USP28 and USP37, present ubiquitin-interacting motifs (UIM) (Figure I5). UIMs are ~20-amino acid -helical regions that bind to ubiquitin (Tanno et al., 2014) and were first discovered within the 26S proteasome subunit PSD4/RPN-10 (Young et al., 1998). The UIM motif has the consensus sequence $X\text{-Ac-Ac-Ac-Ac-}\Phi\text{-X-X-Ala-X-X-X-Ser-X-X-Ac-X-X-X-X}$, where Φ represents a large hydrophobic residue (typically Leu), Ac represents an acidic residue (Glu, Asp), and X represents residues that are less well conserved (Hofmann & Falquet, 2001). Some deubiquitinases from the USP family also possess zinc-finger ubiquitin-binding domains (ZnF-UBPs), that in some cases have been demonstrated to identify the carboxyl-terminal Gly-Gly motif of unattached ubiquitin (Clague et al., 2019). USP29 might also have a ZnF-UBP.

The first target described for USP29 protein was the tumour suppressor p53 (Liu et al., 2011). Liu and colleagues reported that, under oxidative stress, USP29 interacts and stabilizes p53 by removing its poly-ubiquitin chains. Moreover, USP29 has been shown to be recruited at double-strand breaks to oppose stress-induced 53BP1 (p53 binding protein 1) foci by preventing the action of the ubiquitin E3-ligase RNF168 and therefore, impairing the ubiquitination of histone H2A (histone 2A) by the RNF8/RNF168 complex and the subsequent recruitment of DNA repair factors (Mosbech et al., 2013). Furthermore, USP29 has been

reported to de-ubiquitinate and stabilize the checkpoint adaptor protein claspin during the S-phase of the cell-cycle (Martín et al., 2015). This protein is required for DNA damage checkpoint and correct DNA replication.

Recently, we have established USP29 as a novel non-canonical regulator of HIF- α (Hypoxia Inducible Factor α). Indeed, in order to identify hypoxia specific DUBs, we carried out an unbiased loss-of function screen using pools of small hairpin RNAs (shRNAs) to individually inhibit the expression of human DUBs. We used the hypoxia-driven LUC reporter as a readout of hypoxia signalling activation. In the three replicates of this experiment, USP29 appeared as one of the strongest hits. The data from the screening showed that silencing USP29 clearly reduced hypoxia-driven HRE-luciferase expression, as well as HIF- α protein accumulation. Interestingly, USP29 binds to the C-terminal region of HIF-1 α subunits and deubiquitinates the protein, in a non-canonical way, independently of O₂/PHDs(Prolyl hydroxylases)/VHL(von Hippel-Lindau) mediated ubiquitination, thus protects HIF- α from proteasomal degradation (Schober et al., 2020) (Figure I6).

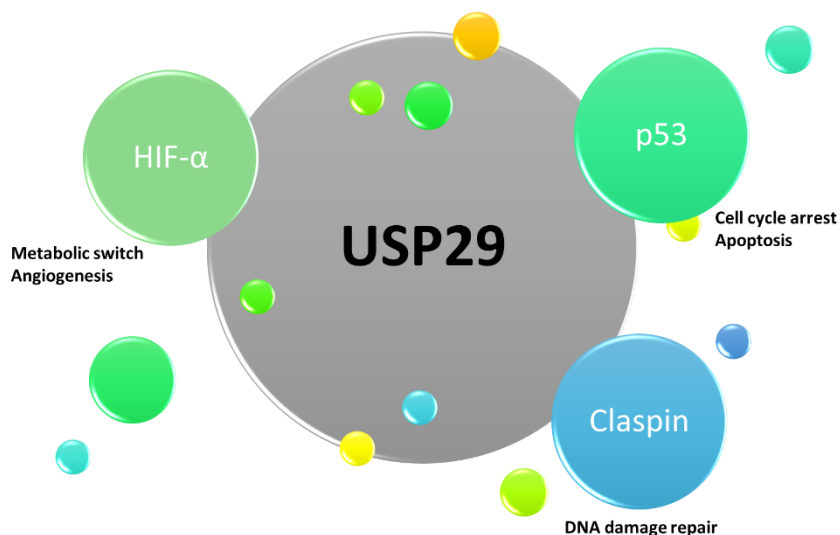


Figure I6: Schematic summary of the proteins reported in the literature as regulated by USP29. The protein stability of these targets has been shown to be regulated by USP29.

Our lab carried out a MassSpec (MS) analysis to identify the USP29 interactome in order to broaden the biochemical characterization of this DUB. Based on the MS result, USP29 interacts with mitochondrial and ribosomal

proteins, proteins involved in the cytoskeletal organisation of the cell, and in concordance with its primarily nuclear localisation with proteins that bind to chromatin, DNA and mRNA. Interestingly, PCNA (Proliferating Cell Nuclear Antigen) was one of the top 10 interacting proteins of USP29, in terms of reproducibility and abundance. Thus, a potential new target of USP29 had appeared.

1.4 Functionality

1.4.1 DNA Damage Tolerance (DDT)

PCNA has, at least, three biological functions: i) it is the eukaryotic DNA sliding clamp, a structurally and functionally conserved family of proteins that encircle and slide on the DNA during DNA replication and repair (Kelman & O'donnell, 1995), ii) it is a polymerase switch factor (Strzalka & Ziemienowicz, 2011), and iii) a recruitment factor in the regulation of the cell cycle and chromatin remodelling (Maga & Hübscher, 2003).

PCNA plays a critical role in DDR, a network of DNA repair and DNA damage checkpoint pathways which negotiate with DNA injuries by coordinating different cellular processes (Aguilera & García-Muse, 2013).

Depending on the type of DNA damage, the reparation takes place in different stages of the cell cycle and by different mechanisms, including the base excision repair (BER), nucleotide excision repair (NER), mismatch repair (MMR), non-homologous end joining (NHEJ) and homologous recombination (HR) (Branzei & Foiani, 2008; Mjelle et al., 2015). PCNA interacts with many proteins involved in the aforementioned DNA repair mechanisms, such as Pol β , FEN1, XPG (DNA repair protein complementing XP-G cells), LIG1, several DNA glycosylases, AP endonuclease 1 (DNA- (apurinic or apyrimidinic site) lyase), XRCC1 (DNA repair protein XRCC1), MSH2 (DNA mismatch repair protein Msh2), MSH3 (DNA mismatch repair protein Msh3) and MSH6 (DNA mismatch repair protein Msh6), and enhances their activities (Fan et al., 2004; Gary et al., 1997; Kleczkowska et al., 2001; Moldovan et al., 2007b; Montecuccio et al., 1998; Sancar et al., 2004).

DNA Damage Tolerance (DTT), also known as Post-replication Repair (PRR) or DNA damage bypass, is another DDR mechanism, responsible for bypassing DNA lesions during replication in order to avoid replication fork slowing and/or stalling (Bi, 2015). DTT is critical to ensure the duplication of the genome as well as to prevent the formation of double-strand breaks. Two different pathways of DNA Damage Tolerance exist, the error-prone translesion synthesis (TLS) and the error-free template switching (TS) (Branzei & Psakhye, 2016) (Figure 17). In eukaryotic organisms, the activation of these pathways relies on the ubiquitination of PCNA (Kanao & Masutani, 2017).

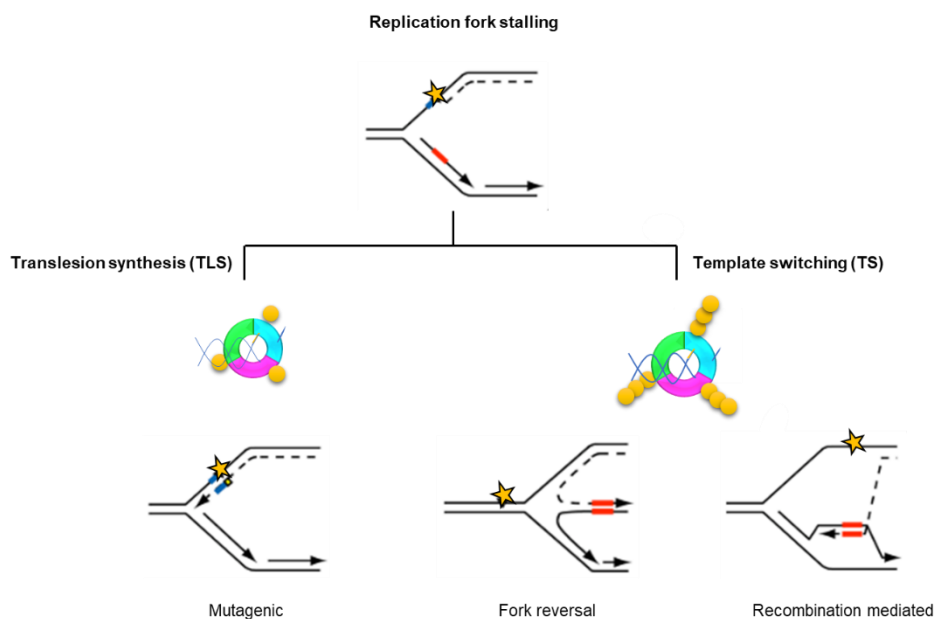


Figure 17: The DNA Damage Tolerance pathways. The yellow stars indicate a lesion in the DNA strands and the dashed line the blocked DNA replication. In the left, translesion synthesis is shown, which allows DNA lesion bypass in an error-prone mode. In the right, the two models proposed for template switching are represented: the formation of a four-way junction or “chicken-foot” intermediate (left) and recombination-mediated template switching involving D-loop formation and strand invasion (right). The templates that polymerases use to bypass the lesion are in blue for TLS and in red for TS. PCNA is represented along each mechanism in mono-Ubiquitinated (TLS) or poly-Ubiquitinated (TS) form. Adapted from (Chang & Cimprich, 2009).

Two different models of template switching have been proposed, in which structural rearrangements of the replication fork are required: fork regression and recombination-mediated template switching. Fork regression is the prevalent TS pathway in mammals while recombination-based TS is dominant in yeast (Vujanovic et al., 2017). At fork regression, the replication fork that has been stalled upon the lesion forms a chicken-foot-like DNA structure (Neelsen & Lopes, 2015) (Figure 17). In this chicken foot structure, the replisome is able to use the

newly synthesized sister strand as a template to avoid and correct the damage. This way, the nascent DNA of the stalled strand has direct access to the nascent homologue undamaged template. Next, the chicken-foot structure is reversed again to continue in a point after the damage and continuing DNA replication in an error-free manner (Hedglin & Benkovic, 2015).

Recombination-mediated TS fills the single-stranded gap that contains the damage (Branzei & Szakal, 2016). Here, the replicative fork that finds the DNA lesion invades the undamaged strand and a displacement loop (D-loop) is formed creating a holiday junction like structure. This way, the stalled strand uses the newly synthesized sister strand as a template bypassing the lesion in an error-free manner (Friedberg, 2005) (Figure 17).

When genotoxic stress causes replication-blocking lesions, RAD6/RAD18, an E2/E3 complex, is recruited to the stalled forks and catalyzes the conjugation of a Ub to the K164 residue of PCNA (Finley et al., 2012). The activity of the E2/E3 complex is enhanced by the phosphorylation of human RAD6 and RAD18 by cyclin-dependent kinase 9 (CDK9) and Cdc7 kinase (Cell division cycle 7-related protein kinase) and ATR/Chk1-dependent c-Jun N-terminal kinase (JNK), respectively (Hedglin & Benkovic, 2015). Mono-Ubiquitinated (mono-Ub) PCNA promotes the activation of the TLS pathway by recruiting the TLS polymerase η at the stalled replication forks (Leung et al., 2019; Watanabe et al., 2004).

The TLS or low-fidelity polymerases belong to three different families: A (Pol ν and Pol θ), B (Pol ζ) and Y (Pol η , Pol κ , Pol ι and Rev1) polymerases families. Due to their lack of proofreading capacity, they are specific for the bypass of different DNA lesions (Prakash et al., 2005). TLS polymerases are recruited to the DNA damage site by mono-Ub-PCNA via their ubiquitin-binding motifs (UBM) in the C-terminal region (Bienko et al., 2005). In addition, Pol η and Pol κ interact with the E3-ligase Rad18 and are directly recruited to DNA damage sites (Bi et al., 2006; Watanabe et al., 2004).

Being highly mutagenic, the activation of TLS must be tightly controlled, and therefore the level of ubiquitinated PCNA must be regulated. The first described enzyme responsible for deubiquitinating mono-Ub-PCNA was the deubiquitinating enzyme (DUB) USP1 (Huang et al., 2006), active during the S

phase of the cell cycle. USP1 is catalytically active and stable in complex with UAF1 (USP1-associated factor1) (Cohn et al., 2007), which in turn is activated by hELG1 (enhanced level of genomic instability 1), an alternative subunit of the RFC (Lee et al., 2010). Consistent with USP1 negatively regulating PCNA, it has been demonstrated that USP1 is autocleaved and therefore, PCNA is ubiquitinated upon UV irradiation (Niimi, Brown & Lehmann, 2009). USP7 has been described as another DUB that deubiquitinates mono-Ub PCNA during the interphase (Kashiwaba et al., 2015). It has been shown that USP7 binds and stabilizes Rad18 and Pol η , therefore acting as an indirect regulator of mono-Ub-PCNA and TLS (Qian et al., 2015; Zlatanou et al., 2016). USP7 is present during the whole cell-cycle (Kashiwaba et al., 2015). It has also been found that, upon UV irradiation, PCNA is deubiquitinated by USP10, following PCNA ISGylation by ISG15 (interferon-stimulated gene 15), which in turn releases Pol η from PCNA, terminating TLS (Park et al., 2014).

It is thought that the switch from TLS to template switching is activated when RPA is accumulated at the ssDNA rather than when PCNA is mono-Ubiquitinated, taking into account that ssDNA is needed for PCNA ubiquitination at K164 (Chang et al., 2006).

PCNA is further poly-Ubiquitinated at K164 (Figure I1) through Ub-K63 chains (Hoege et al., 2002) by MMS2-UBC13 and DNA-dependent ubiquitin ligase HTLF (Helicase-like transcription factor) and SHPRH (SNF2 histone linker PHD RING helicase) to activate an error-free lesion bypass through the template switching pathway (Motegi et al., 2008). However, the mechanism by which poly-Ub-PCNA activates TS is yet to be understood.

Poly-Ubiquitination of PCNA has been identified as a key factor in template switching (Chiu et al., 2006), but it is still not clear how this poly-Ubiquitination of PCNA is reversed.

Poly-Ub-PCNA is difficult to detect since it exists at a much lower abundance than mono-Ub-PCNA (Masuda & Masutani, 2019). Moreover, studies performed in mammalian cell lines have proved that mono-Ub-PCNA is induced at the same time that poly-Ub-PCNA when treating the cells with UV irradiation, MMS (methyl methanesulfonate), MMC (3-Methylmethcathinone), CPT (Camptothecin) or HU

(hydroxyurea) (Brun et al., 2010; Chiu et al., 2006; Motegi et al., 2008; Vujanovic et al., 2017), which complicates even more the task of studying the poly-Ubiquitination of PCNA.

1.4.2 DNA replication: the catalytic subunit of polymerase δ , p125

DNA replication ensures that the entire genome is copied only once and faithfully during the S phase of the cell cycle (Bruck et al., 2015). Thus, the tightly controlled process is essential for living organisms to continue propagating the species.

The replisome is the molecular machine that coordinates the biochemical activities required for an optimal chromosome replication (Yeeles et al., 2017). DNA replication is initiated in eukaryotes by the binding of ORC (Origin Recognition Complex) to the *ori* (origin of replication) during the G₁ phase of the cell cycle (Huilin Li & Stillman, 2012). The ORC complex then serves as an anchor platform for the pre-replicative complex (pre-RC). The pre-RC includes the licensing cofactor Cdt1 (DNA replication factor Cdt1), the 4ATPase (adenosine triphosphatase), Cdc6 (cell division control protein 6 homologue) and the hexameric Mcm2-7 (minichromosome maintenance proteins 2-7) helicase complex (Evrin et al., 2014). The pre-RC is then activated and converted into the initiation complex by the action of cyclin-dependent kinases (CDK) and Dbf4-dependent kinases (DDK) (Bruck et al., 2015; Tanaka et al., 2007). These kinases phosphorylate the CMG helicase complex formed by Cdc45 (Cell division control protein 45 homologue), Mcm2-7 and GINS (DNA replication complex GINS protein SLD5), activating the complex in order to separate the parental DNA strands and form two single-stranded DNA (ssDNA) to allow the replisome to synthesize the new DNA (Bell & Labib, 2016; Tognetti et al., 2015). Replication Protein A (RPA) binds then to ssDNA to prevent it from winding back on itself or from forming secondary structures, keeping DNA unwounded for the next step (Zou et al., 2006).

The enzymes that continue the duplication of the parental DNA are the three replicative DNA polymerases α , δ , and ϵ (Pol α , Pol δ , and Pol ϵ) (Yu, Gan, &

Zhang, 2017), which are members of the Family B of polymerases, together with the herpesvirus DNA polymerases, and the bacteriophage T4 polymerase.

The complex of the Polymerase α and the primase synthesize the nucleic acid primer necessary for the duplication of both the leading and lagging strands (Baranovskiy et al., 2018). Replication factor C (RFC) then loads PCNA on the primer/template junction (Hedglin & Benkovic, 2017). PCNA encircles the duplex and tethers the replicative polymerases increasing their processivity by sliding along the double-stranded DNA helix (Moldovan et al., 2007a). Pol ϵ is responsible for the replication of the leading-strand (Stodola & Burgers, 2017). In contrast to the continuous leading strand synthesis, lagging strand is replicated discontinuously in Okazaki fragments (Okazaki et al., 1968). Pol δ elongates the primers synthesized by Pol α in 5'-3' direction and when it reaches the 5' terminus of the previous Okazaki fragment, Pol δ displaces short 5' flap structures, which are cleaved by flap endonuclease 1 (FEN1) and other nucleases, by replacing most of the DNA incorporated by the error-prone Pol α (Kahli et al., 2019). FEN1 is anchored to PCNA and degrades the initiator primer before fragment ligation by DNA ligase I, which also interacts with PCNA (Finger et al., 2012) (Figure 18). The RFC catalyzes the loading of PCNA onto DNA, by binding to the 3' end of the primed DNA and thus, opening the PCNA ring by hydrolyzing ATP (Tsurimoto & Stillman, 1991).

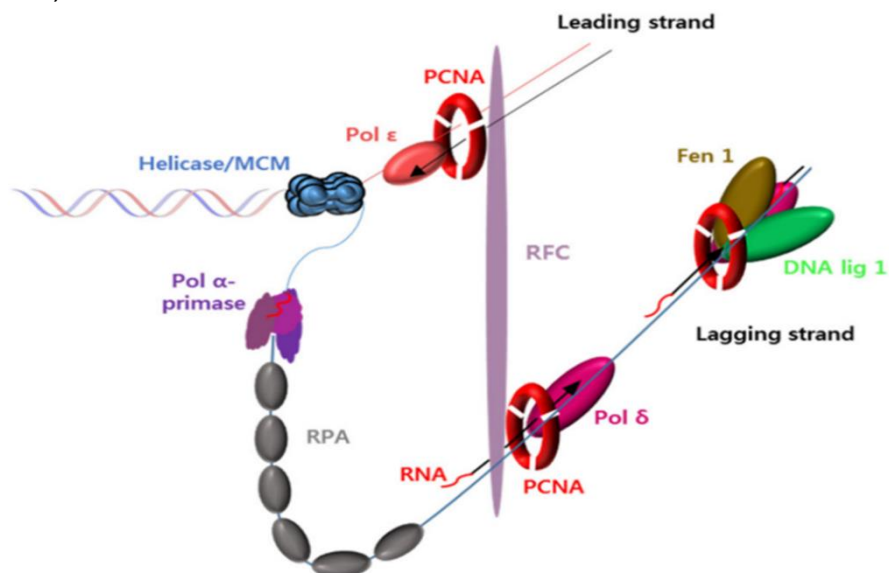


Figure 18: Eukaryotic DNA replication. The MCM helicase complex unwinds the DNA duplex. RFC loads PCNA and Pol ϵ and Pol δ to synthesize the leading strand and lagging strand, respectively. The lagging strand is primed by Pol α and then Pol δ elongates it discontinuously. The single-stranded DNA (ssDNA) is coated by Replication Protein A (RPA). The red tail represents the priming RNA synthesized by the polymerase α (Park, Jeong, Han, Yu, & Jang, 2016).

Human Pol δ is a heterotetrameric complex consisting of: i) the catalytic subunit p125; ii) p50 (also referred to as the B-subunit), which acts as a scaffold; iii) p68 (also known as p66), and iv) the regulatory subunit p12 (Figure I9) (Lancey et al., 2020). The catalytic subunit (p125) holds the polymerase and exonuclease activities (Lee, Wang, Zhang, Zhang, & Lee, 2017).

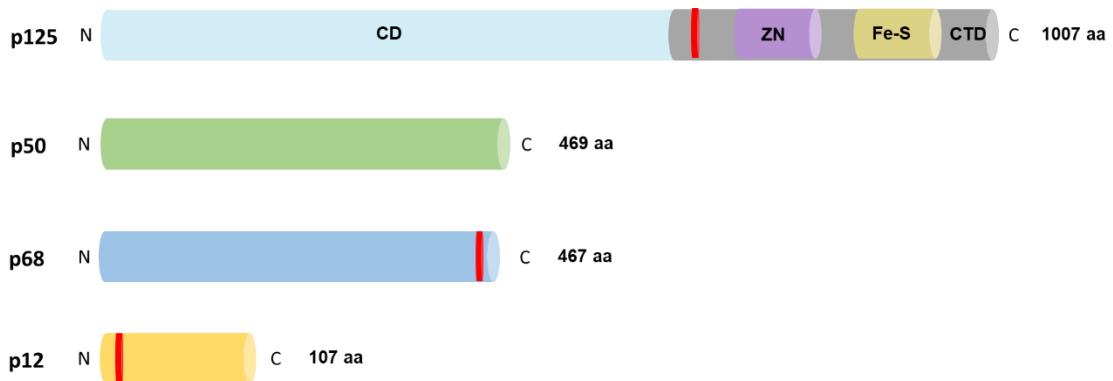


Figure I9: Schematic representation of Pol δ subunits. The PIP-box motifs for each subunit are represented (red). In the case of the catalytic subunit, p125, there are four different domains: CD: catalytic domain (blue); CTD: C-terminal domain (grey); ZN: Zinc finger (purple) and Fe-S: iron-sulfur cluster (yellow).

Several experiments have reported that the four subunits of Pol δ interact with PCNA. Until recently, only the interaction of p68 had been structurally characterized. Like many PCNA-binding proteins, p68 has a short specific sequence called PIP-box (PCNA interacting protein-box), through which p68 binds to PCNA with an affinity of 1.5 μ M (Bruning & Shamoo, 2004). Moreover, the phosphorylation of the residue S458, located in this PIP-box, by protein kinase A (PKA), decreases its interaction affinity with PCNA and the processivity of Pol δ (Rahmeh et al., 2012). The smallest subunit of Pol δ , p12, interacts with PCNA via a non-canonical PIP-box located at its N terminus (Gonzalez-Magaña et al., 2019). p12 is also thought to bridge p125 and p50 subassemblies in the polymerase δ complex (Xie et al., 2002).

It has been shown that there is a weak interaction between the catalytic subunit of Pol δ and PCNA (Hao Li et al., 2006). However, until very recently, no structural data existed about the binding of p125 to PCNA. After analysing the sequence of p125, two potential non-canonical PIP-box sequences were found

in the C-terminus, which could be the potential interaction sites with PCNA. Moreover, Acharya and colleagues had discovered that yeast Pol δ showed less processivity during DNA synthesis after mutation of one of the two potential PIP-boxes in the p125 yeast homologue Pol3 (Acharya et al., 2011), suggesting this PIP-box as the potential PCNA binding site for p125. Later, during this thesis-work, this data was confirmed by the cryo-EM structure of human Pol δ bound to PCNA and DNA determined by Lancey and colleagues (Lancey et al., 2020).

Hypothesis and Aims

PCNA has been identified as one of the top10 interacting proteins of USP29 by mass spectrometry. USP29's sequence contains a canonical PIP-box motif. Hence, we hypothesize a direct interaction between the two proteins and a role for PCNA/USP29 as a crossroad in the DDT pathway template switching through at least two non-mutually exclusive mechanisms: the de-ubiquitination of PCNA and/or PCNA-interacting proteins by USP29.

PCNA interacts with all the subunits of Pol δ (p125, p50, p68 and p12), but until recently, only the interaction with p68 had been structurally characterized. We hypothesize that p125, the catalytic subunit of human polymerase δ , interacts with the PIP-box site on the front face of PCNA through a divergent PIP-motif.

The specific objectives of this thesis are:

1. To characterize the interaction between the human PCNA and USP29 proteins as well as the role of USP29 as a DUB for PCNA.
2. To study the regulation of USP29.
3. To structurally characterize USP29.
4. To structurally characterize the interaction between PCNA and the catalytic subunit of DNA polymerase δ (p125).

Material and Methods

1. Materials

Chemicals and siRNAs were purchased from Sigma-Aldrich unless stated otherwise. All tissue culture media were purchased from Gibco and custom oligo primers were purchased from Invitrogen. All columns and chromatography systems used were from GE Healthcare. The synthetic peptides used in this thesis were purchased from the company A peptide in lyophilized form.

2. Methods

2.1 *Molecular biology*

2.1.1 *Polymerase chain reaction (PCR)*

Polymerase chain reaction is used to amplify double-stranded DNA from single or doubled stranded DNA template. This allows the introduction of point mutations, restriction enzyme sites, flanking sequences, or tags by modifications of the primers used for the amplification. Primers anneal to complementary target DNA and enable DNA polymerase to synthesize new DNA molecules replicating the target sequence and also incorporating the primers' modified sequence.

DNA was amplified via PCR using KOD Hot Start DNA Polymerase (EMD Millipore). After an initial denaturation step for 5 minutes at 95 °C, 30 cycles using the following scheme were performed: denaturation at 95 °C for 20 seconds, annealing at primer-dependent melting temperature (T_m) for 15 seconds, and elongation at 70 °C for 30-90 seconds (depending on the length of the DNA). Finally, a 10 min elongation step was included to complete the elongation.

2.2.2 *In-Fusion® HD Cloning*

To insert cDNAs into expression vectors In-Fusion® HD Cloning (Clontech), a method which takes advantage of DNA recombination technology, was used. Thus, the destination vector was linearized by single or double digestion and the insert was amplified by PCR using specific primers (Table M1) that create complementary overhangs to the vector backbone at the site of insertion. Then, the linearized vector and PCR product were gel-purified (with the gel purification kit QIAEX® II from Qiagen) and the In-Fusion® reaction was set up with a molar insert:vector-ratio of 6:1. After that, the In-Fusion reaction was diluted 1:10 and 2.5 µl were used to transform 50 µl competent Stellar™ *E. coli* cells.

Table M1: Summary of the strategies used to clone the indicated plasmids.

<i>In-Fusion® HD Cloning primers (F: forward; R: Reverse)</i>			
<i>Insert donor</i>	<i>Vector acceptor</i>	<i>Final plasmid</i>	<i>Sequence (5' → 3')</i>
mRuby2-PCNA	<i>Myc-clover-</i> HIFDM	<i>Myc-clover-PCNA</i>	F: ACGAGCTGTACAAGGAATTCGAGGCGCGCCTGGTC R: TTAATTAAGGTACCGCTAAGATCCTTCTTCATCCTC
HA-USP29	<i>GFP-</i> USP29	<i>GFP-USP29PH</i>	F: CTTCGAATTCTGCAGTCATCTCTCTAAAGGTATGTGG R: TAGATCCGGTGGATCCTACTGAGATTTGTTTTGGTGG
HA-USP29	<i>GFP-</i> USP29	<i>GFP-USP29ΔPH</i>	F: CTTCGAATTCTGCAGTCGACAAATCTCAGCAACCCATGA R: TAGATCCGGTGGATCCTCAAGCAGGTCTGTACAAAGAG
pET11d- USP29PH	pET29	<i>pET29-USP29PH</i>	Ligation
pET11d- USP29PH	pHisP2	<i>pHisP2-USP29PH</i>	F: TATTTTCAGGGCGCCATGATCTCTCTAAGGGTATGTGG R: TTGAATCCGGATCCTCACATATTCCTGCTTTCGAACAC
GFP-USP29PH	pOPINE	<i>pOPINE-USP29PH</i>	F: AGGAGATATACCATGATGATCTCTCTGAAGGTATGT R: GTGATGGTGTGTTTCTGAGACTTGTCTGGTGGATTATG
GFP-USP29PH	pOPING	<i>pOPING-USP29PH</i>	F: GCGTAGCTGAAACCGGCATGATCTCTCTGAAGGTATGT R: GTGATGGTGTGTTTCTGAGACTTGTCTGGTGGATTATG
HA-USP29	pHisP2	<i>pHisP2-USP29</i>	F: TATTTTCAGGGCGCCATGATCTCTCTAAGGGTATGTGG R: TTGAATCCGGATCCTCAAGCAGGTCTGTACAAAGAGT
HA-USP29	pET21a- Cpf1	<i>pET21a-USP29</i>	F: AGAAGGAGATATACATATGATCTCTCTGAAGGTATGTGG R: GCTCGAATCCGGATCCAGCAGGTCTGTACAAAGAGTC
HA-USP29	pOPINE	<i>pOPINE-USP29</i>	F: AGGAGATATACCATGATGATCTCTCTGAAGGTATGT R: GTGATGGTGTGTTTAGCAGGTCTGTACAAAGAGTC
HA-USP29	pOPING	<i>pOPING-USP29</i>	F: GCGTAGCTGAAACCGGCATGATCTCTCTGAAGGTATGT R: GTGATGGTGTGTTTAGCAGGTCTGTACAAAGAGTCAC

The human gene of full-length USP29 was cloned into the expression vectors pHisP2 and pET21a. The pHisP2-USP29 and pET21a-USP29 constructs were designed with a His₆-tag at the N-terminus and C-terminus, respectively, followed, or preceded, by the sequence for TEV protease cleavage (ENLYFQG), for His₆-tag removal after purification.

A synthetic gene of the N-terminal region of USP29 corresponding to the PH domain (residues 1-108 of USP29) with codons optimized for expression in *E. coli* was cloned into the expression vectors pET11d and pET29. Both constructs were designed with a Strep-tag at the N-terminus to facilitate protein purification by affinity chromatography followed by a specific sequence for TEV protease cleavage for Strep-tag removal after purification. In the pET29-USP29PH

construct the gene of interest is fused to N-terminal ubiquitin, which provides high expression levels, and a His-tag inserted in one of the loops of ubiquitin for purification by Ni²⁺ affinity chromatography. The human gene of USP29PH was also cloned into the expression vector pHisP2 (with a His₆-tag at the N-terminus followed by the TEV protease cleavage sequence).

The full-length USP29 and the isolated PH domain of USP29 human sequences were cloned into the mammalian expression vectors pOPING and pOPINE (<https://www.opf.rc-harwell.ac.uk/OPPF/protocols/cloning.jsp>). The four constructs (pOPING-USP29, pOPING-USP29PH, pOPINE-USP29 and pOPINE-USP29PH) were designed with a His₆-tag at the C-terminus to facilitate protein purification by affinity chromatography. The tag can be removed from the protein with Carboxypeptidase A. In the case of pOPING, the expressed protein also contains a secretion signal sequence (MGILPSPGMPALLSLVSLLSVLLMGCVAETG) at the N-terminus.

2.2.3 Ligation

The only plasmid that was generated by ligation was pET29-USP29PH. The destination vector, in this case pET29, was linearized by double digestion (BamHI/NcoI). The insert, USP29PH, was generated by digestion of the pET11d-USP29PH plasmid with the same restriction enzymes. Next, the linearized vector and digested insert were gel purified. The ligation reaction was set up with an insert:vector-ratio of 6:1, 1 µl of freshly prepared ligation buffer (300 mM Tris pH 7.5, 100 mM MgCl₂, 100 mM DTT and 2mM ATP) and 1 µl of T4 ligase in a final volume of 10 µl. After 16 h at room temperature, 2 µl of the reaction were used to transform 50 µl competent Stellar™ *E. coli* cells.

2.2.4 Mutagenesis

QuikChange® II XL Site-Directed Mutagenesis (Agilent Technologies) as well as In-Fusion® HD Cloning (Clontech) kits were used to introduce single or multiple point mutations from double-stranded DNA plasmids. As for the QuikChange® II XL Site-Directed Mutagenesis Kit, the mutations were introduced by amplification of 100 ng of template DNA with 0.25 µM forward and reverse primers (Table M2), in the presence of reaction buffer (6% (v/v) Quik solution®,

0.1 mM dNTPs) with 1.25 units PfuUltra HF DNA Polymerase. PCR cycles were set as follows: 1 minute at 95 °C, 18 cycles of 50 seconds at 95 °C, 50 seconds at 60 °C and 7 minutes at 68 °C with a final elongation cycle of 7 min at 68°C. Template DNA was digested with 5 units of Dpn1 for 1 h at 37 °C and subsequently one sixth of the reaction was used to transform competent XL10-Gold (Agilent Technologies) *E. coli* cells.

With In-Fusion® HD Cloning (Clontech) the mutations were introduced by amplification of 5 ng of template DNA with 300 nM forward and reverse primers (Table M3), in the presence of 12.5 µL of CloneAmp HiFi PCR Premix in a final volume of 25 µL. PCR cycles were set as follows: 30 cycles of 10 seconds at 98 °C, 10 seconds at 55 °C and 5 seconds/Kb at 72 °C. The PCR product was gel-purified with a gel purification kit (QIAEX® II from Quiagen) and subsequently the In-Fusion® reaction was set up with 100 ng of the gel-purified linear construct. 2.5 µL of the reaction were transformed into competent Stellar™ *E. coli* cells.

Table M2: Summary of the primers used for plasmid mutagenesis.

<i>QuikChange® II XL Site-Directed Mutagenesis</i>		
<i>Result vector</i>	<i>AA change</i>	<i>Sequence (5' → 3')</i>
GFP-USP29 V39T	V39T	F:GCAAAGACAAAAGGAAATTAAACTGACGGTCACTTTCAAATCTGG R: CCAGATTTGAAAGTGACCGTCAGTTTAATTTCTTTGTCTTTGC
GFP-USP29 I50T	I50T	F: CTGGAAAATTTATAAGAACGTTTCAGCTGAGCAACAACATTAG R: CTAATGTTGTGCTCAGCTGAAACGTTCTTATAAATTTCCAG
GFP-USP29 TM	I50T	F: CTGGAAAATTTATAAGAACGTTTCAGCTGAGCAACAACATTAG R: CTAATGTTGTGCTCAGCTGAAACGTTCTTATAAATTTCCAG

Table M3: Summary of the primers used for plasmid In-Fusion® HD mutagenesis (F: forward; R: reverse)

<i>In-Fusion® HD Mutagenesis</i>		
<i>Result vector</i>	<i>AA change</i>	<i>Sequence (5' → 3')</i>
GFP-USP29 V30T	V30T	F:TGAAACAACGCAAAGACAAAAGGAAATTAAACTGG R: CTTTGCGTTGTTTCAATGAGAGCTTCTTTCAG
GFP-USP29 V30/39T	V30T	F: TGAAACAACGCAAAGACAAAAGGAAATTAAACTGG R: CTTTGCGTTGTTTCAATGAGAGCTTCTTTCAG

2.2.5 DNA amplification

Amplification of circular plasmid DNA (with a bacterial origin of replication and an antibiotic resistance for selection purposes) was carried out by transforming

the DNA into chemically competent *E. coli* XL10-Gold (Agilent Technologies) or Stellar™ (Clontech) cells. 5 ng of plasmid DNA were incubated with 50 µl of competent bacteria for 30 min on ice. Bacteria were then heat-shocked in a 42 °C water bath for 45 seconds and after 2 minutes on ice, 500 µl of SOC-medium was added. Bacteria were allowed to grow for 1 hour at 37 °C in a shaker (220 rpm) before plating 1:10 and 9:10 of the culture onto LB plates containing the selection antibiotic (50 µg/ml kanamycin or 100 µg/ml ampicillin). Plates were incubated overnight at 37 °C and single colonies were picked and inoculated into antibiotic containing LB-medium and allowed to grow for 16 hours. The GeneJET Plasmid Miniprep Kit (Thermo Fisher Scientific), the QIAGEN® Plasmid Maxi Kit and the QIAGEN® Plasmid Giga Kit were used for plasmid purification from mini- (5 ml), maxi- (200 ml), and giga-cultures (2000 ml), respectively.

All sequences were verified by restriction digestion and DNA sequencing with appropriate primers. Sequencing was done by the company STABvida.

2.2.6 Restriction digestion

Restriction digestions were carried out by incubating 10 units of enzyme per µg of DNA in appropriate buffer for at least 1 hour at 37 °C. DNA fragments were separated by size on agarose gels containing SYBR® Safe DNA Gel Stain for visualization of DNA under UV exposure. Agarose gel percentage was chosen between 0.7 and 2%, depending on the expected DNA fragment size.

2.2 Cell Biology

2.2.1 Cell culture

2.2.1.1 Small scale

Human Embryonic Kidney 293 cells (HEK293) were cultured in DMEM + GlutaMAX™ supplemented with 5 % FBS at 37 °C and 5 % O₂. Sub-confluent plates were trypsinised and cells for experiments were plated at a density of 31,600 cells/cm² in 35, 60 or 100 mm cell plates.

2.2.1.2 Large scale

HEK293FT cells were cultured in DMEM + GlutaMAX™ supplemented with 5 % FBS at 37 °C and 5 % O₂. Sub-confluent plates were trypsinised and cells

for experiments were plated at a density of 5,000 cells/cm² in roller bottles of 2,156 cm².

2.2.2 DNA transfection

2.2.2.1 Small scale

After 24 hours, cells were transfected with 2.5 µg of DNA per 300,000 cells, using Lipofectamine® 2000 (Thermo-Fisher Scientific) at a Lipofectamine:DNA ratio of 2:1 using Opti-MEM medium. Next, the transfection mix was added to the culture media. Cells were harvested 24 hours post-transfection, unless stated otherwise, to be further processed.

2.2.2.2 Large scale

After 4 days, cells were transfected with 0.5 mg of DNA per 250 mL of serum free DMEM, using Polyethylenimine Hydrochloride (PEI MAX 40K) at a PEI MAX:DNA ratio of 2:1 using serum free DMEM. The DNA was previously cleaned with 80 µL of chloroform per 0.5 mg of DNA. Then, transfection mix was added to the culture media. Cells were harvested 48 hours post-transfection unless stated otherwise to be further processed.

2.2.3 siRNA transfection

In order to silence the expression of endogenous or overexpressed proteins, cells were transfected with 20 nM siRNAs (Table M4). The first transfection of the siRNAs with Lipofectamine® 2000 (3 µl Lipofectamine® 2000 per 20 nM of siRNA) was made in suspension at the moment of plating. 24 h later, the cells were transfected again with the siRNAs (and eventually with the corresponding DNA) after a medium change. Cells were harvested 48 h after the first transfection to be further processed.

Table M4: Summary of the siRNAs used.

<i>siRNAs</i>		
<i>Target</i>	<i>Sequence (5' → 3')</i>	<i>Reference</i>
Control	CUACAUCCGAUCGAUGdTdT	Lab validated
USP29	GGUCACUUCAAUCUGGAdTdT	Lab validated

2.2.4 DNA damage induction by ultraviolet radiation

To induce DNA damage in the HEK293 cells, the Stratalinker® UV Crosslinker (Stratagene) was used. Two days after seeding the cells, the medium was removed, and PBS (10 mM phosphate, 140 mM chloride, 153 mM sodium, 4.5 mM potassium) was added in a minimal volume. The plate was put in the Stratalinker and irradiated with 3000 J/m² or 30 J/m², and left for 1 hour or 16 hours, respectively, with the medium previously removed, before harvesting the cells.

2.2.5 Cell synchronization

For arresting HEK293 cells at G₁/S boundary (prior to DNA replication) a double thymidine block was performed (Thomas & Lingwood, 1975; Whitfield et al., 2002). Briefly, cells were plated at a density of 5,000 cells/cm² in 100 mm cell plates. After 8 hours, cells were treated with 2 mM thymidine for 16 hours and then washed twice with PBS and incubated in fresh medium for 8 hours. Cells were treated again with 2 mM thymidine for 16 hours and the resulting G₁/S-enriched cells were twice washed with PBS and released for 2 additional hours in the presence of fresh medium to finally harvest and to analyse the cell cycle. After the first hour of release cells were irradiated or not with UV as previously explained.

2.2.6 Cell cycle analysis

Harvested cells were suspended in 1 mL of PBS, fixed drop by drop with 2.5 mL of absolute ethanol (70% final ethanol concentration) and incubated overnight at -20 °C for fixation. Then, cells were centrifuged and suspended in 200-500 µL of PI staining solution (RNase 25 µg/ml, Triton X-100 0,05%, PI: 1 µg/ml). Finally, samples were incubated for 20-40 minutes at 37 °C and analysed by flow-cytometry, using the cell analyser BD FACSCanto™ II and the FlowJo™ Software to analyse the obtained data.

2.3 Biochemistry

2.3.1 Western Blotting

Cells were lysed in 1.5x Laemmli (50 mM Tris-HCl pH 6.8, 1.25% SDS, 15% glycerol), lysates were frozen, boiled at 95 °C for 15 min and then sonicated. Protein quantification was performed with the DC™ Protein Assay (BioRad). Between 10 and 40 µg of protein were loaded on a self-cast SDS polyacrylamide (Bio-Rad) gel (7.5 %, 10 % or 12 %) or a 4-15 % gradient gel (Bio-Rad) and migrated on Tris/Glycine/SDS running buffer (BioRad) at 160 V for 90 min and 100 V for 60 min, respectively. Then, proteins were transferred into a PVDF-membrane (EMD Millipore) with 100 V for 1 h at 4 °C using Tris/Glycine transfer buffer (Bio-Rad). Membranes were stained with amidoblack, air-dried, rehydrated by washing with ethanol, followed by 2 washes with TNT (50 mM Tris-HCl pH 7.4, 150 mM NaCl, 0.1 % Triton X-100) and 1 wash with TN (50 mM Tris-HCl pH 7.4, 150 mM NaCl). The membranes were then blocked for 1 hour with 5 % milk in TN and incubated with the primary antibody (diluted in 5 % milk in TN) at 4 °C overnight. After 3 washes with TNT, 1 wash with TN and a short blocking step (5 % milk in TN), membranes were incubated with the HRP-conjugated secondary antibody for 1 h. After further washing steps, home-made ECL (solution A: 100 mM Tris-HCl pH 8.5, 0.4 mM coumaric acid, 2.5 mM luminol; solution B: 100 mM Tris-HCl, 2% H₂O₂; solution A:solution B = 1:1) was incubated on the membranes for 1 min and signal was detected with Amersham Hyperfilm ECL (GE Healthcare Life Sciences).

Table M5: Summary of the antibodies used for WBs.

<i>Antibodies</i>			
<i>Target</i>	<i>Reference</i>	<i>Dilution</i>	<i>Secondary</i>
β-actin	Sigma A5441	1 : 50 000	mouse 1 : 20000
FLAG M2-HRP	Sigma A8592	1 : 1 000	-
GFP	Roche 11 814 460 001	1 : 1 000	mouse 1 : 5000
HA	Covance 16B12	1 : 10 000	mouse 1 : 10 000
HIF-1α	Home-made (Richard et al, 1999)	1 : 5 000	rabbit 1 : 5000
His-tag	Novagen 70796-3	1 : 1000	mouse 1 : 5000
H2A.X	Abcam ab11175	1 : 5000	rabbit 1 : 5000
H2A.X (pS139)	BD Pharmingen 560443	1 : 1000	mouse 1 :5000

LaminA	Abcam ab8980	1 : 1000	mouse 1 : 5000
Myc	Cell signaling 2276	1 : 1 000	mouse 1 : 5000
NP 84	Abcam ab487	1 : 5 000	mouse 1 : 5000
PCNA	Chromotek 16D10	1 : 2 000	rat 1 : 5000
PCNA K164Ub	Cell Signaling 13439	1 : 1 000	rabbit 1 : 1000
Tubulin	SIGMA T9026	1 : 10 000	mouse 1 : 10 000
USP29	Abcam ab57545	1 : 5 000	mouse 1 : 5000
Secondary antibodies			
anti-mouse-HRP	Promega W4021		
anti-rabbit-HRP	Promega W4011		
anti-rat-HRP	Jackson Lab 112-035-003		

2.3.2 Subcellular Fractionation assay

Typically, between 2×10^6 and 6×10^6 HEK293 cells were used for each extraction. Cells were harvested by trypsinization, resuspended in PBS, and counted in order to normalize all the conditions. Cells were lysed in freshly prepared ice-cold A buffer [10 mM HEPES pH 7.9, 100 mM KCl, 1,5 mM MgCl₂, 340 mM sucrose, 10% glycerol, 1 mM DTT, 1 µg/ml aprotinin, 1 µg/ml leupeptin, 1 µg/ml pepstatin, 0.1 mM AEBSF (4-(2-aminoethyl) benzenesulfonyl fluoride hydrochloride), 1 mM sodium-orthovanadate, 10 mM NaF, 2 mM NEM (N-Ethylmaleimide)] 1 µL per 20,000 cells. 10% of the lysate was stored into Laemmli 2x (1:1 ratio) and kept for whole cellular extract analysis. After incubating the rest of the lysate for 5 minutes on ice with 0.1% Triton X-100, the sample was centrifuged (4 minutes at 1,300 g at 4 °C). Then, the supernatant was recovered and centrifuged for 15 minutes at 20.000 g at 4 °C. The clarified supernatant (cytoplasm fraction) was stored into Laemmli 2x (1:1 ratio) and kept for analysis, while the pellet was discharged. The pellet from the initial centrifugation (consisting of intact nuclei) was washed once with ice-cold A buffer and incubated in freshly prepared B buffer (3 mM EDTA, 0.2 mM EGTA, 1mM DTT, 1 µg/ml aprotinin, 1 µg/ml leupeptin, 1 µg/ml pepstatin, 0.1 mM AEBSF, 1 mM sodium-orthovanadate, 10 mM NaF, 2 mM NEM) for 30 min at 4 °C. The lysate was centrifuged (5 min, 7,000 g, 4 °C) and the supernatant (soluble nuclear fraction) was separated and stored into Laemmli 2x (1:1 ratio) for analysis. The pellet was washed once in one volume of ice-cold B buffer (5 min, 7,000 g at 4 °C). This

extract constituted the chromatin-associated or insoluble nuclear fraction. This last fraction and the whole cell extract were sonicated (15 sec, 10% amplitude). All fractions were quantitated by DC™ Protein Assay (BioRad) and 10 µg or 70 µg were resolved by 12% and 10% SDS-PAGE, respectively, and Western blotted as described above.

2.3.3 Protein co-immunoprecipitation

HEK293 cells were transfected with the GFP-tagged protein of interest and 24 h post-transfection cells were lysed on ice with lysis buffer (50 mM Tris-HCl pH 8, 120 mM NaCl, 1 mM EDTA, 1 % IGEPAL CA-630, 40 mM β-Glycerolphosphate, 1 µg/ml Leupeptin, 1 µg/ml Aprotinin, 1 µg/ml Pepstatin A). Lysates were centrifuged for 15 min at 13,000 g at 4 °C and the supernatant was diluted with Co-IP buffer (50 mM Tris-HCl pH 8, 120 mM NaCl, 1 mM EDTA, 40 mM β-Glycerolphosphate, 1 µg/ml Leupeptin, 1 µg/ml Aprotinin, 1 µg/ml Pepstatin A) to reduce detergent concentration to 0.2%. The diluted lysate was incubated for 1 h at 4 °C with 15 µl pre-washed bab-20 (Chromotek) beads for pre-clearing. The lysate was then incubated with 15 µl pre-washed GFP-traps® overnight at 4 °C. The beads were subjected to 3 washes of 30 minutes with dilution buffer and 1 washing with PBS before the bound protein was eluted from the beads by boiling them for 10 min in elution buffer (250 mM Tris-HCl pH 7.5, 40% glycerol, 4% SDS, 0.2% bromophenol blue, 5% β-mercaptoethanol). Input sample and eluates were analysed by Western blotting.

2.3.4 Protein expression and purification

2.3.4.1 Expression and purification of PCNA

Human PCNA (UniProt: P12004) was produced in *E. coli* BL21(DE3) Rosetta cells grown in ZYP-5052 auto-induction rich medium (Studier, 2005) to obtain protein with natural isotopic abundance. Cells were grown for 2 h at 37 °C and were left for expression induction at 20 °C for 16 h. For PCNA uniform ²H, ¹³C, U-¹⁵N isotope enrichment, cells were grown in M9 minimal medium prepared in 99.8%-²H₂O (CIL), and containing 1 g/L 99%-¹⁵NH₄Cl and 2 g/L 97%-²H₇, 99%-¹³C₆-glucose (CIL) supplemented with 1 g/L of isotope enriched Celtone (CIL).

A PCNA clone with an N-terminal His₆-tag and the HRV 3C protease cleavage site in a pET-derived plasmid was used. The protein was purified from the soluble fraction by Co²⁺ affinity chromatography and was cleaved by HRV 3C protease during dialysis to remove the imidazole used to elute the protein. The solution was chromatographed again on the Co²⁺ loaded column to remove the protease (which also has a His₆-tag) and uncleaved PCNA protein. The protein from the flow-through of the second Co²⁺ affinity chromatography was loaded on a Q-Sepharose column and eluted with a NaCl gradient. PCNA containing fractions were finally polished by gel filtration chromatography in PBS pH 7.0. Protein elution from the columns was monitored by absorbance at 280 nm and confirmed by SDS-PAGE. The 12 % Tris-glycine gels were stained with Coomassie brilliant blue and destained with 30% acetic acid in ethanol.

The purified protein contained the non-native sequence GPH at the N-terminus. PCNA stock solutions were flash-frozen in liquid nitrogen and stored at -80 °C. The protein concentrations were measured by absorbance at 280 nm using the extinction coefficient calculated from the amino acid composition (15,930 M⁻¹ cm⁻¹) with the ExPASy ProtParam tool (Gasteiger et al., 2003).

2.3.4.2 Expression and purification of USP29 and USP29PH in bacteria

Human USP29 (UniProt: Q9HBJ7) and USP29PH were produced in different *E.coli* strains grown in LB medium or in ZYP-5052 auto-induction rich medium (Studier, 2005) unless stated otherwise. Cells grown in LB at 37 °C were induced at O.D.₆₀₀ = 0.8 with 1 mM IPTG for 16 h at 20 °C, while cells grown in auto-induction ZYP-5052 medium for 2 h at 37 °C, were left for induction at 20 °C for 16 h. All cultures were harvested by centrifugation and resuspended in lysis buffer (20 mM Tris pH 8.0, 300 mM NaCl, 1 mM DTT) in the presence of protease inhibitors (1 tablet *Complete EDTA-free* per 50 mL). The cell suspensions were sonicated and ultracentrifuged (1 h, 40,000 rpm) to monitor the presence of induced protein in the soluble or insoluble fraction. Different clones of USP29 and USP29PH were used in the purification attempts, as shown in Table M6.

The chromatography techniques and procedures used to purify USP29 and USP29PH cloned in the different expression vectors are described below.

Ni²⁺ affinity chromatography: with a HisTrap 5 mL column equilibrated in 20 mM Tris-HCl pH 8.0, 300 mM NaCl, 1 mM DTT and eluted with a first step of 0.025 M imidazole and a second one of 0.5 M imidazole in 5 CV.

StrepTactin sepharose affinity chromatography: using a StrepTactin column equilibrated in 20 mM Tris-HCl pH 8.0, 150 mM NaCl, 1mM DTT and eluted with 2.5 mM desthiobiotine.

TEV protease cleavage: Selected protein containing chromatography fractions were incubated with TEV protease in a 1:30 ratio (1 mg TEV: 30 mg protein) and simultaneously dialyzed against 20 mM Tris pH 8.0, 300 mM NaCl, 1 mM DTT at 4 °C for 16 h (in order to remove imidazol)

Gel filtration: a Superdex 200 26/60 column was used equilibrated in 20 mM Tris pH 8.0, 300 mM NaCl, 1 mM DTT.

Anionic exchange: a MonoQ 5/5 HR column was used equilibrated in 20 mM Tris pH 8.0, 300 mM NaCl, 1 mM DTT. Elution was done with a linear gradient to 1 M NaCl in 25 CV.

Protein refolding: The protein solubilized under denaturing conditions was refolded drop by drop by 1:10 or 1:100 dilution into stirred cold 20 mM, Tris pH 8.0, 300 mM NaCl and 1 mM DTT.

To test conditions for soluble protein expression, the USP29PH constructs were produced at a small scale in the *E.coli* strain Rosetta pLys grown in LB medium supplemented with 2.5 mM glycine betaine and 1 M D-sorbitol (Oganessian et al., 2007).

As most of the USP29PH protein was found to be insoluble, solubilization trials were performed. The Rosetta pLys cells expressing USP29PH were sonicated and centrifuged twice to isolate the pellets, which were washed using four different detergent conditions:

- Control: 20mM Tris pH 8; 800 mM NaCl; 1mM DTT
- SDS: 20mM Tris pH 8; 800 mM NaCl; 1mM DTT; SDS 1%
- DDM: 20mM Tris pH 8; 800 mM NaCl; 1mM DTT; DDM 1%
- CHAPS: 20mM Tris pH 8; 800 mM NaCl; 1mM DTT; CHAPS 5%

- Triton: 20mM Tris pH 8; 800 mM NaCl; 1mM DTT; Triton 1%

Table M6: Summary of the different expression vectors used for the purification trials of USP29 and USP29PH in bacterial cells.

USP29	USP29PH
Expression in <i>E.coli</i>	
pHisP2-USP29	pET11d-USP29PH
pET21a-USP29	pET29-USP29PH
	pHisP2-USP29PH

2.3.4.3 Expression and purification of USP29 and USP29PH in mammalian cells

Expression and purification of both USP29 and USP29PH was also attempted in mammalian cells, specifically HEK293FT cells.

The construct pOPINE-USP29 was transiently expressed for 48 hours and one week in 0.5 L of culture media (DMEM + GlutaMAX™ supplemented with 5 % FBS) and in roller-bottles at 37 °C and 5 % O₂. The culture was harvested by centrifugation and resuspended in lysis buffer (50 mM Tris pH 8.0, 150 mM NaCl, 1 mM DTT, 0.001% Tween-20, 1 mM o-vanadate, 10 mM NaF and 1 mM β-glycerophosphate) in the presence of protease inhibitors (1 tablet *Complete EDTA-free* per 50 mL).

The following tables summarize the constructs used for the purification of USP29 and USP29PH (Table M7) and the purification steps followed for each construct (Table M8).

Table M7: Summary of the different expression vectors used for the purification trials of USP29 and USP29PH in mammalian cells.

USP29	USP29PH
-------	---------

Expression in mammalian cells	
pOPINE-USP29	pOPINE-USP29PH
pOPING-USP29	pOPING-USP29PH

Table M8: Summary of the purification steps followed for the purification trials of USP29 and USP29PH.

<i>Construct</i>	<i>Purification steps</i>
pHisP2-USP29	No expression
pET21a-USP29	Ni ²⁺ affinity chromatography TEV incubation Ni ²⁺ affinity chromatography Gel filtration chromatography Anionic exchange chromatography
pET11d-USP29PH	No expression
pET29-USP29PH	Ni ²⁺ affinity chromatography StrepTactin chromatography TEV incubation Ni ²⁺ affinity chromatography Refolding from Urea Ni ²⁺ affinity chromatography
pHisP2-USP29PH	Ni ²⁺ affinity chromatography Refolding from Guanidinium chloride Ni ²⁺ affinity chromatography
pOPINE-USP29	Ni ²⁺ affinity chromatography
pOPING-USP29	No expression
pOPINE-USP29PH	No purification
pOPING-USP29PH	No expression

2.3.5 Peptide design

The design of the USP29 and p125 fragments (Table M9) to study their interaction with PCNA was based on five criteria: i) the presence of a PIP-box sequence, ii) the net charge at pH 7.0 (the higher the net charge the higher the solubility of the peptide), iii) the presence of Tyr or Trp residues (to facilitate concentration measurement by UV light absorbance), iv) the disorder prediction of the sequence (since PCNA binding sequences are frequently predicted to be disordered (Prestel et al., 2019a)), and v) the sequence length. The length was chosen between 12 residues, which is the shortest p21-derived peptide found to bind PCNA (Zheleva et al., 2000), and 28 residues, which were previously used

to study the binding of the PIP sequence of p15PAF (De Biasio et al., 2015). When judged necessary, non-native residues were added to favour solubility or enable the concentration measurement).

Table M9: Sequences of the designed peptides. The PIP box sequence are colored red. Non-native residues introduced to favour solubility or to enable concentration measurement are colored blue.

<i>Peptides</i>		
<i>Name</i>	<i>Sequence</i>	<i>Order prediction</i>
USP29's canonical PIP box ₄₆₇₋₄₈₄ (long sequence)	LSIQNSLDLFFKEELEY	Disordered
USP29's canonical PIP box ₄₅₈₋₄₈₅ (short sequence)	LHQETKPLPLSIQNSLDLFFKEELEYN	Disordered
USP29's non-canonical C-t PIP box ₈₄₆₋₈₅₈	YDFQKQAWFTYND	Non disordered
USP29's disordered non-canonical PIP box ₇₃₈₋₇₄₉ (short sequence)	YGIIESIIDEFLQQ	Disordered
USP29's disordered non-canonical PIP box ₇₃₂₋₇₅₆ (long sequence)	YEQLQQCIIESIIDEFLQQAPPGVR	Disordered
p125's PIP box ₉₉₆₋₁₀₁₀	YRRGTGKVGGLLAFKRR	Non disordered

2.4 Structural biology and biophysics

2.4.1 Isothermal titration calorimetry (ITC)

ITC is a quantitative biophysical technique used to determine the thermodynamic parameters of molecular interactions in solution by measuring the energy of the binding reaction (Pierce et al., 1999). The ITC is based on an adiabatic process, in which the released or absorbed heat of the reaction is balanced by a thermic core to keep the reference and the sample cells at the same temperature. The increase (endothermic reaction) or decrease (exothermic reaction) in the applied energy by the thermic core after each injection of the ligand is plotted in a thermogram against the molar ratio between the ligand and the protein. The profile of the curve is determined by the c-value, which is calculated using the equation: $c = n \cdot K_d \cdot M$, where n is the stoichiometry of the

binding, K_d is the dissociation constant and M is the concentration of the protein. The stoichiometry of the reaction, the dissociation constant as well as the enthalpy (ΔH) and the entropy changes (ΔS) can be directly determined from the thermogram. The molar ratio at the middle of the thermogram indicates the stoichiometry of the reaction while the curve fitting to a binding model provides the K_d . The amount of released energy allows calculating the enthalpy and entropy variations. From these initial measurements it is possible to calculate the change in the Gibbs free energy (ΔG) using the relationship $\Delta G = \Delta H - T\Delta S$.

A Microcal PEAQ-ITC (Malvern) calorimetry system was used to analyse the binding of the p125 peptide to PCNA. PCNA was placed in the cell and the p125 peptide in the syringe, both in PBS at pH 7.0. The experiments were performed at 25 °C. The binding isotherms were analysed by non-linear least-squares fitting of the experimental data to a model assuming a single set of equivalent sites, using the Malvern software.

2.4.2 Nuclear magnetic resonance (NMR) spectroscopy

NMR is an analytical technique used for determining the structure and dynamics of molecules. NMR is based on the principle that many nuclei have a quantum mechanical property known as spin. The most common nuclei analysed in proteins by NMR are ^1H , ^{13}C and ^{15}N because of their favourable magnetic properties (spin quantum number $I=1/2$) and their ubiquity in the polypeptide chain. In a simple NMR experiment, an external magnetic field is applied to the sample, and then an energy transfer is possible between the low-energy state and the high-energy state of the nuclear spin. The energy transfer takes place at a wavelength that corresponds to radiofrequencies and when the spin returns to its ground level, energy is emitted at the same frequency. The frequency that matches this transfer (resonant frequency) is measured and processed in order to yield the NMR spectrum. The precise resonant frequency of the nuclei within a molecule depends on the local chemical environment (chemical shift, δ). It is customary to adopt tetramethylsilane (TMS) as the chemical shift reference. In this way, the chemical shift is independent of the magnetic field and is expressed as ppm (parts per million of the field). Since TMS is not soluble in water, similar

compounds are used instead, such as DSS (sodium trimethylsilylpropanesulfonate).

In protein NMR, the frequency of the nuclei will depend on the type of the amino acid and also on its particular chemical environment, which is modulated by the secondary, tertiary, and quaternary structure of the protein, as well as the binding of ligands and by the solvent conditions, namely, pH, salt and temperature.

The ^1H - ^{15}N -HSQC (Heteronuclear Single Quantum Coherence) spectrum of a protein shows all ^1H - ^{15}N correlations. These are mainly in the backbone amide groups, but also in the side chains of arginines, tryptophanes, histidines, glutamines, asparagines and lysines. The spectrum is rather like a fingerprint of a protein and it is a very useful tool for protein-ligand binding studies, particularly to map the region of interaction and measuring the affinity. Heteronuclear ^1H - ^{15}N correlations can be also measured in the Transverse Relaxation Optimized Spectroscopy (TROSY) mode, which provides increased resolution at the expense of some sensitivity loss. With this strategy the signal that relax most slowly is selected, facilitating the observation of the NMR spectrum. TROSY is especially advantageous for slowly tumbling large deuterated proteins, but it may also be helpful with small non-deuterated proteins.

^1H - ^{15}N TROSY spectra of perdeuterated PCNA were recorded at 35 °C on a Bruker Advance III 800 MHz (18.8 T) spectrometer equipped with a cryogenically cooled triple resonance z-gradient probe. A 400 μL sample of 50 μM U- $[\text{}^2\text{H}, \text{}^{13}\text{C}, \text{}^{15}\text{N}]$ PCNA in PBS, pH 7.0, 0.01 % NaN_3 , 20 μM DSS, and 5% D_2O was placed in a 5 mm Shigemi NMR tube (without plunger) and defined volumes of the USP29's non-canonical PIP box peptides (USP29⁷³²⁻⁷⁵⁶ and USP29⁷³⁸⁻⁷⁴⁹) or increasing volumes of the p125's PIP box peptide stock solutions at 11.25 mM, 3.6 mM and 3.9 mM, respectively, were added and mixed (by capping and inverting several times the NMR tube). In the case of USP29⁷³²⁻⁷⁵⁶ and USP29⁷³⁸⁻⁷⁴⁹ peptides a 30-fold excess was directly added with respect to PCNA. The peptide solutions were prepared in the same buffer as the PCNA samples (except that no NaN_3 , DSS or D_2O was added). For that purpose, and to remove unwanted salts from the synthetic peptides, the lyophilized powders were

dissolved in PBS pH 7.0 and passed through a PD-10 Minitrap G25 column. BEST (Band selective excitation short transient) ^1H - ^{15}N -TROSY spectra were measured with 256 indirect points for a total duration of 21.5 h. The NMR titration of PCNA with the canonical PIP box peptides (USP29⁴⁵⁴⁻⁴⁸⁵ and USP29⁴⁶⁷⁻⁴⁸⁴) were done in the same conditions as the previous peptides except that the peptides stock solutions were 3 mM and 3.76 mM respectively, and that the intermediate titration points were monitored with ^1H - ^{15}N HMQC spectra using 124 indirect points and a total duration of 10.6 h. In the case of the C-terminal non-canonical PIP box peptide (USP29⁸⁴⁶⁻⁸⁵⁸), only a 3.1-fold excess of the peptide could be added with respect to ^2H - ^{15}N -labeled PCNA, since the peptide was of limited solubility (0.32 mM) at pH 7.0 and no titration was performed.

The titrations allowed for an extensive transfer of NMR signal assignment from free PCNA to peptide-bound PCNA spectra. The Chemical Shift Perturbations (CSP) in the NMR signals of PCNA caused by peptide binding were computed as the weighted average distance between the backbone amide ^1H and ^{15}N chemical shifts in the free and bound states, with an error of ± 0.005 ppm (estimated from the spectral resolution in both dimensions). The analysis of the CSPs (for those residues with CSP larger than the average plus one standard deviation) was performed by fitting of the values to a single-site binding model using Prism (GraphPad software). In the case of the canonical PIP-box peptides of USP29 the reported K_d is the one derived from residue G127, with the fitting error as an estimate of its uncertainty, while in the case of the p125 peptide the reported K_d is the average over all selected residues, with the standard deviation as an estimate of its uncertainty.

The equation used to calculate CSP from the ^1H and ^{15}N shifts is:

$$CSP = \sqrt{\frac{1}{2}(\Delta\delta_H^2 + \frac{\Delta\delta_N^2}{5})}$$

The equation to calculate the dissociation constant from the CSP values is (assuming a simple 1:1 binding stoichiometry):

$$CSP = K_d + [P] + x[P] - \sqrt{\frac{(K_d + [P] + x[P])^2 - (4x[P]^2)}{2[P]CSP_{max}}}$$

where K_d is the dissociation constant, $[P]$ is the total protein concentration (considered constant), x is the molar ratio ($[\text{ligand}]/[\text{protein}]$), CSP is the measured chemical shift perturbation, and CSP_{max} is the maximum CSP at saturation. The adjustable parameters are CSP_{max} and K_d .

Results

1. Characterization of the interaction between USP29 and PCNA

1.1 Validation of mass spectrometry data

Our lab's previous proteomics approach to explore the USP29 interactome revealed that PCNA was one of the top 10 interacting proteins of USP29. The interaction between ectopically expressed USP29 and endogenous PCNA was validated by colP experiments.

At the beginning of this PhD thesis we aimed at confirming the interaction by colP using recombinantly produced PCNA (no recombinant USP29 was available at that time). Ectopic USP29 was able to interact with recombinant PCNA (Figure R1), but only when the N-terminal His-tag had been removed as part of the protein purification process (no interaction was detected using His-PCNA).

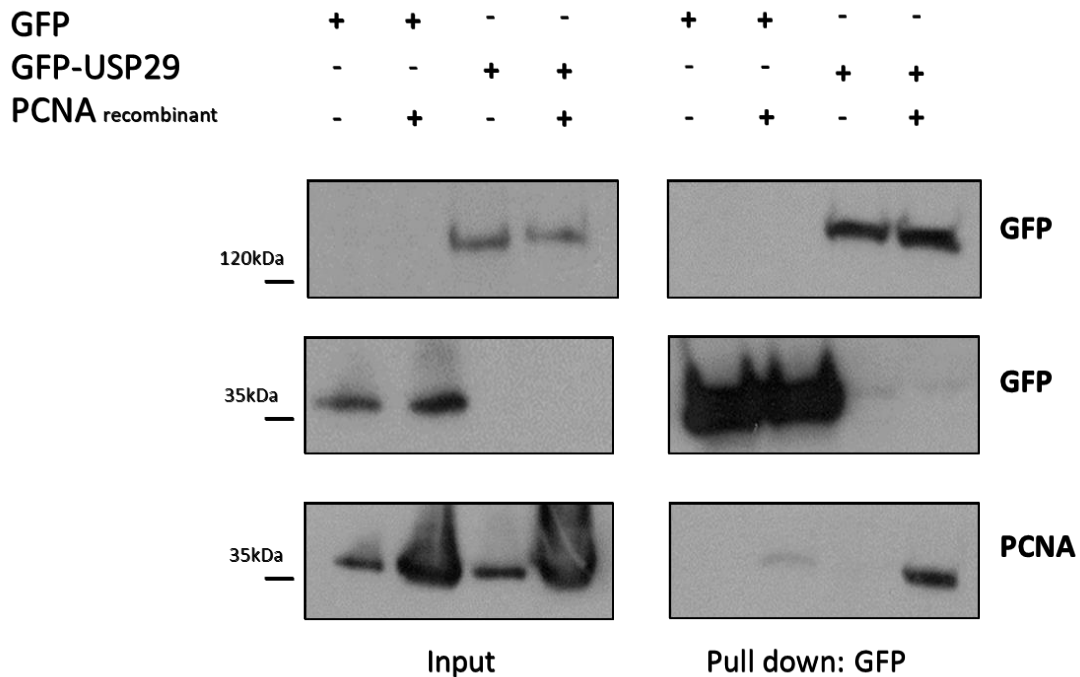


Figure R1: Recombinant PCNA interacts with USP29. HEK293 cells were transfected with GFP and GFP-USP29 and lysed 24h post-transcription. After addition of recombinant PCNA, GFP and GFP-fusion proteins were co-immunoprecipitated in native conditions with GFP-traps® and eluates (together with 2.5% of the total lysed extracts) were subjected to SDS-PAGE followed by WB against the indicated proteins.

1.2 *The role of USP29 as a DUB for PCNA*

The interaction led us to hypothesized a role for USP29 as a PCNA deubiquitinating enzyme, particularly for poly-Ubiquitinated PCNA (poly-Ub PCNA), which has been reported to occur in response to DNA damage (Edmunds et al., 2008; Motegi et al., 2006). Initial attempts to detect poly-ubiquitinated PCNA upon DNA damage induced by UV irradiation using conventional ubiquitination assays failed. We next adapted the protocol described by Vujanovic and colleagues (Vujanovic et al., 2017), which uses a highly specific antibody recognizing Ub K164-PCNA and cell fractionation to enrich poly-Ub PCNA into the chromatin-associated nuclear fraction (N) (Figure R2A). Using this experimental set-up, we demonstrated that the ectopic expression of USP29 decreased the levels of PCNA poly-Ub upon UV irradiation (Figure R2B). In contrast, PCNA poly-Ub did not change upon the expression of the catalytically inactive mutant USP29^{C294S} (Figure R2B).

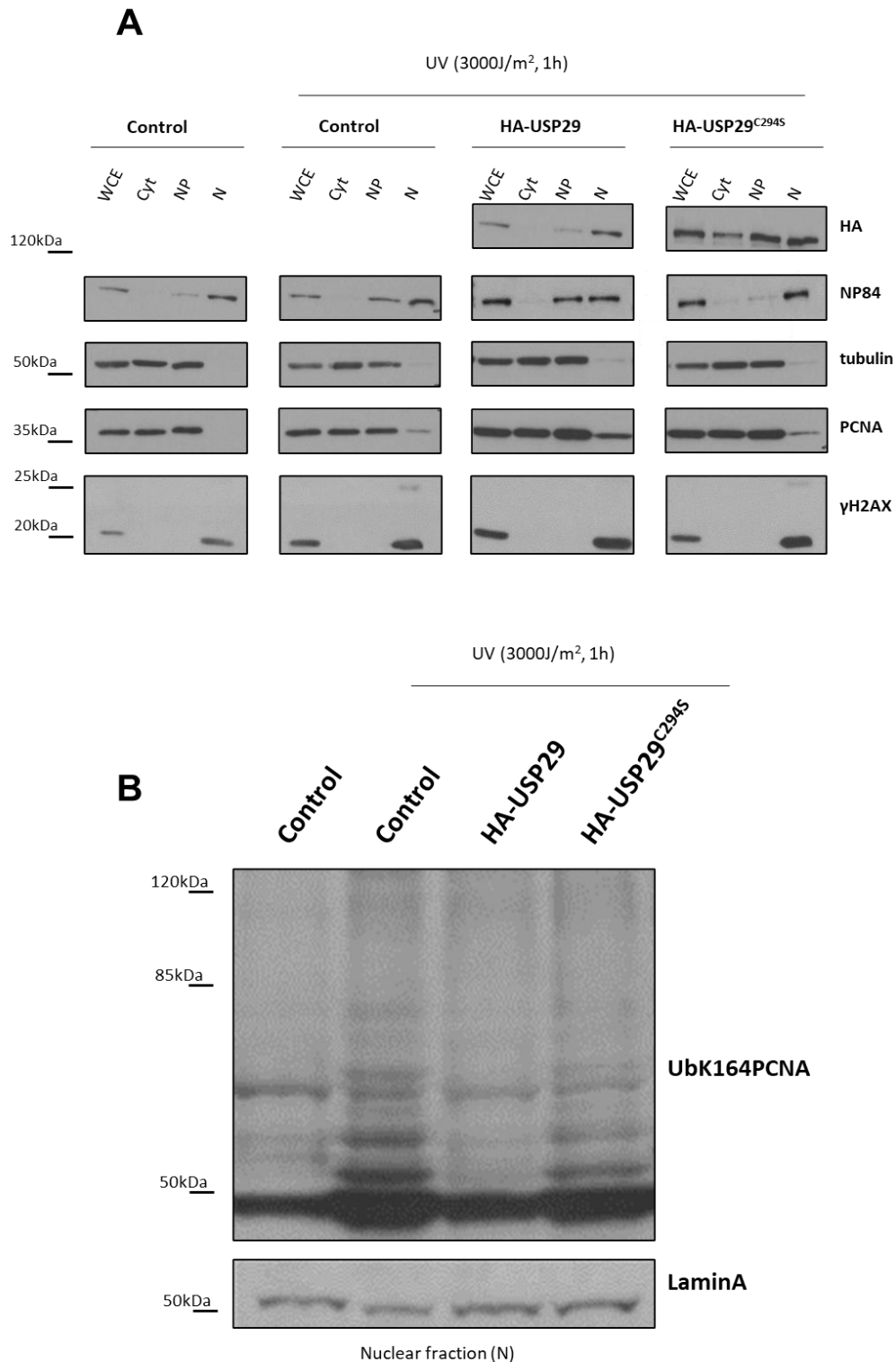


Figure R2: USP29 decreases PCNA poly-Ubiquitination upon DNA damage. (A) HEK293 cells were transfected with empty vector, HA-USP29 or HA-USP29^{C294S}, non-treated or treated with UV irradiation (3000 J/m²) and then subjected to a fractionation protocol (WCE: Whole Cell Extract; Cyt: Cytoplasm; NP: Nucleoplasm; N: Nucleus). Each fraction was loaded onto an SDS-PAGE and analysed by immuno-blotting using the indicated antibodies: NP84 as control for the nuclear fraction; tubulin as control for the cytoplasm fraction and γH2AX as control of the UV irradiation. **(B)** The chromatin-associated nuclear fractions (N) were analysed using anti-UbK164PCNA. Lamin A was used as loading control.

To corroborate the role of USP29 as a DUB for poly-Ub PCNA, an additional fractionation assay was performed using a complementary strategy. This time, the HEK293 cells were silenced for USP29 48 hours before UV irradiation. However, we did not detect a reproducible and consistent increase in poly-Ub PCNA upon silencing of USP29 (Figure R3C).

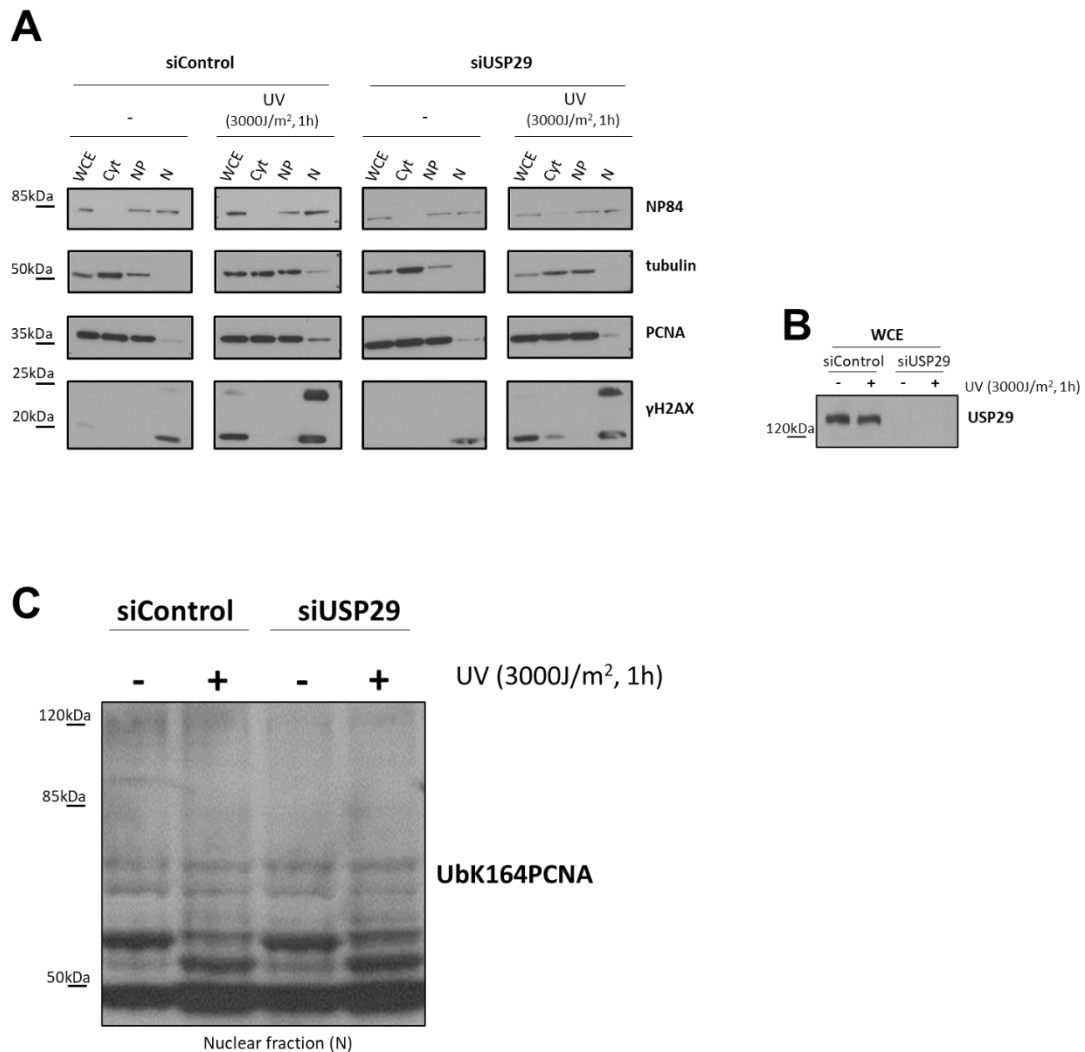


Figure R3: The silencing of USP29 does not increase PCNA poly-Ubiquitination upon DNA damage. (A) HEK293 cells were transfected with siControl or siUSP29 and non-treated or treated with UV irradiation (3000 J/m²) and then subjected to a fractionation protocol. Each fraction was loaded onto an SDS-PAGE and analysed using the indicated antibodies. (B) USP29 silencing efficacy was analysed through the detection of exogenous HA-USP29 by immuno-blotting using anti-HA. (C) Upon cell fractionation, the chromatin-associated nuclear fractions (N) were analysed by immuno-blotting using anti-UbK164PCNA.

To boost PCNA poly-Ubiquitination levels, and since PCNA poly-Ubiquitination mainly occurs upon replication stress during the S phase of the cell cycle (Leung et al., 2019), HEK 293 cells were synchronized at this phase by a double blockage with thymidine prior to UV irradiation (Figure R4B). Thymidine is an inhibitor of the DNA synthesis (Schvartzman, 1984) and this is a very efficient method to synchronize multiple cell lines (Thomas & Lingwood, 1975; Whitfield et al., 2002). Cells were treated twice with 2 mM thymidine for 16 hours before UV irradiation. Although thymidine doubled the percentage of cells in S phase (Figure R4A), no differences in poly-Ub PCNA were found between asynchronized or synchronized cells (Figure R4).

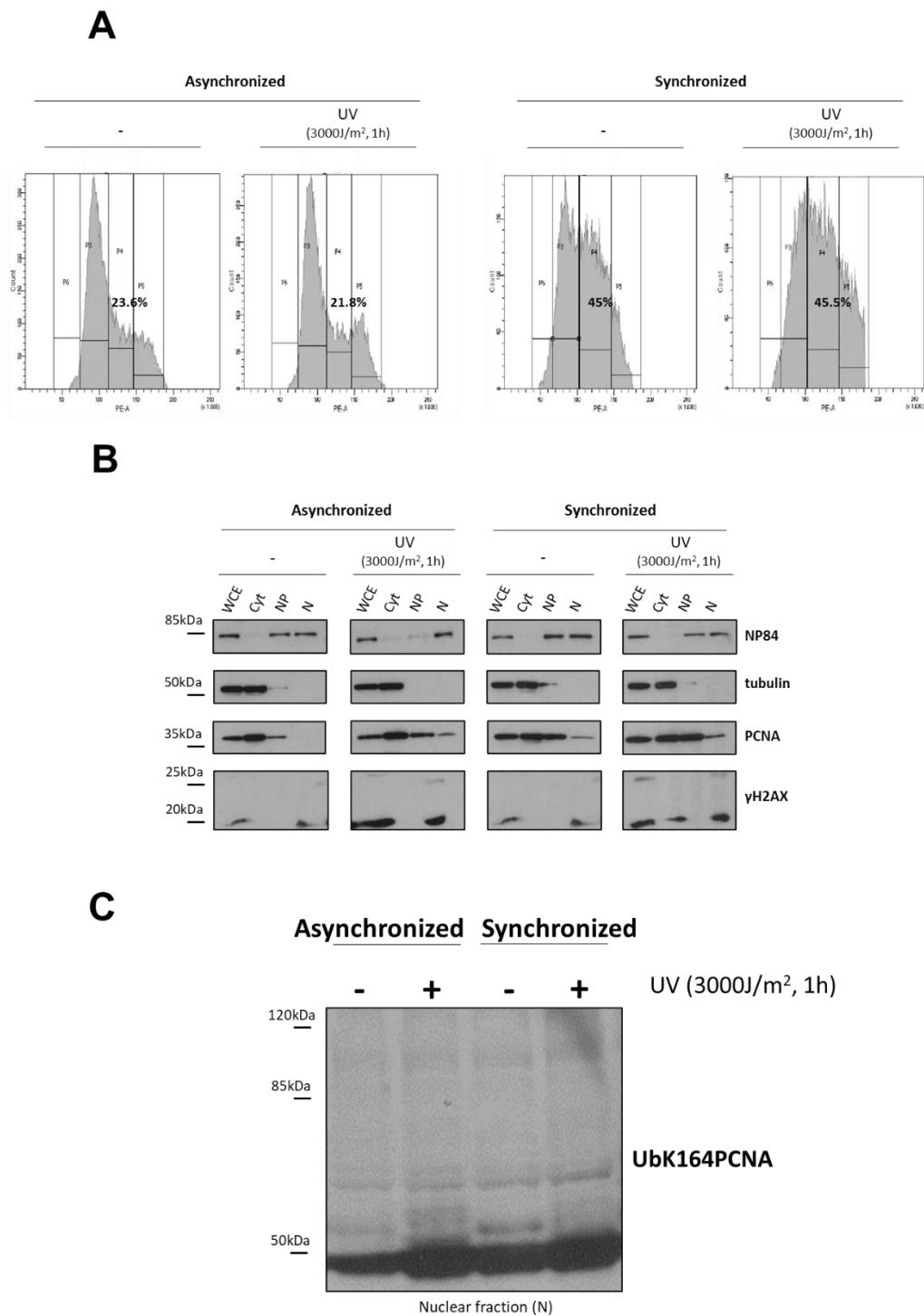


Figure R4: The synchronization of cells at S phase does not increase PCNA poly-Ubiquitination upon DNA damage. (A) HEK293 cells were non-treated and treated with UV irradiation (3000 J/m²) and then subjected to a fractionation protocol. Each fraction was loaded onto an SDS-PAGE and analysed using the indicated antibodies. **(B)** FACS analysis of the control and synchronized cells at S phase without and with UV irradiation (3000 J/m²). The numbers show the percentage of the cells at S phase. **(C)** Upon cell fractionation, the chromatin-associated nuclear fractions (N) were analysed by immuno-blotting using anti-UbK164PCNA.

1.3 USP29's PIP box sequences and interactions with PCNA

Three potential PIP-box sequences (Figure R5 and Figure R6) were detected within the USP29 sequence. Therefore, different synthetic peptides corresponding to the three potential PIP-boxes were designed in order to analyse their possible binding to PCNA by solution NMR, which is a sensitive technique to detect even weak binding and to map the binding site on PCNA. For this purpose we took advantage of the availability of the PCNA resonance assignments (Sánchez et al., 2007).

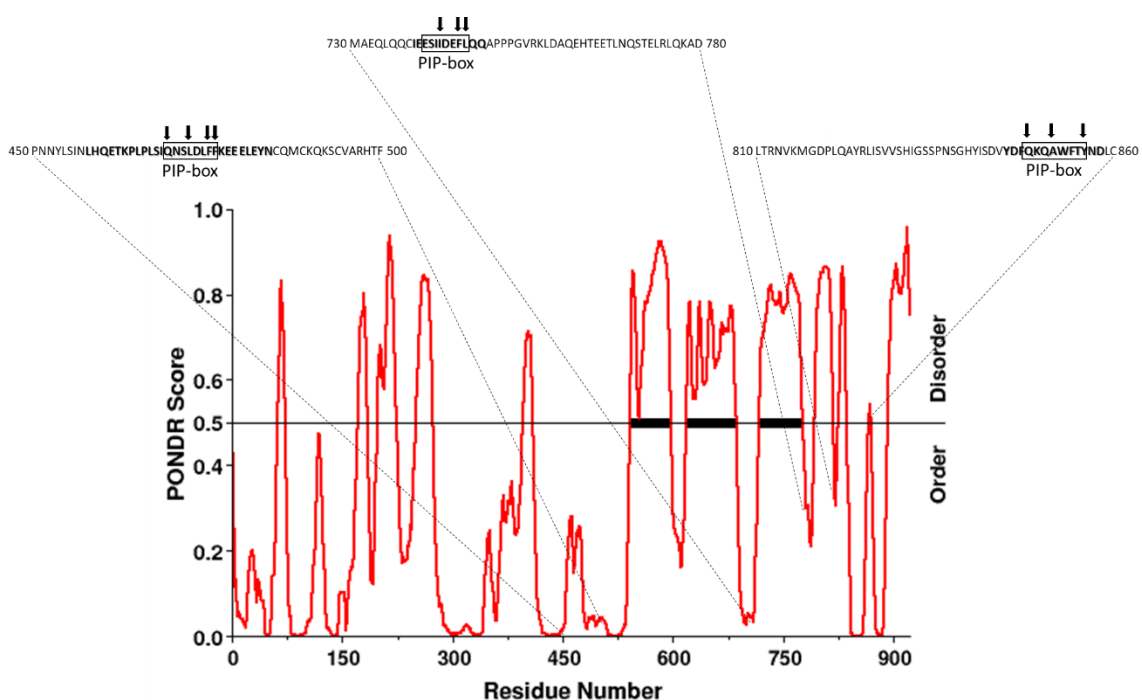


Figure R5: Prediction of structural disorder along the USP29 sequence. The red line shows the disorder prediction profile by the PONDR server (Predictor Of Naturally Disordered Regions (<http://www.pondr.com>), and the black line the threshold line at 0.5. Residues encompassing the peptides used for the biophysical characterization with PCNA are indicated in bold characters, those belonging to canonical or divergent PCNA interacting motifs are boxed. The consensus residues in the PIP motifs are indicated by arrows.

Figure R5 shows a prediction of the structural disorder of the USP29 protein. This is relevant because PCNA binding motifs are frequently found in intrinsically disordered protein regions (Prestel et al., 2019a). In Figure R6 the five peptides used to study the PCNA-UPS29 interaction are described.

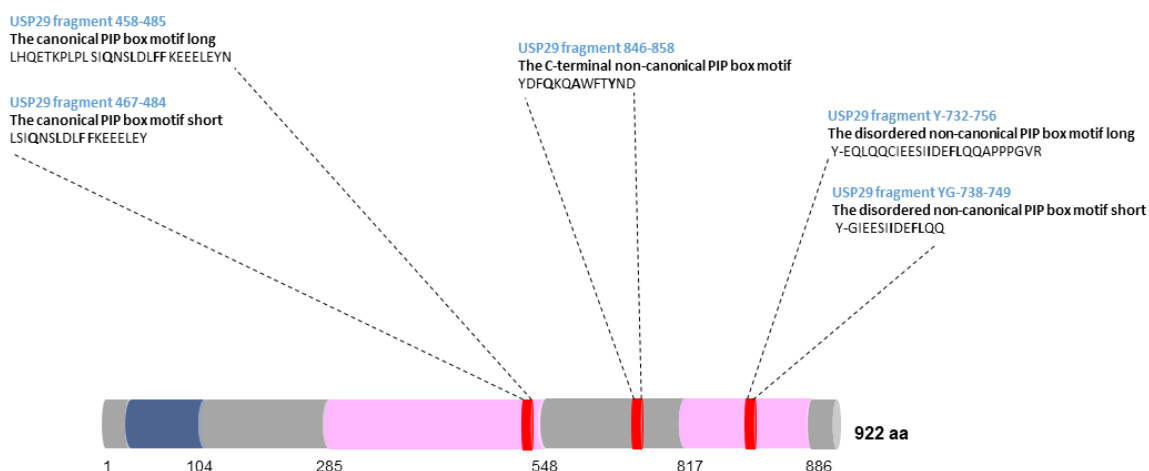


Figure R6: Scheme with the location along the USP29 sequence corresponding to the potential PIP box peptides of USP29 used in this thesis project.

1.3.1 USP29's canonical PIP box motif

The first USP29's potential PIP box which was analysed was the canonical one. Two peptides of different length around the canonical PIP-box sequence were designed: a 17 residue long (fragment USP29⁴⁶⁷⁻⁴⁸⁴), and a longer 27 residue long peptide (fragment USP29⁴⁵⁴⁻⁴⁸⁵) which included residues at the N- and C- terminal ends that might also interact with PCNA.

The interaction of PCNA with both peptides was characterized by solution NMR. Uniformly, ²H-¹³C, ¹⁵N-labeled PCNA was titrated with unlabelled USP29 peptides and chemical shift perturbations of PCNA backbone amide signals were analysed (Figure R7A and Figure R8A). A few new sharp signals in the central region of the spectra come from the excess peptide (natural abundance ¹⁵N NMR signals). Some perturbed residues were observed whose signals gradually shifted along the titration, implying a fast exchange regime on the NMR time scale (Figure R7B and Figure R8B), but the changes were very small, indicating a weak binding. The dissociation constant calculated from the signal of residue G127, one of the residues with chemical shift perturbation (CSP) larger than the average plus one standard deviation, was of 2.8 ± 0.1 mM at 35 °C for the short peptide (Figure R7C) and of 3 ± 1 mM at 35 °C for the long peptide (Figure R8C). The plot of the CSPs versus the PCNA residues (Figure R7D and Figure R8D)

showed a similar pattern as for p21 binding (De Biasio et al., 2012), suggesting a similar mode of binding. Mapping the perturbed residues on the three-dimensional structure of PCNA (Figure R7E and Figure R8E), show a cluster in the pocket where the short helix of p21 binds PCNA, indicating that USP29's canonical PIP box also binds to this pocket.

Interestingly, the binding between the short peptide and PCNA is better defined than the one with the long peptide. This result could be due to favourable electrostatic interactions between PCNA and the free chain ends of the short peptide.

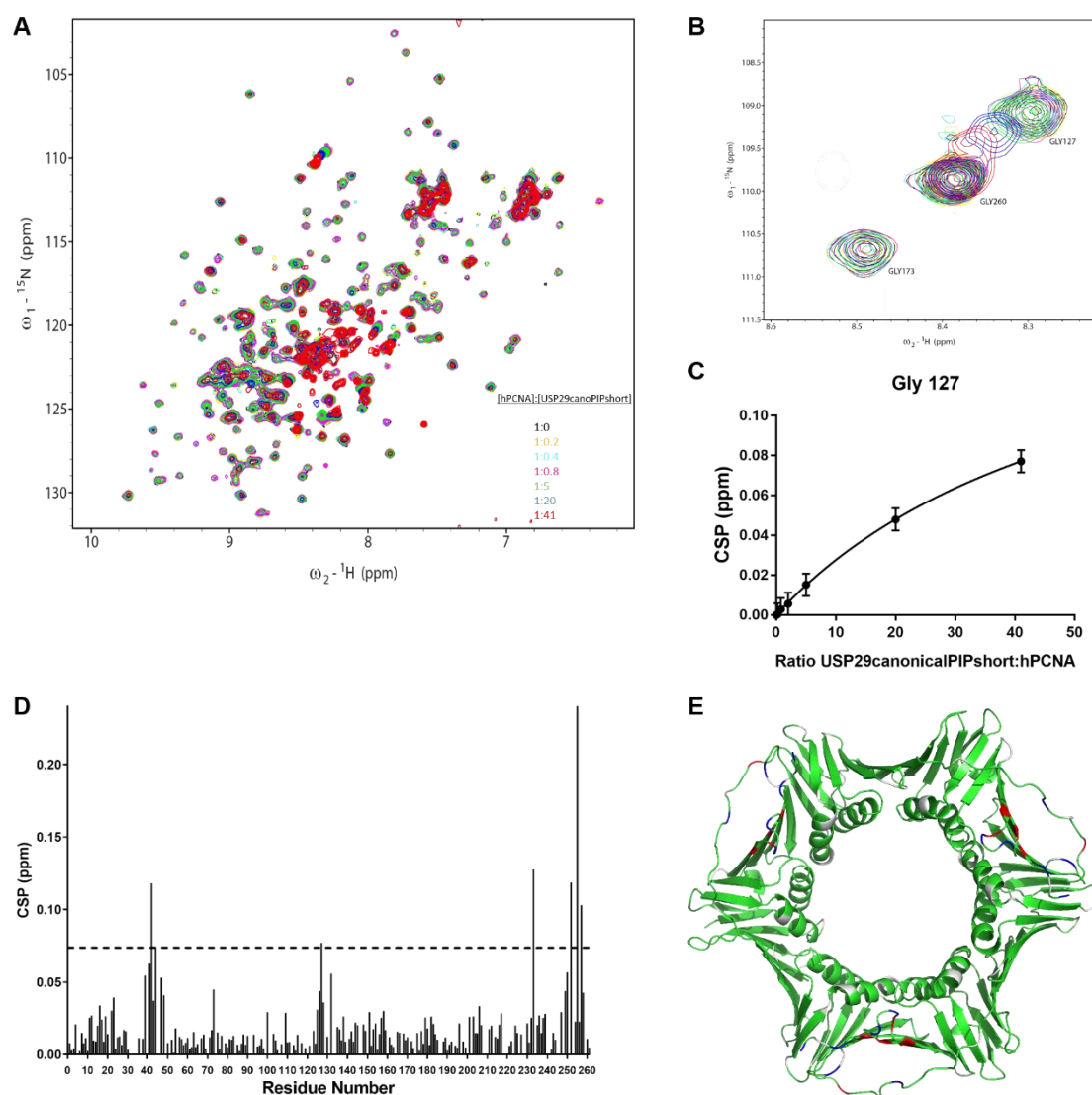


Figure R7: NMR analysis of the PCNA interaction with the short peptide comprising the USP29 canonical PIP box. (A) Superposition of ^1H - ^{15}N HMQC spectra of 50 μM PCNA in the absence (black) and increasing amounts (different colours) of USP29⁴⁶⁷⁻⁴⁸⁴ PIP box peptide. Spectra were acquired at 35°C in PBS pH 7.0. (B) Region of the NMR spectra of PCNA in the presence of increasing amounts of USP29 canonical PIP short peptide (from black to red) showing the shift of G127 signal. (C) Chemical shift perturbation of the amide signal of residue G127 at different peptide:PCNA ratios. The symbols correspond to the experimental data, the bars correspond to the experimental error and the continuous line to the best fit to a model of one set of identical binding sites. (D) Chemical shift perturbations (CSP) of PCNA backbone amide ^1H and ^{15}N NMR resonances induced by USP29⁴⁶⁷⁻⁴⁸⁴. The dashed line indicates the average plus two standard deviations. (E) Mapping of the peptide binding on the three-dimensional structure of PCNA. Residues with CSP values higher than the average plus one standard deviation are marked in red and higher than the average plus two standard deviations in blue.

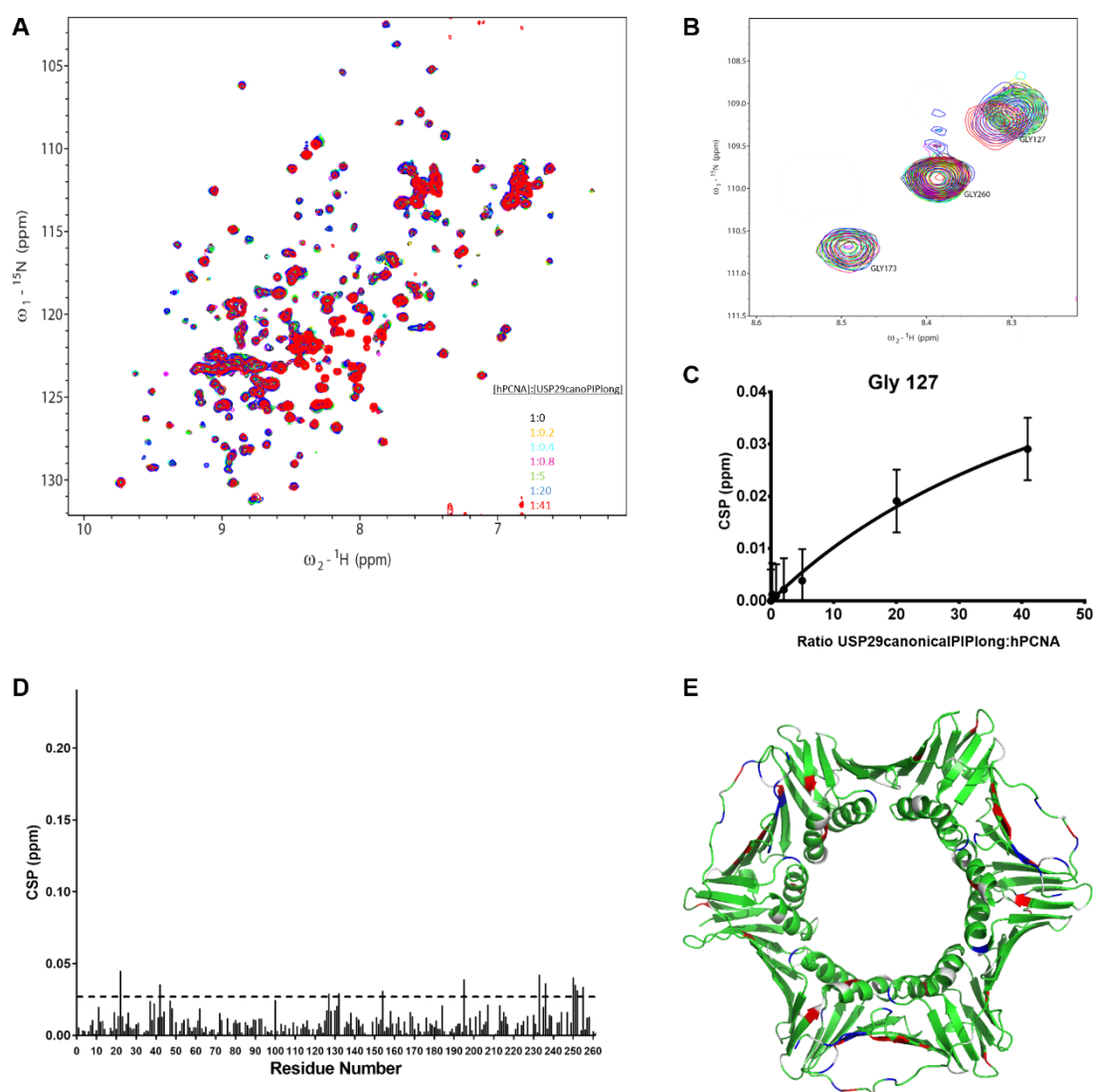


Figure R8: NMR analysis of PCNA interaction with the long peptide comprising the USP29 canonical PIP box. **(A)** Superposition of ${}^1\text{H}$ - ${}^{15}\text{N}$ HMQC spectra of $50\ \mu\text{M}$ PCNA in the absence (black) and increasing amounts (different colors) of USP29⁴⁵⁸⁻⁴⁸⁵ PIP box peptide. Spectra were acquired at 35°C in PBS pH 7.0. **(B)** Region of the NMR spectra of PCNA in the presence of increasing amounts of USP29 canonical PIP long peptide (from black to red) showing the titration of G127 signal. **(C)** Chemical shift perturbation of the amide signal of G127 residue at different USP29:PCNA ratios. The symbols correspond to the experimental data, the bars correspond to the measurement error and the continuous line to the best fit to a model of one set of identical binding sites. **(D)** Combined chemical shift perturbations (CSP) of PCNA backbone amide ${}^1\text{H}$ and ${}^{15}\text{N}$ NMR resonances induced by USP29⁴⁵⁸⁻⁴⁸⁵. The dashed line indicates the average plus two standard deviations. **(E)** Mapping of the peptide binding on the three-dimensional structure of PCNA. Residues with CSP values higher than the average plus one standard deviation are marked in red and higher than the average plus two standard deviations in blue.

Since the binding affinity between PCNA and the canonical PIP-box sequence of USP29 was very low the biological relevance of this PIP-box sequence was put into question. In order to verify whether this was the PCNA binding site, a new construct of USP29 was generated in which the PIP-box sequence was disrupted by mutation of the two phenylalanines into two alanines and a coIP assay was performed.

This USP29 mutant, expected to abolish the binding, was still able to interact with PCNA, as shown in Figure R9. These data suggest that the canonical USP29 PIP-box (⁴⁷⁰QNSLDLFF⁴⁷⁷) is not required for PCNA interaction.

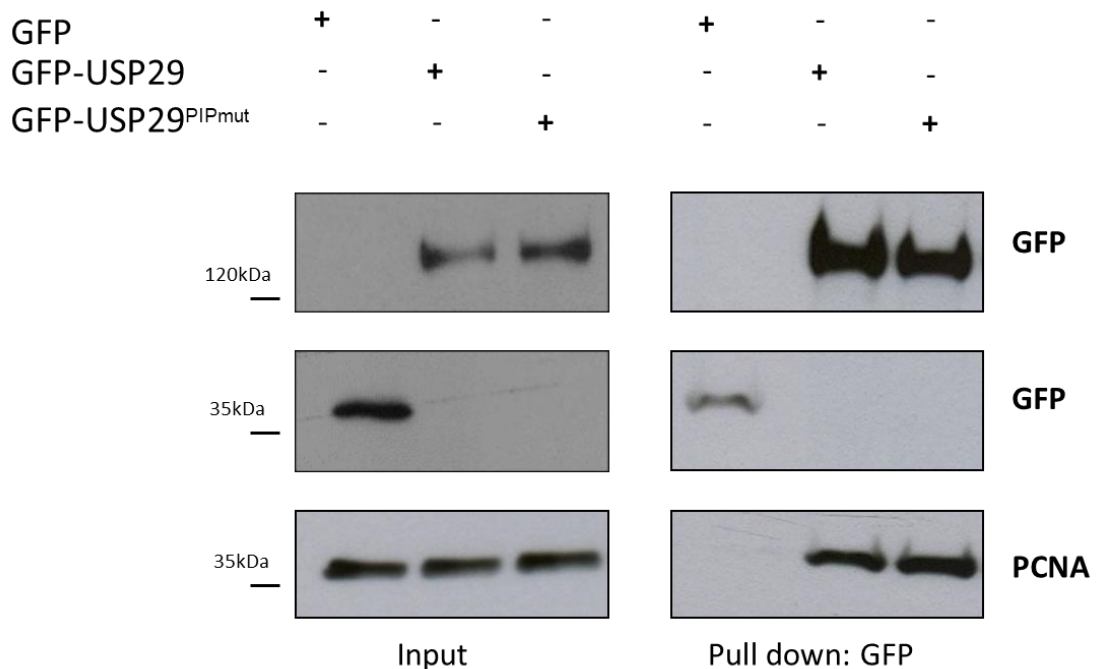


Figure R9: The canonical USP29 PIP-box (⁴⁷⁰QNSLDLFF⁴⁷⁷) does not mediate the interaction with PCNA. HEK293 cells were transfected with GFP, GFP-USP29 and GFP-USP29^{PIPmut} and lysed 24 h post-transfection. The interaction with endogenous PCNA was analysed by coIP. GFP and GFP-fusion proteins were co-immunoprecipitated in native conditions with GFP-traps® and eluates (together with 2.5% of the total lysed extracts) were subjected to SDS-PAGE followed by WB against the indicated proteins.

1.3.2 USP29's non-canonical PIP box motifs

Due to the low affinity of the canonical USP29's PIP box for PCNA, and considering that PIP-boxes do not always have a canonical sequence (Prestel et al., 2019b), a search was carried out to identify potential non-canonical PIP-box motifs within the USP29 sequence. Two different sequences were considered as possible candidates (Figure R6). The fragment USP29⁸⁴⁶⁻⁸⁵⁸ was selected to analyse the first non-canonical PIP-box, while to test the second non-canonical PIP-box two different peptides in length were designed (USP29⁷³²⁻⁷⁵⁶ and USP29⁷³⁸⁻⁷⁴⁹). These fragments were located at a predicted IDR of USP29 (Figure R5). The same type of experimental analysis as for the canonical PIP-box peptides was performed with these two potential non-canonical PIP-box sequences.

Unlabelled non-canonical USP29 peptides were added in excess to uniformly ²H-¹³C, ¹⁵N-labeled PCNA and chemical shift perturbations of PCNA backbone amide signals were analysed (Figure R10A, Figure R11A and Figure R12A). The G127 residue, located in the IDCL which is a typical area where the PIP-boxes bind (Freudenthal et al., 2009), did not shift, or shifted very little, upon the addition of the excess of the non-canonical PIP-box peptides (Figure R10B, Figure R11B and Figure R12B) indicating no binding. The plot of CSPs versus the PCNA residues (Figure R10C, Figure R11C and Figure R12C) does not result in a clear pattern as for the canonical PIP peptides, and the slightly perturbed residues do not cluster on a defined region on PCNA (Figure R10D, Figure R11D and Figure R12D), consistent with no specific binding.

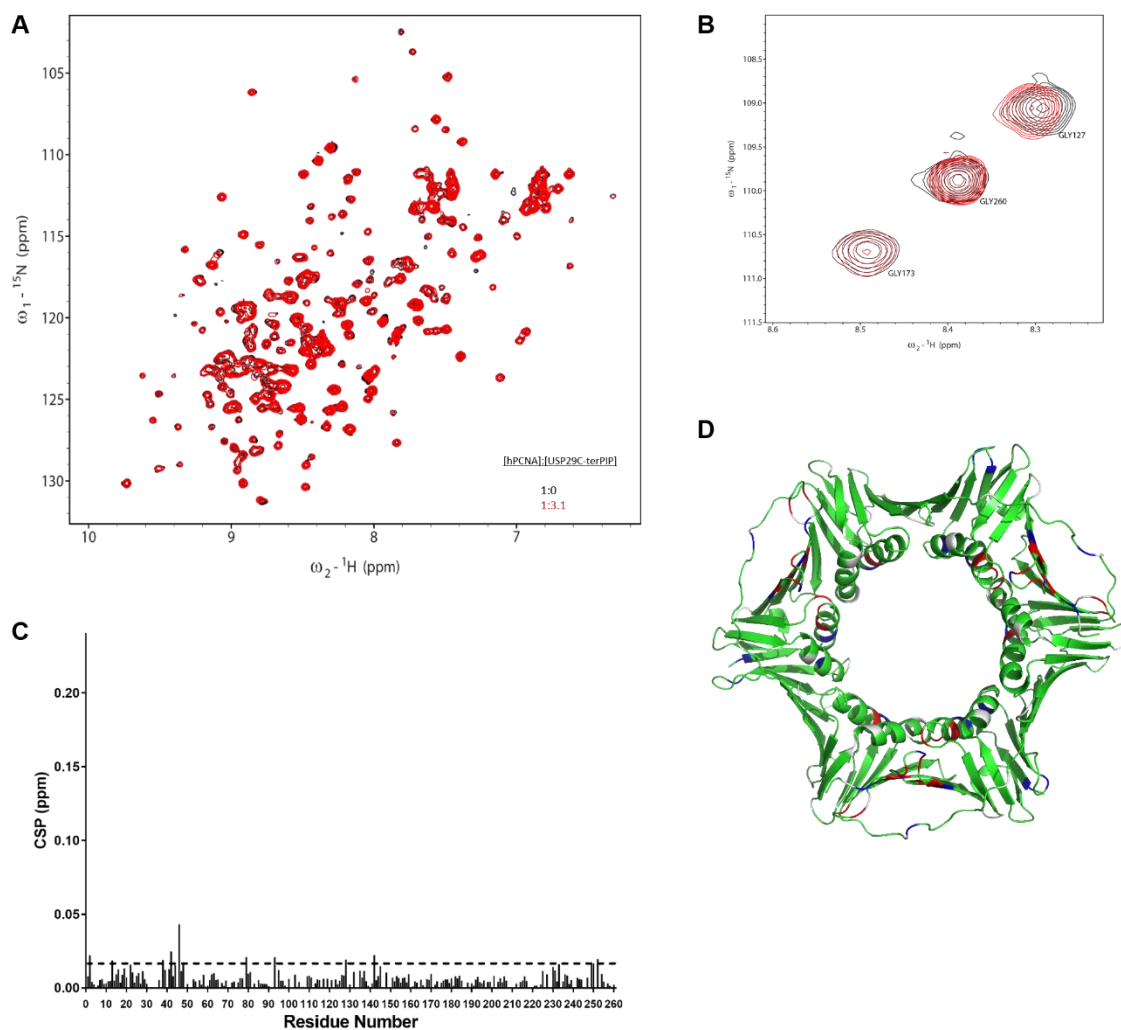


Figure R10: NMR analysis of the USP29 C-terminal non-canonical PIP box peptide (USP29⁸⁴⁶⁻⁸⁵⁸) interaction with PCNA. (A) Superposition of ¹H-¹⁵N HMQC spectra of 50 μM PCNA in the absence (black) and 3.1-fold excess (red) of USP29⁸⁴⁶⁻⁸⁵⁸ PIP box peptide. Spectra were acquired at 35 °C in PBS pH 7.0. **(B)** Region of the NMR spectra displayed in A showing the small shift in the G127 signal. **(C)** Chemical shift perturbations (CSP) of PCNA backbone amide ¹H and ¹⁵N NMR resonances induced by USP29⁸⁴⁶⁻⁸⁵⁸. The dashed line indicates the average plus two standard deviations. **(D)** Mapping of the peptide binding on the three-dimensional structure of PCNA. Residues with CSP values higher than the average plus one standard deviation are marked in red and higher than the average plus two standard deviations in blue.

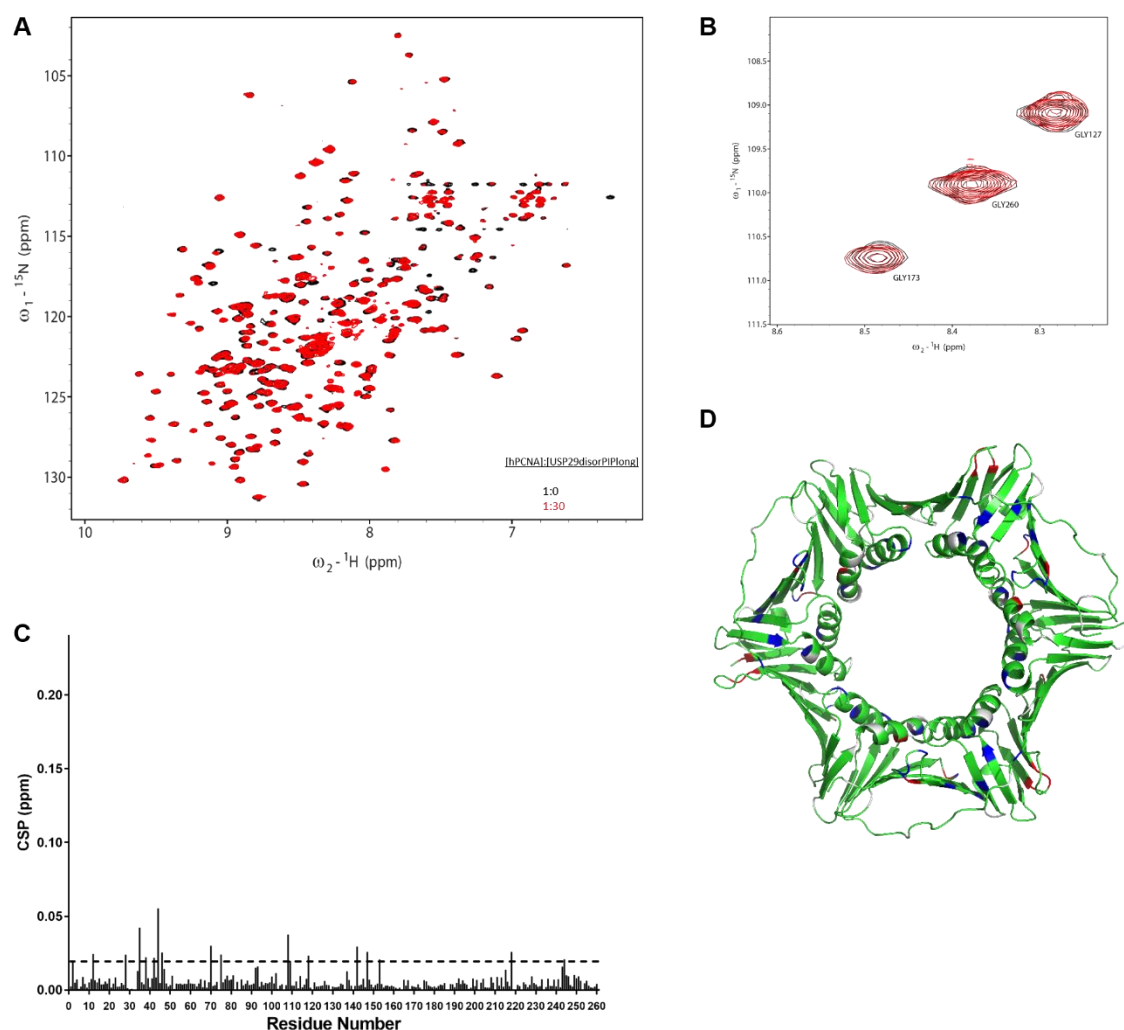


Figure R11: NMR analysis of the USP29 disordered non-canonical PIP box short peptide (USP29⁷³⁸⁻⁷⁴⁹) interaction with PCNA. (A) Superposition of ¹H-¹⁵N TROSY spectra of 50 μM PCNA in the absence (black) and 30-fold excess (red) of USP29⁷³⁸⁻⁷⁴⁹ PIP box peptide. Spectra were acquired at 35°C in PBS pH 7.0. **(B)** Region of the NMR spectra displayed in A showing the G127 signal. **(C)** Chemical shift perturbations (CSP) of PCNA backbone amide ¹H and ¹⁵N NMR resonances induced by USP29⁷³⁸⁻⁷⁴⁹. The dashed line indicates the average plus two standard deviations. **(D)** Mapping of the peptide binding on the three-dimensional structure of PCNA. Residues with CSP values higher than the average plus one standard deviation are marked in red and higher than the average plus two standard deviations in blue.

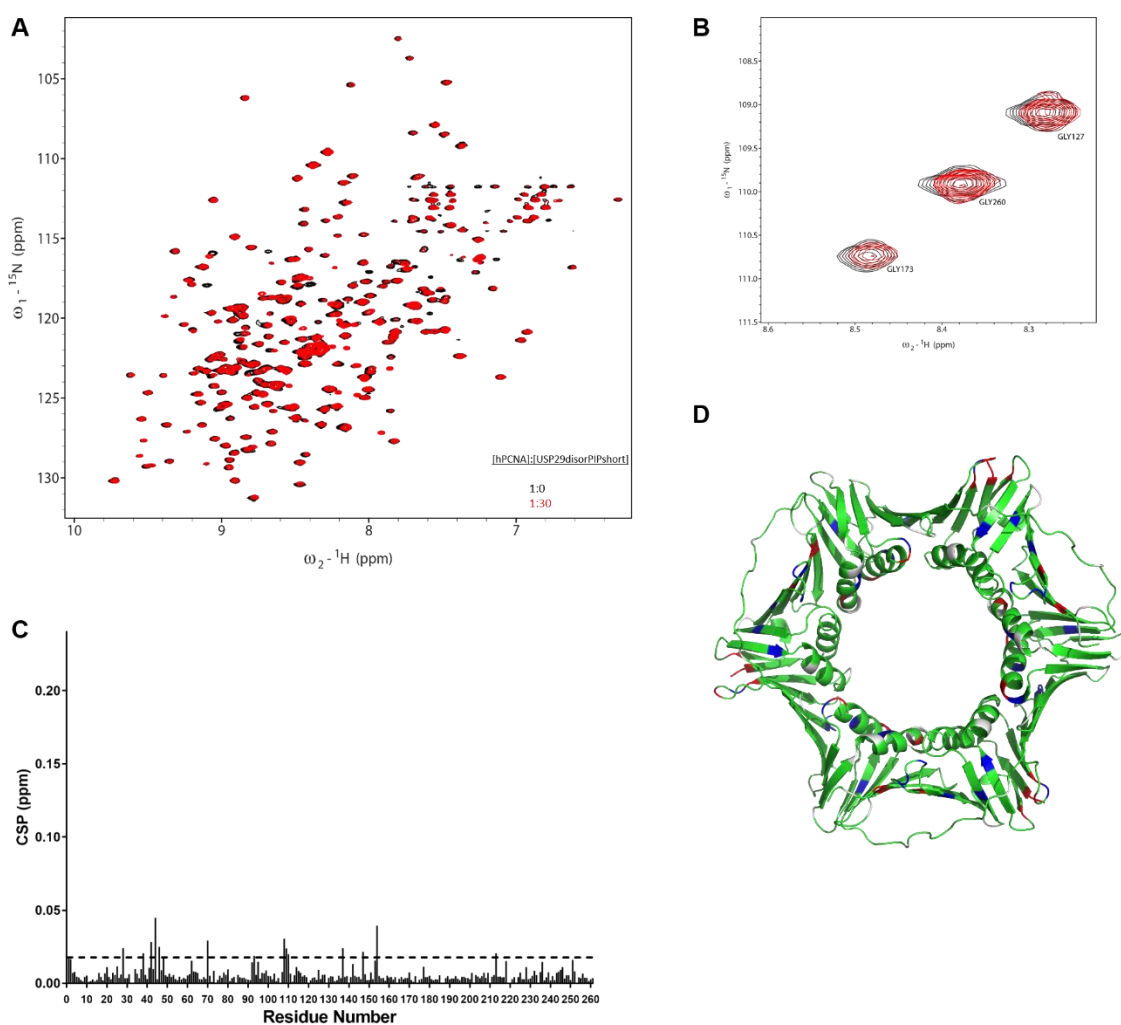


Figure R12: NMR analysis of the USP29 disordered non-canonical PIP box long peptide (USP29⁷³²⁻⁷⁵⁶) interaction with PCNA. (A) Superposition of ¹H-¹⁵N TROSY spectra of 50 μM PCNA in the absence (black) and 30-fold excess (red) of USP29⁷³²⁻⁷⁵⁶ PIP box peptide. Spectra were acquired at 35°C in PBS pH 7.0. **(B)** Region of the NMR spectra displayed in A showing the G127 signal. **(C)** Chemical shift perturbations (CSP) of PCNA backbone amide ¹H and ¹⁵N NMR resonances induced by USP29⁷³²⁻⁷⁵⁶. The dashed line indicates the average plus two standard deviations. **(D)** Mapping of the peptide binding on the three-dimensional structure of PCNA. Residues with CSP values higher than the average plus one standard deviation are marked in red and higher than the average plus two standard deviations in blue.

1.4 USP29PH mediates USP29 and PCNA interaction

Based on the prediction with DELTA-BLAST, USP29 contains a PH domain. This domain has been found in many kinases, isoforms of phospholipase C, GTPases and nucleotide-exchange factors (Musacchio et al., 1993). In general, the PH domain is related to proteins relevant in signal transduction and cytoskeletal function (Wang, Shaw, Winkelmann, & Shaw, 1994). Furthermore, the PH domain has been reported to play a role in protein-protein interactions (Drugan et al., 2000). In fact, a conserved cluster of hydrophobic residues on the surface of the PH domains could be a site for this kind of binding (Downing et al., 1994). Therefore, we hypothesized that the PH domain of USP29 was responsible for the binding of USP29 with PCNA.

To prove this hypothesis, two different truncated forms of USP29 were generated: one that comprised only the PH domain (USP29PH) and a second one without the PH domain (USP29 Δ PH) (Figure R13). Co-immunoprecipitation analysis with the truncated forms of USP29 (Figure R14A and Figure R14B) showed that USP29PH is necessary and sufficient to interact with endogenous or recombinant PCNA (Figure R14C).

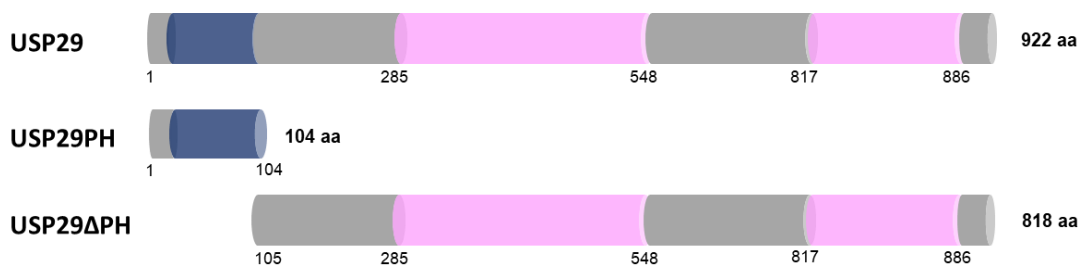


Figure R13: Scheme of the different constructs of USP29 used in this thesis to study the role of the PH domain in the interaction with PCNA.

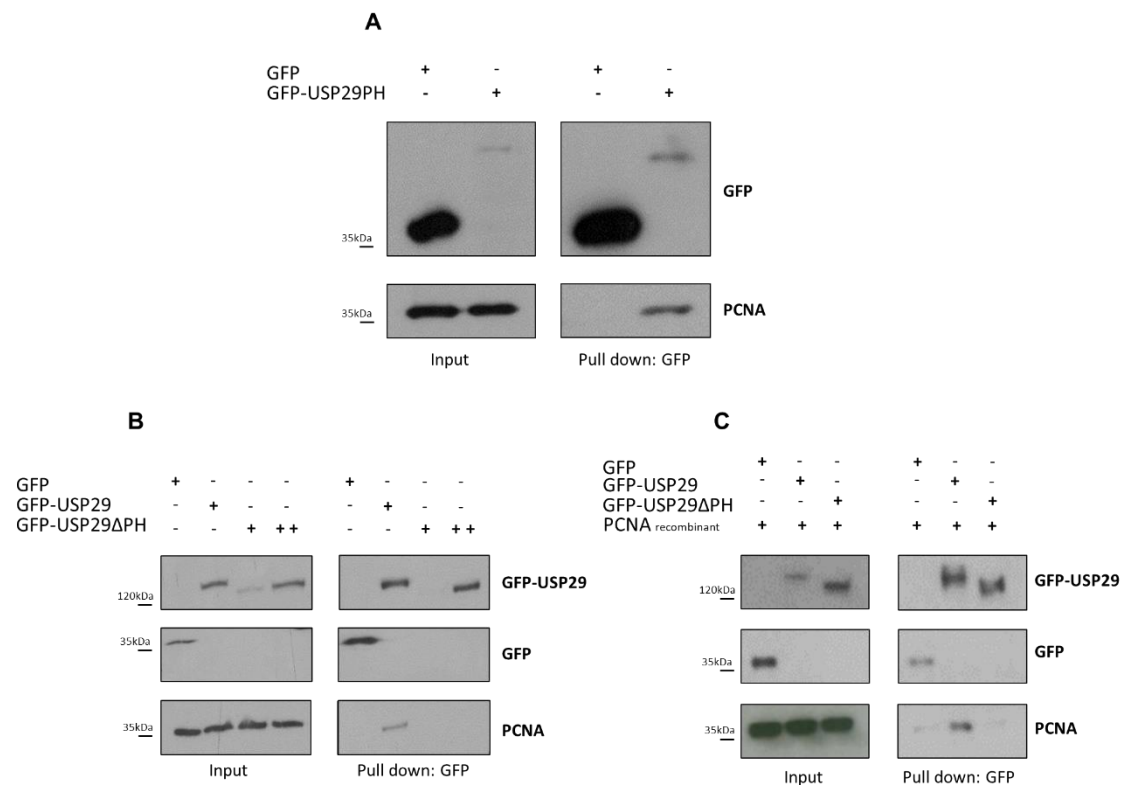


Figure R14: USP29 PH domain mediates USP29 interaction with PCNA. HEK293 cells were transfected with GFP, GFP-USP29PH, GFP-USP29 or GFP-USP29 Δ PH and lysed 24h post-transfection. The interaction with endogenous (A), (B) or recombinant (C) PCNA was analysed by coIP. GFP and GFP-fusion proteins were co-immunoprecipitated in native conditions with GFP-traps® and eluates (together with 2.5% of the total lysed extracts) were subjected to SDS-PAGE followed by WB against the indicated proteins.

2. USP29 regulation

2.1 USP29 dimer/oligomerization

Previous results from our group have shown that the catalytically inactive USP29^{C249S} is very unstable. Moreover, the ectopic expression of USP29 eliminates the poly-Ub chains and accumulates USP29^{C249S} stabilizing it. The fact that USP29 was able to remove poly-ubiquitin chains from USP29^{C249S} suggested that USP29 interacted with other USP29 molecules. *In cellulo* coIP (Figure R15) confirmed that USP29 dimerizes (and/or oligomerizes).

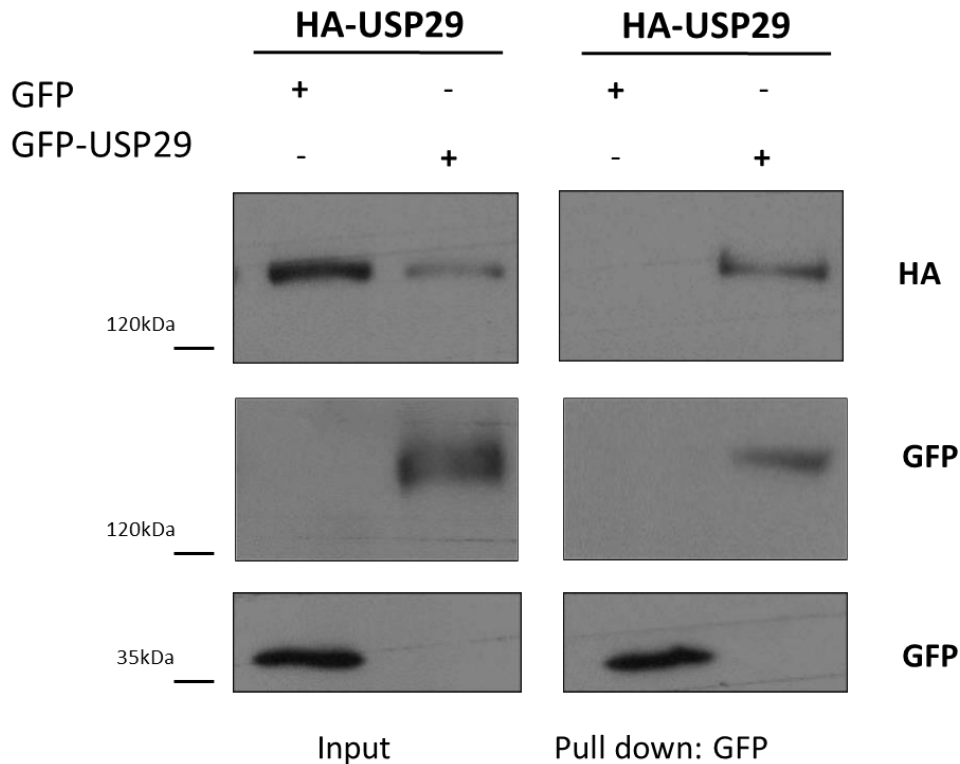


Figure R15: USP29 oligomerizes. HEK293 cells were co-transfected with HA-USP29 and GFP or GFP-USP29 and lysed 24 h post-transfection. The interaction between HA-USP29 and GFP-USP29 was analysed by coIP. GFP and GFP-fusion proteins were co-immunoprecipitated in native conditions with GFP-traps® and eluates (together with 2.5% of the total lysed extracts) were subjected to SDS-PAGE followed by WB against the indicated proteins.

Based on the fact that the PH domains have been identified, among other functions, as protein-protein interacting domains, the truncated USP29 constructs (Figure R13) were used to determine whether the dimer/oligomerization occurs via the PH domain. Pull down experiments show that USP29PH is sufficient (Figure R16A) and necessary (Figure R16B) for USP29 dimer/oligomerization.

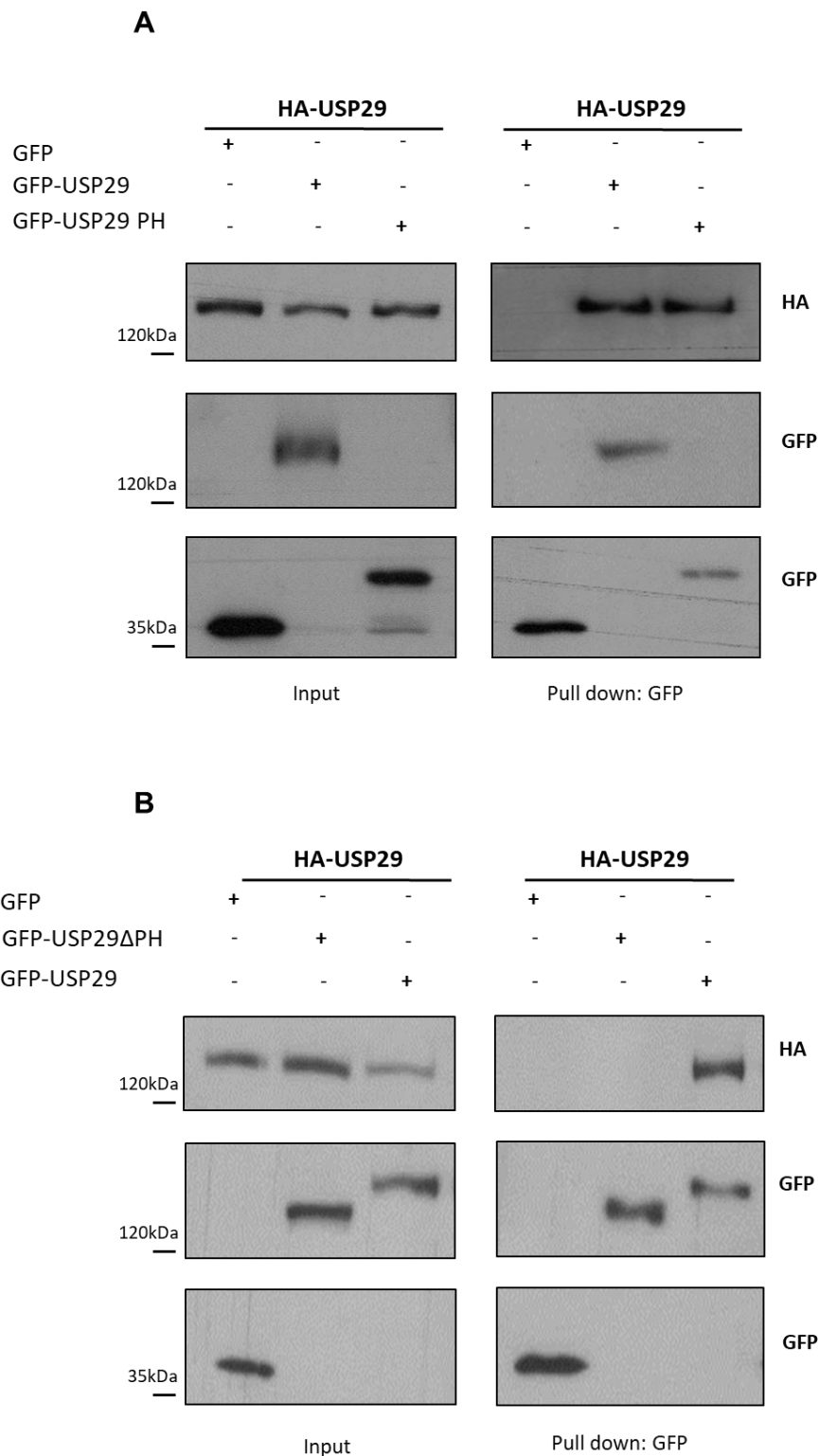


Figure R16: The PH domain of USP29 mediates USP29 dimer/oligomerization. HEK293 cells were co-transfected with HA-USP29 and GFP, GFP-USP29, GFP-USP29PH or GFP-USP29 Δ PH and lysed 24 h post-transfection. The interactions between HA-USP29 and GFP-USP29PH (A) or GFP-USP29 Δ PH (B) were analysed by coIP. GFP and GFP-fusion proteins were co-immunoprecipitated in native conditions with GFP-traps® and eluates (together with 2.5% of the total lysed extracts) were subjected to SDS-PAGE followed by WB against the indicated proteins.

2.2 Characterization of the potential PH dimerization interface by mutagenesis

While the 3D structure of USP29 is still unknown, the N-terminal PH domain of USP37, which is a close homologue to USP29, has been crystalized. This structure shows a symmetric dimer with the two protomers interacting through their main β -sheets. The sequence homology between the PH domains of USP29 and USP37 is 48%, suggesting that their structures are highly similar. A homology model of the PH domain of USP29 was built based on the crystal structure of the corresponding domain of USP37 (PDB 3u12) showing a cluster of hydrophobic residues within the dimer interface (Figure R17).

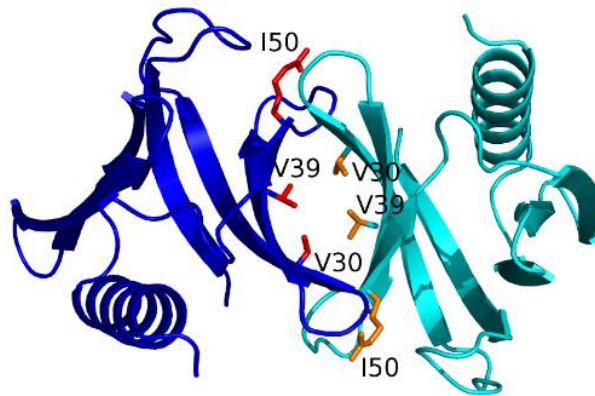


Figure R17: Modelization of USP29PH dimer. Model from SWISS-MODEL SERVER (Waterhouse et al., 2018) using the crystal structure of the PH domain of USP37 (PDB 3u12) as template. The potential residues that could mediate the interaction between the PH domains of USP29 are shown as sticks and labelled.

These hydrophobic residues (V30, V39 and I50) form part of the β -sheet structure and favour this type of secondary structure. We reasoned that mutation of these residues for Thr (another β -sheet favourable amino acid but of polar nature) should disrupt the hydrophobic core and the dimer but preserve the monomeric fold of the PH domain of USP29.

Our previous results showed that the expression of USP29 abolishes USP29^{C249S} poly-Ubiquitination and stabilizes this catalytically inactive mutant. Therefore, it was assumed that any mutation impairing the interaction between USP29 and USP29^{C249S} should avoid the accumulation of the catalytically inactive protein. In order to investigate this hypothesis, the three hydrophobic residues were mutated individually and the impact of those mutants on USP29^{C249S} was analysed (Figure R18A).

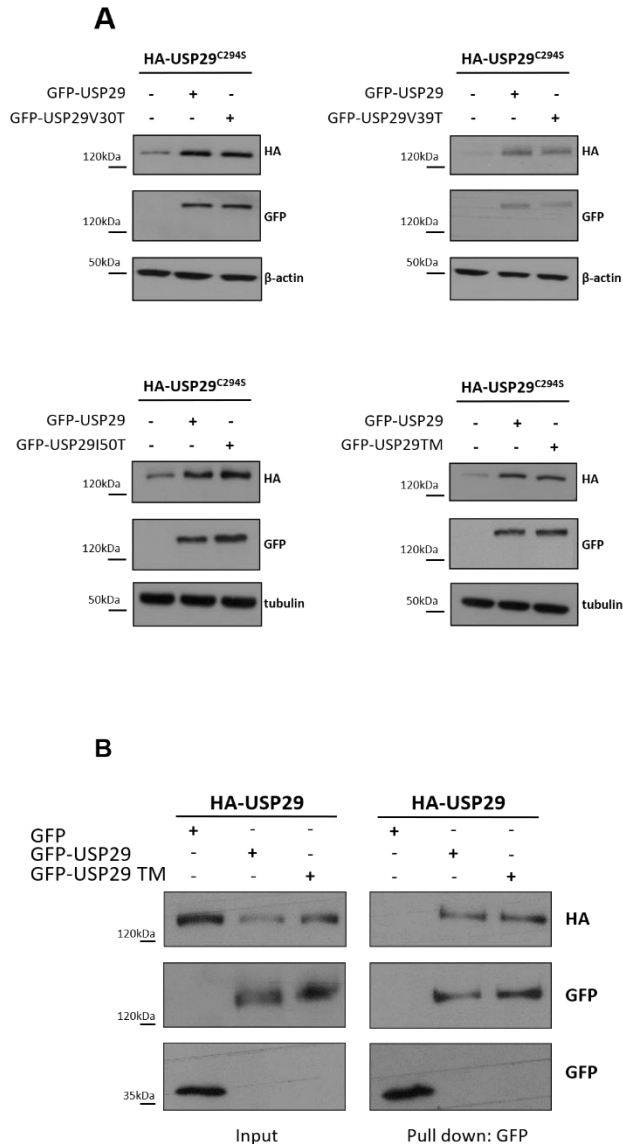


Figure R18: Effect of the residues identified as potential mediators of USP29 dimerization on the stabilization of the catalytically inactive USP29^{C294S} mutant. (A) HEK293 cells were co-transfected with HA-USP29^{C294S} and empty vector, GFP-USP29 or GFPUSP29V30T; GFP-USP29V39T; GFPUSPI50T or GFP-USP29TM. WCE were subjected to SDS-PAGE followed by immunoblotting with the indicated antibodies. **(B)** HEK293 cells were co-transfected with HA-USP29 and GFP, GFP-USP29 or GFP-USP29TM and lysed 24h post-transfection. The interaction between HA-USP29 and GFP-USP29TM was analysed by coIP. GFP and GFP-fusion proteins were co-immunoprecipitated in native conditions with GFP-traps® and eluates (together with 2.5% of the total lysed extracts) were subjected to SDS-PAGE followed by WB against indicated proteins.

The three mutants accumulate USP29^{C249S} as the USP29 WT does. To exclude that there was some redundancy between the three residues a USP29 triple mutant was generated. Contrary to expectations, this mutant was still capable of accumulating USP29^{C249S} (Figure R18A). Moreover, USP29TM interacts with USP29 similarly to the wild type (Figure R18B).

2.3 USP29PH acts as a dominant negative for USP29

USP29PH expression levels in HEK293 cells are consistently lower than those of full length USP29 when transfecting the same amount of both plasmids. To evaluate whether USP29PH was unstable, cells were treated either with the proteasome inhibitor, MG132 or the autophagy inhibitor, chloroquine. Significant accumulation of USP29PH was only perceived upon inhibition of the proteasome. Autophagy was clearly inhibited as indicated by the appearance of the lipidated LC3 band (Figure R19A). These data suggested that the proteasome machinery, and not the autophagic one, was implicated in USP29PH degradation.

The half-life of USP29PH was checked in a cycloheximide (CHX) experiment. Cycloheximide is a protein synthesis inhibitor used to measure the half-life of a protein. The CHX was added in the cells transfected with USP29PH and the expression of USP29PH was checked at different time points. Interestingly, the half-life of USP29PH increased significantly in the presence of USP29, suggesting that USP29 stabilizes USP29PH as it did with USP29^{C249S} (Figure R19B). To assess whether this stabilization was dependent on the catalytic activity of USP29, USP29PH was co-expressed together with both catalytically active USP29 or inactive USP29^{C294S} (Figure R19C). As expected, USP29PH was exclusively accumulated in the presence of active USP29.

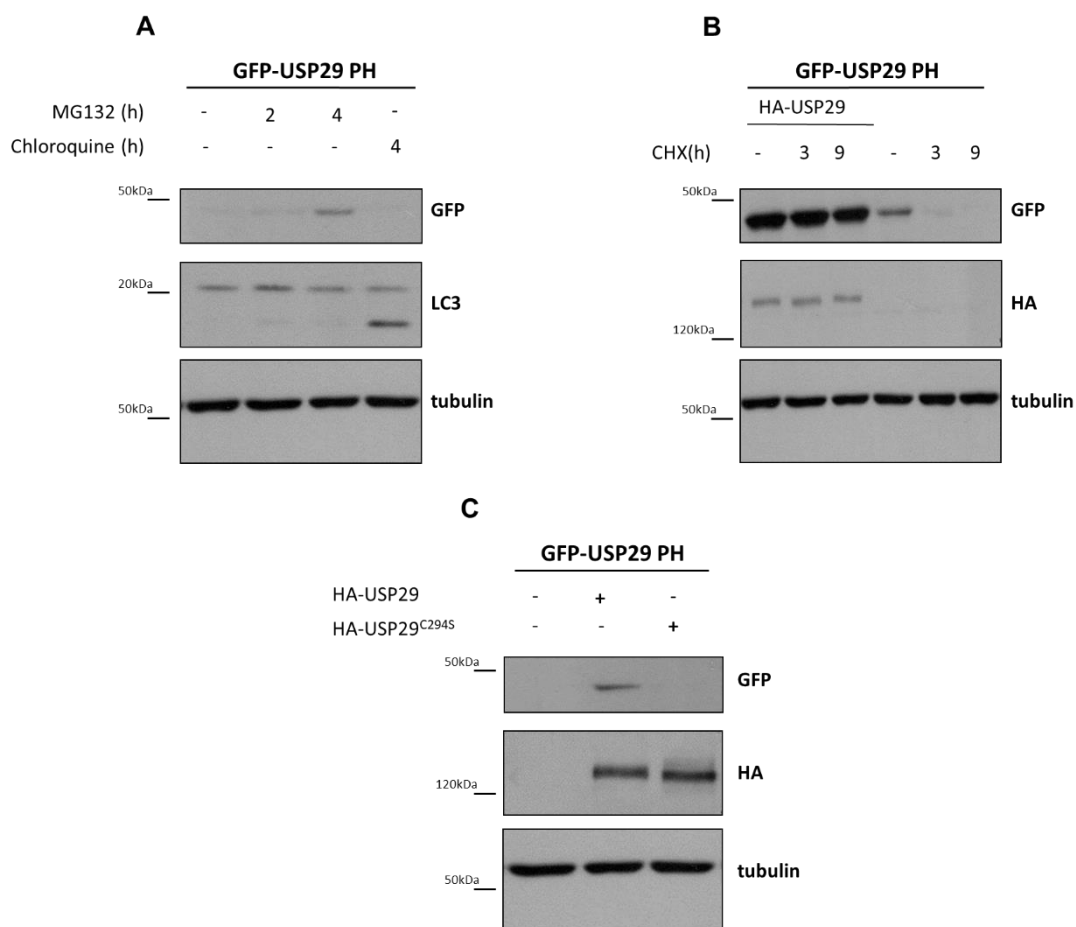


Figure R19: USP29 stabilizes USP29PH by protecting it from proteasome-mediated degradation. (A) HEK293 cells were transfected with GFP-USP29PH and left untreated or treated with MG132 (2h and 4h) or with chloroquine 4h prior to lysis. WCE were subjected to SDS-PAGE followed by WB against the indicated proteins. (B) HEK293 cells were co-transfected with GFP-USP29PH and HA-USP29 or empty vector and treated with cycloheximide (20 μ g/ μ L) to inhibit protein synthesis. Cell extracts were prepared at the indicated time points. GFP-USP29PH protein levels were determined by Western Blotting. (C) HEK293 cells were co-transfected with GFP-USP29PH and empty vector, HA-USP29 or HA-USP29^{C294S}. WCE were subjected to WB against the indicated proteins.

The PH domain of USP29 is supposed to have no catalytic activity, but it could have a regulatory effect on USP29. To investigate this possible role of the PH domain, USP29 was ectopically expressed in HEK293 cells together with increasing amounts of USP29PH. Interestingly, USP29 protein levels decreased while USP29PH levels increased (Figure R20A). To corroborate that USP29PH was indeed affecting the catalytic activity of USP29, the impact on HIF1- α , a novel USP29's target, was studied. Increasing amounts of USP29PH impaired accumulation of HIF-1 α upon hypoxia (Figure R20B). The expression of USP29PH seems to work as a dominant negative affecting the USP29 activity and, therefore, reducing USP29 and USP29's target HIF1- α protein levels. Thus,

it can be concluded that USP29PH is necessary for USP29 dimer/oligomerization (Figure R16) and activity (Figure R20).

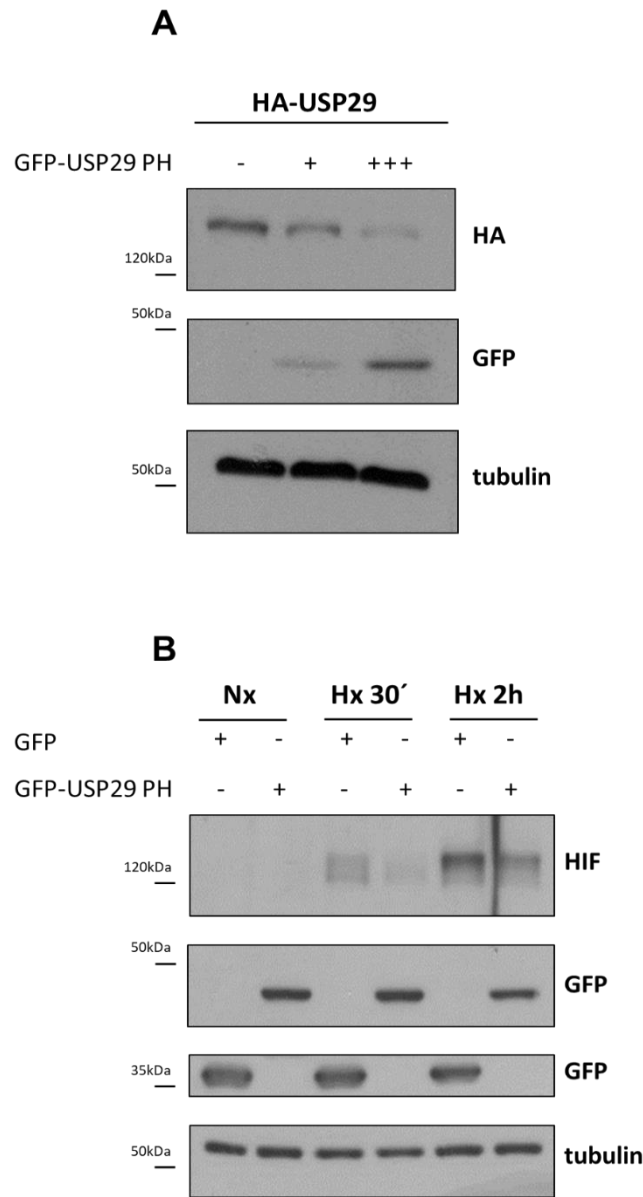


Figure R20: USP29 PH is a dominant negative for USP29 activity. (A) HEK293 cells were co-transfected with HA-USP29 and empty vector or increasing quantities of GFP-USP29PH. WCE were subjected to SDS-PAGE followed by immunoblotting with HA, GFP and tubulin antibodies. **(B)** HEK293 cells were transfected with GFP or GFP-USP29PH and leave them in normoxia (Nx, 20% O₂), 30 minutes or 2 hours of hypoxia (Hx, 1% O₂). WCE were subjected to SDS-PAGE followed by immunoblotting with HA, GFP and tubulin antibodies.

3. Structural analysis of USP29

3.1 USP29 and USP29PH proteins expression and purification

3.1.1 Expression and purification of USP29 in bacteria

To gain insight into the structure-function relationship of USP29 we aimed to produce the pure protein for structural analysis. For that purpose, the generation of recombinant USP29 and/or USP29PH was necessary.

To express and purify USP29 protein in *Escherichia coli* (*E. Coli*), two different constructs were used: pHisP2-USP29 (with an N-t His-tag sequence) and pET21a-USP29 (with a C-t His-tag sequence).

Expression tests with pHisP2-USP29 were performed in *E. coli* BL21 Star (DE3) strain harbouring the pRARE2 plasmid. This strain facilitates the expression of long genes by stabilizing long mRNA (messenger RNA), and pRARE2 codes for human tRNAs (transfer RNAs) reading rare codons in bacteria. Two different expression conditions were tested: 3 h at 37 °C or 16 h at 20 °C. However, the USP29 protein was not expressed in any of these growth conditions (Figure R21).

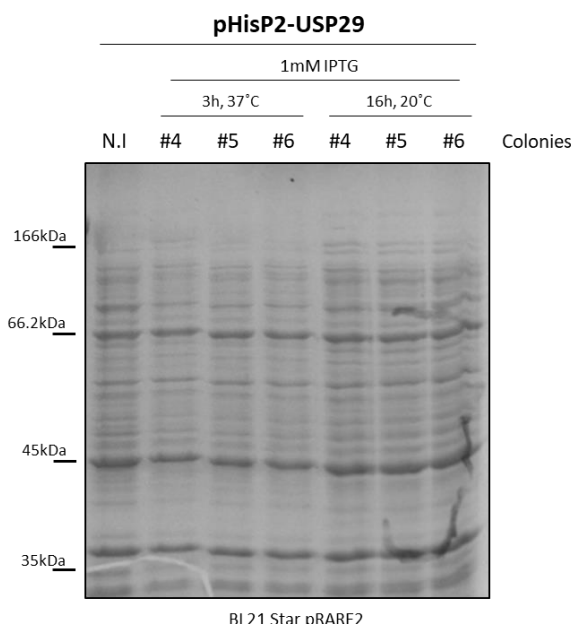


Figure R21: USP29 (pHisP2) is not expressed in BL21 (DE3) Star pRARE2. A Tris-glycine 8 % SDS-PAGE was run with a non-induced colony (N.I) and the indicated colonies from the two different growth conditions after induction with 1 mM IPTG (Isopropyl β -D-1-thiogalactopyranoside). The gel was stained with Coomassie Brilliant Blue. The expected molecular weight of USP29 is 107 kDa.

Similarly, the expression test was performed to check pET21a-USP29 in BL21 (DE3) Star pRARE2 (Figure R22A). This clone produced a protein in induced cultures that was consistent with the size of USP29 (107 kDa), with similar levels at the two tested temperatures. It was decided to scale up the growth to 6 L of LB for 16 h at 20 °C since lower temperatures generally favour the production of soluble versus insoluble protein. After cell harvesting, lysis and ultracentrifugation, the expressed protein was found mainly in the insoluble fraction (Figure R22B).

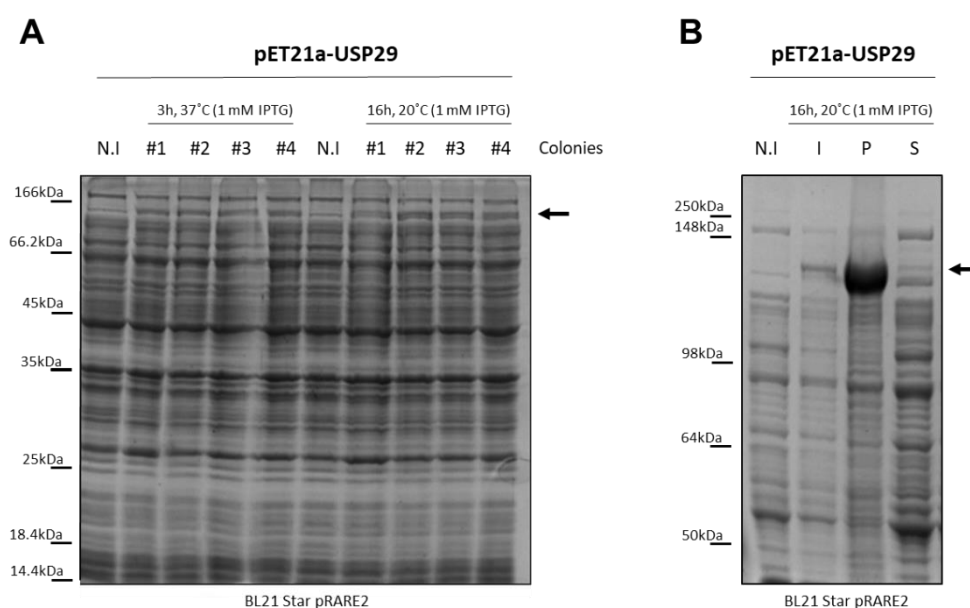


Figure R22: USP29 in pET21a is expressed as insoluble protein in BL21(DE3) Star pRARE2. (A) A Tris-glycine 8 % SDS-PAGE was run with a non-induced colony (N.I) and the indicated colonies from the two different growth conditions after induction with 1 mM IPTG. The band corresponding to the molecular weight of His₆-USP29 is indicated with an arrow. **(B)** The non-induced (N.I), induced with 1 mM IPTG (I) and the pellet (P) and supernatant (S) samples of the high-scale growth were run in a Tris-glycine 8 % SDS-PAGE.

The possible protein present in the soluble fraction was captured by a Ni²⁺ affinity chromatography. After incubation of the eluted fractions with TEV (Tobacco Etch Virus) protease and elimination of the imidazol by dialysis, it was loaded again on the same column, and the flow-through was separated by gel filtration. The protein eluted in the exclusion volume, together with other proteins, suggesting that USP29 formed high molecular weight aggregates. An attempt to increase the purity of the protein by anion-exchange chromatography was done (the calculated pI of the protein is 5.6), but very little and impure protein was

recovered (Figure R23). Thus, the strategy for obtaining full-length USP29 using *E. coli* as an expression system was abandoned.

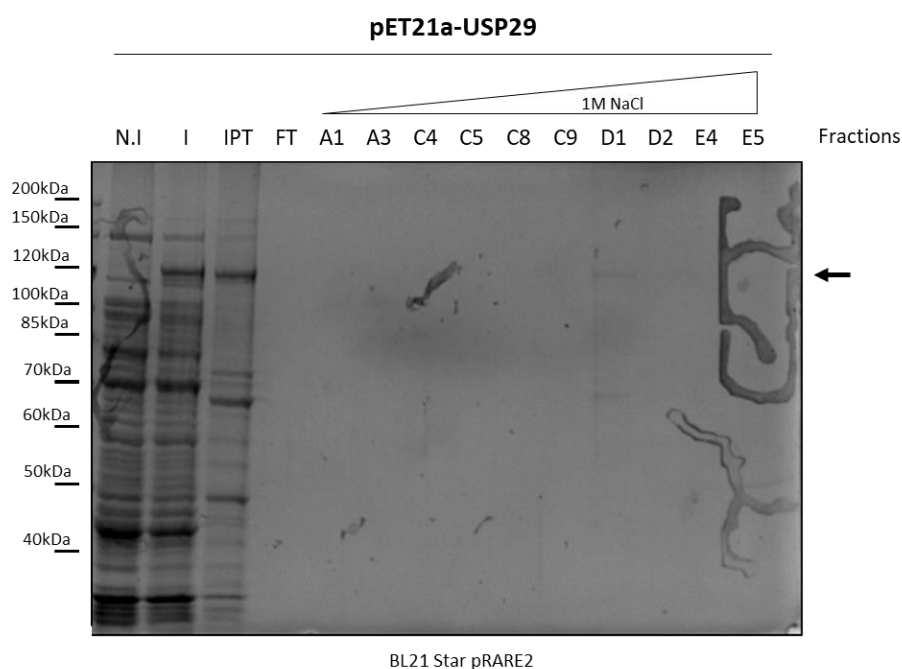


Figure R23: SDS-PAGE analysis of the last purification step of USP29 from bacterial cells. A Tris-glycine 8 % SDS-PAGE was loaded with a non-induced (N.I) and induced (I) culture samples as well as with the fractions from the anion exchange chromatography together with the input (IPT) and flow-through (FT) on a MonoQ HR 5/5 column. A faint band corresponding to the molecular weight of His₆-USP29 is indicated with an arrow in fraction D1.

3.1.2 Expression and purification of USP29PH in bacteria

Three different clones were used in order to express and purify the PH domain of USP29: pET11d-USP29PH (with and N-t Strep tag), pET29-USP29PH (fused to an N-terminal Ubiquitin, with His and Strep tags) and pHisP2-USP29PH (with and N-t His tag).

In the case of pET11d-USP29PH, two different *E.coli* strains were tried: BL21(DE3) (with induction at 37 °C and 20 °C) and ArticExpress (DE3). This last strain is induced at low temperatures (15 °C) to express chaperones that facilitate the folding of highly expressed proteins, to increase the yield of soluble protein. However, no protein expression was observed using these conditions and strains (Figure R24). The molecular weight of this construct is 15 KDa.

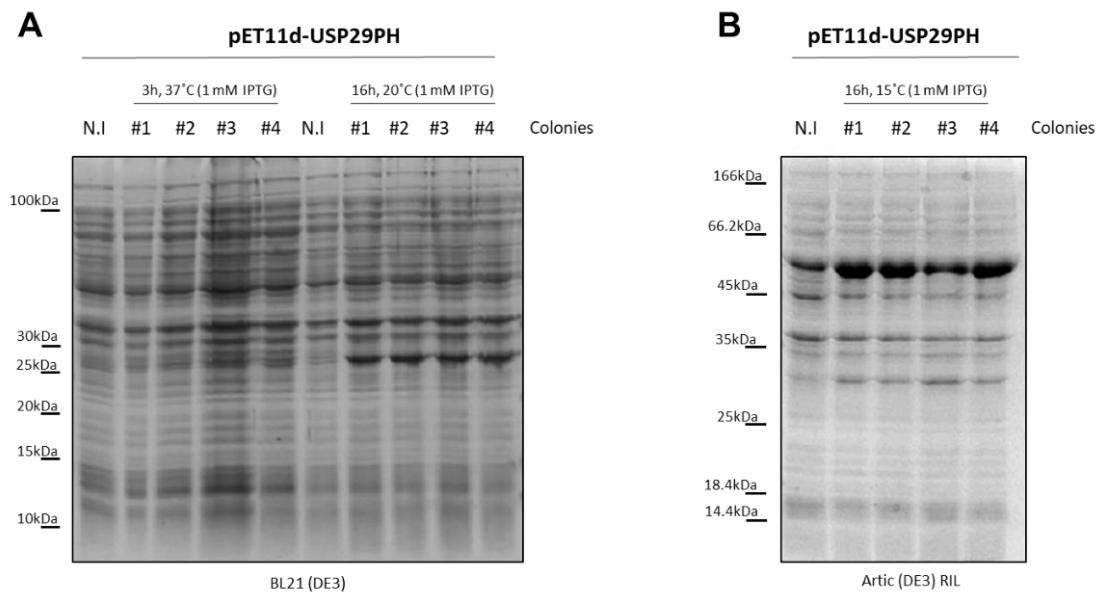


Figure R24: USP29PH cloned into pET11d vector is not expressed in neither BL21 (DE3) nor in Artic (DE3) RIL. (A) (B) Tris-glycine 12 % SDS-PAGE were loaded with non-induced (N.I) samples and the samples corresponding to several bacterial colonies induced at different temperatures and times.

An expression test was also performed with pET29-USP29PH (with an N-t fusion to ubiquitin, 28 kDa) in BL21(DE3) cells at two different temperatures and induction times. There was protein expression in both conditions, as assessed by SDS-PAGE and Coomassie staining (Figure R25).

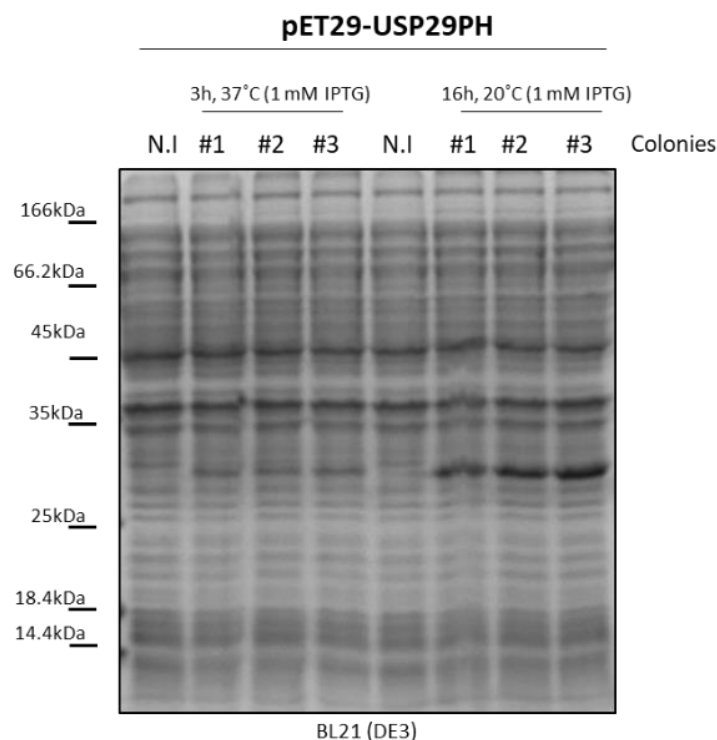


Figure R25: USP29PH in pET29 is expressed in BL21 (DE3) bacterial cells. A Tris-glycine 12 % SDS-PAGE was loaded with non-induced (N.I) samples and the samples corresponding to the colonies induced at different temperatures and times.

Considering that USP29PH showed higher expression levels at 20 °C and 16 h, it was decided to scale up the growth in these conditions. Furthermore, an autoinducible ZYP5052 medium that allows reaching higher bacterial densities than the LB medium was used. While the USP29PH protein was mostly found in the insoluble fraction (P) (Figure R26A), the possible protein present in the soluble fraction was captured by Ni²⁺ affinity chromatography. After tag cleavage with TEV protease and subsequent Ni²⁺ affinity chromatography, no protein was found in the flow-through (FT; Figure R26B). The most likely interpretation for this result is that there was no USP29PH protein in the soluble fraction.

The insoluble protein was attempted to recover from the inclusion bodies by solubilization in lysis buffer containing 8 M urea and ultracentrifugation for 3 h. The solubilised fraction was refolded by dilution and the possible soluble protein was captured by Ni²⁺ affinity chromatography. However, no protein was detected

in the elution because the protein could not be solubilized from the inclusion bodies even with 8M urea.

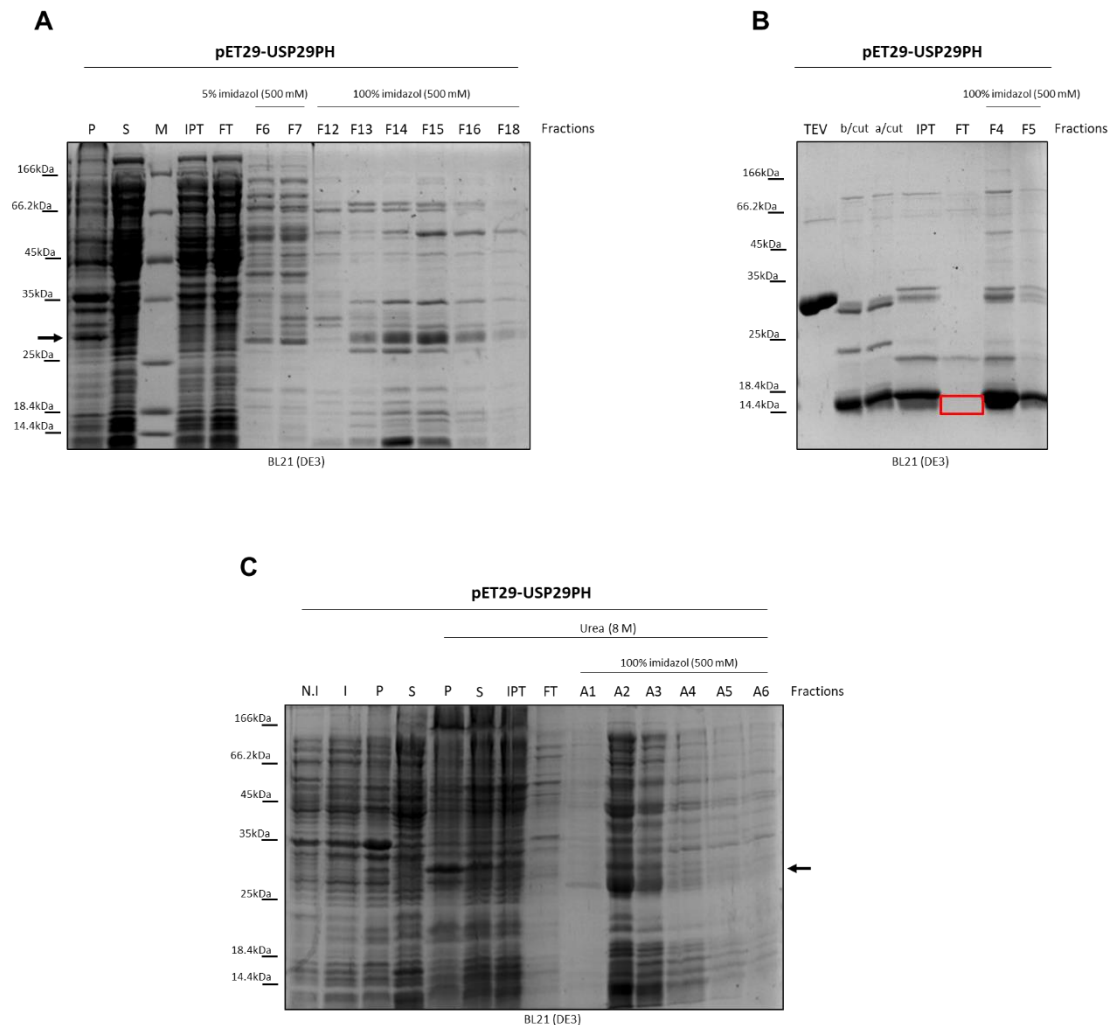


Figure R26: USP29PH in pET29 is expressed as inclusion bodies and could not be purified. (A) A Tris-glycine 12 % SDS-PAGE were loaded with the pellet (P) and supernatant (S) samples and the samples corresponding to the nickel affinity chromatography performed; the input (IPT) and the flow-through (FT) of the HisTrap column and the fractions corresponding to the 0.025 M imidazol and 0.5 M imidazol eluted fractions. The arrow shows the band at 28 KDa corresponding to the molecular weight of Ubq-His₆-Strep-USP29PH. **(B)** A Tris-glycine 12 % SDS-PAGE was loaded with the samples corresponding to the second nickel affinity chromatography. As controls, the TEV protease, the protein before cutting with TEV (b/cut) and the protein after cutting with TEV (a/cut) were loaded. Also, the input (IPT), flow-through (FT) and two fractions eluted at 0.5 M imidazol on the last HisTrap column were loaded. The red square shows where USP29PH without tag (13 kDa) should be. **(C)** A Tris-glycine 12 % SDS-PAGE was loaded with samples corresponding to the trial of purification of USP29PH from the inclusion bodies. As negative control a non-induced sample was loaded and as positive control and induced sample and the pellet (P) and supernatant (S) of the lysed bacterial cells were loaded. The pellet (P) and supernatant (S) from the resuspension of inclusion bodies with 8 M urea were also loaded, as well as the samples corresponding to the HisTrap column chromatography of the refolded urea soluble fraction (IPT). The arrow points to 28 KDa corresponding to the molecular weight of Ubq-His₆-Strep-USP29PH.

The construct pET29-USP29PH was also expressed in the *E.coli* strain Rosetta pLys to further test the solubilization of the protein. After a trial of the expression of USP29PH at different concentrations of IPTG, it was observed that the expression increased at lower IPTG concentrations (Figure R27).

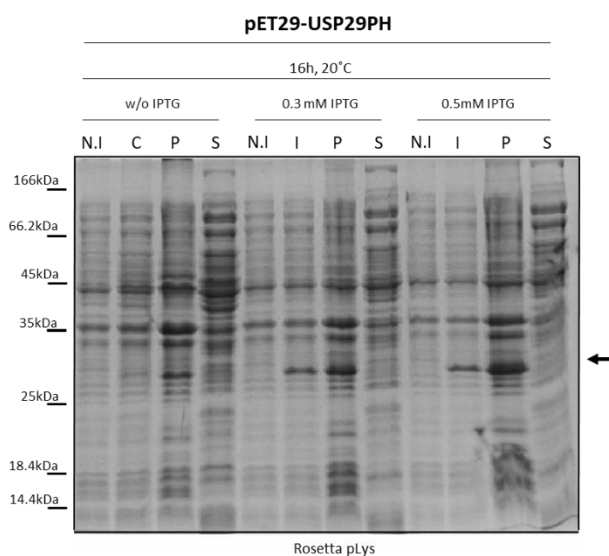


Figure R27: USP29PH is expressed in Rosetta pLys bacterial cells. A Tris-glycine 12 % SDS-PAGE were loaded with non-induced (N.I) samples and the samples corresponding to the colonies induced at different IPTG concentrations. The insoluble (P) and soluble (S) fractions were separated and loaded for each condition. The arrow shows the band corresponding to Ubq-His₆-Strep-USP29PH.

The high-scale growth (6 L) for pET29-USP29PH expression in Rosetta pLys cells was done in LB medium. After sonication and ultracentrifugation, USP29PH was predominantly found in the insoluble fraction. Nonetheless, a Ni²⁺ affinity chromatography of the soluble fraction was run trying to capture the possible soluble protein (Figure R28). However, no protein was found in the eluted fractions of the Ni²⁺affinity chromatography (Figure R28A).

The inclusion bodies were solubilized in 8 M urea containing lysis buffer and ultracentrifuged for 3 h. The soluble fraction was refolded and the solution was

loaded on a Ni²⁺affinity column. No USP29PH was detected in the elution because the protein remained insoluble even in 8 M urea (Figure R28B).

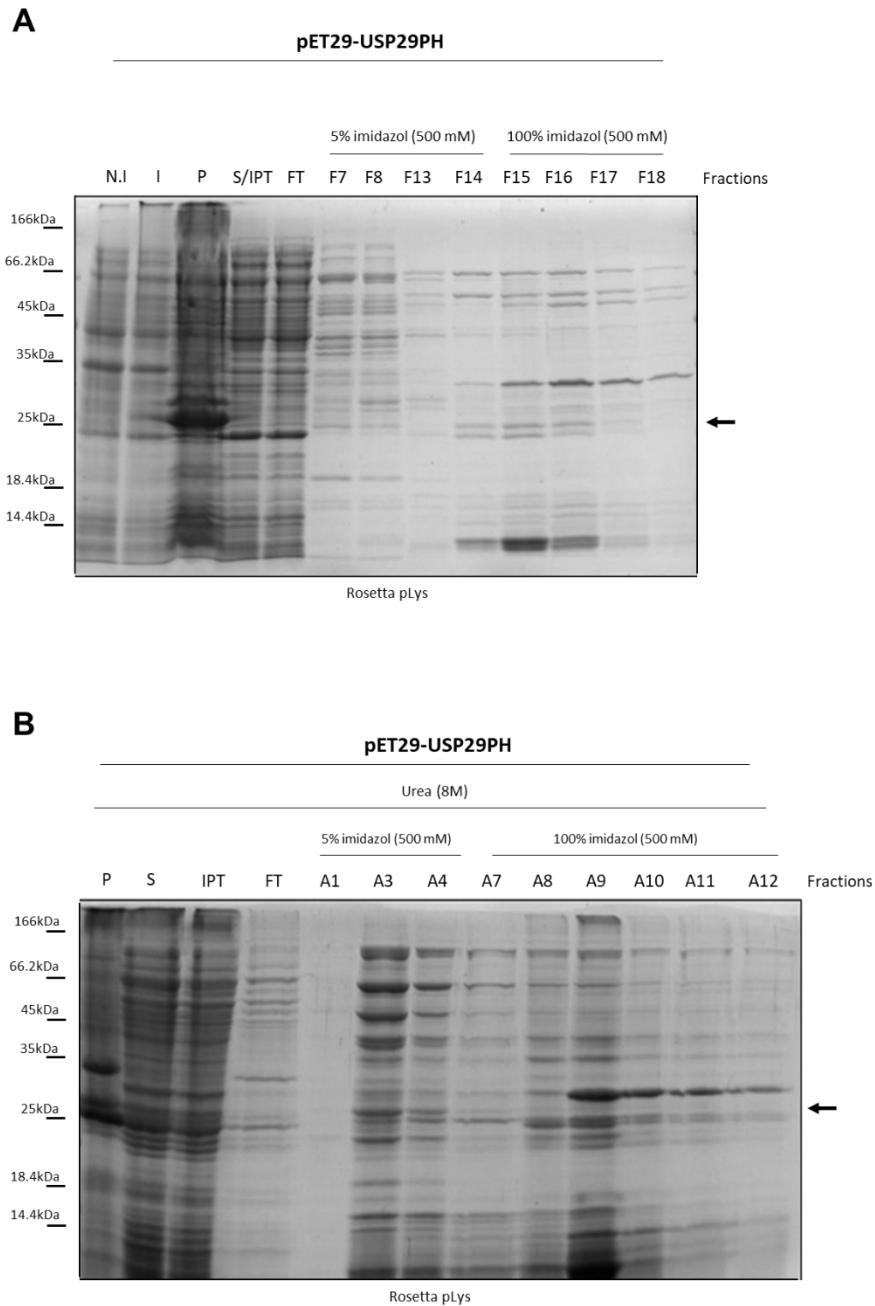


Figure R28: USP29PH in pET29 is expressed as inclusion bodies and could not be purified. (A) A Tris-glycine 12 % SDS-PAGE were loaded with the pellet (P) and supernatant (S) samples and the samples corresponding to the first nickel affinity chromatography; the input (IPT) and the flow-through (FT) of the HisTrap column and the fractions corresponding to the 0.025 M imidazol and 0.5 M imidazol elution. The arrow shows the band at 28 KDa corresponding to the molecular weight of Ubq- His₆-Strep-USP29PH. **(B)** A Tris-glycine 12 % SDS-PAGE was loaded with samples corresponding to the trial of purification of USP29PH from the insoluble fraction. The pellet (P) and supernatant (S) from the resuspension with 8 M Urea were also loaded, as well as the samples corresponding to the 0.025 M imidazol and 0.5 M imidazol eluted fractions of the HisTrap column chromatography of the refolded soluble fraction (IPT) from the urea resuspension. The arrow shows the band at 28 KDa corresponding to the molecular weight of Ubq-His₆-Strep-USP29PH.

A reason for the poor solubility of USP29PH could be protein attachment to membranes, but different solubilization trials using four different detergents (SDS (Sodium Dodecyl Sulfate), CHAPS ((3-((3-cholamidopropyl) dimethylammonio)-1-propanesulfonate)), DDM (n-Dodecyl-beta-Maltoside) and Triton X-100) were unsuccessful in recovering the protein in soluble form (Figure R29).

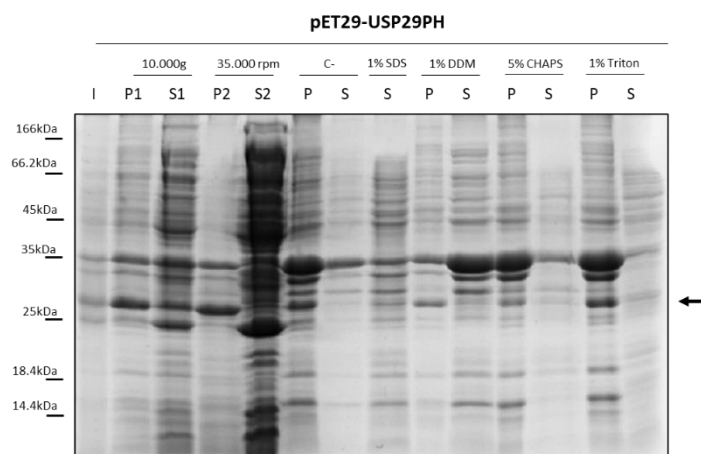


Figure R29: USP29PH is mainly expressed in the inclusion bodies after stringent membrane washings. A Tris-glycine 12 % SDS-PAGE were loaded with an induced (I) sample of pET29-USP29PH expression test and the samples corresponding to the insoluble (P) and soluble (S) fractions of each condition. The arrow shows the band at 28 KDa corresponding to the molecular weight of Ubq-His₆-Strep-USP29PH.

The clone pHisP2-USP29PH showed good expression levels in both Rosetta pLys and BL21 (DE3) Star pRARE2 cells at two different induction temperatures and times (Figure R30).

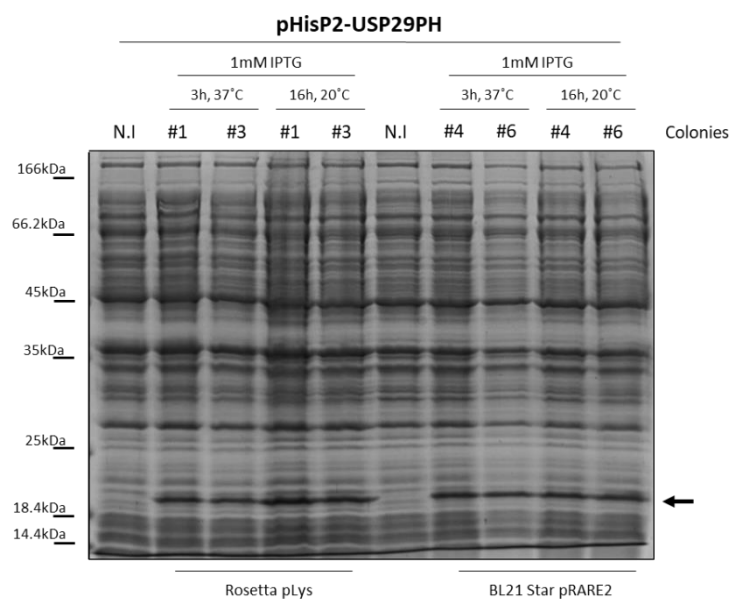


Figure R30: USP29PH in pHisP2 is expressed in Rosetta pLys and in BL21 (DE3) Star pRARE2. A Tris-glycine 12 % SDS-PAGE was loaded with non-induced (N.I) samples and the samples corresponding to the colonies induced at different temperatures and times.

For pHisP2-USP29PH high-scale (6 L) expression in BL21(DE3) Star pRARE2 cells was done in ZYP5052 auto-inducible medium. Cultures were harvested by centrifugation and resuspended in lysis buffer. After sonication and ultracentrifugation, USP29PH was predominantly found in the insoluble fraction. Nevertheless, a Ni²⁺ affinity chromatography was run trying to capture the protein present in the soluble fraction, however, no protein was found (Figure R31A).

The insoluble His₆-USP29PH was resuspended in lysis buffer containing 8 M urea but the protein could not be solubilized (Figure R31B).

The pellet was then resuspended in 20 mM Tris-HCl pH 8.0, 6 M guanidinium chloride yielding soluble protein after ultracentrifugation (Figure R31B). The supernatant was refolded by dilution into cold buffer and the refolded protein solution (after removal of precipitated material) was loaded on a Ni²⁺affinity chromatography. However, no USP29PH was recovered, probably because it was not properly refolded.

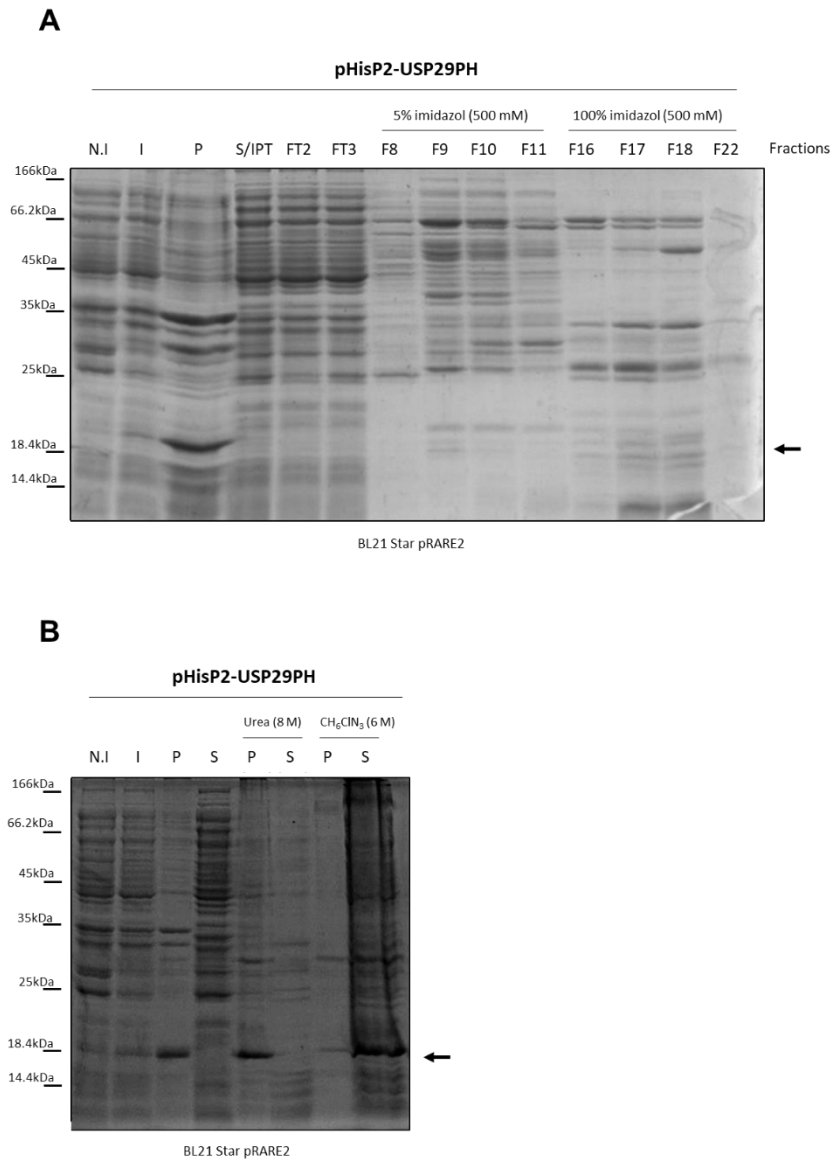


Figure R31: USP29PH in pHisp2 is expressed as inclusion bodies. (A) A Tris-glycine 12 % SDS-PAGE was loaded with the pellet (P) and supernatant (S/IPT) samples, as well as the samples corresponding to the nickel affinity chromatography of the soluble fraction: the supernatant used as the input (S/IPT), the flow-through (FT) of the HisTrap column, and the fractions corresponding to the 0.025 M imidazol and 0.5 M imidazol elutions. The arrow shows the band at 18 kDa corresponding to the molecular weight of His₆-USP29PH. **(B)** A Tris-glycine 12 % SDS-PAGE was loaded with samples corresponding to the solubilization trials of USP29PH from the inclusion bodies. Negative and positive control samples of non-induced (N.I) and induced (I) protein from the expression test were loaded. The pellet (P) and supernatant (S) from the lysed cells, the solubilization with 8 M urea and the solubilization with 6 M guanidinium chloride (CH₆CIN₃) were loaded. The arrow shows the band at 18 kDa corresponding to the molecular weight of His₆-USP29PH.

The final attempt for USP29PH purification using *E.coli* as the expression system was to grow the three constructs in media supplemented with additives that stabilize protein structure as described by Oganessian and colleagues (Oganessian et al., 2007). Thus, the three constructs were grown in Rosetta pLys cells in LB medium supplemented with 2.5 mM glycine betaine, and 1 M D-sorbitol. The culture was induced the first day with 0.2 mM IPTG and it was grown for 5 days at 18 °C. The cultures were harvested by centrifugation and separated into insoluble and soluble fractions. No expression was seen in neither of the three constructs (Figure R32). Therefore, the strategy for obtaining USP29PH from *E. coli* expression was abandoned.

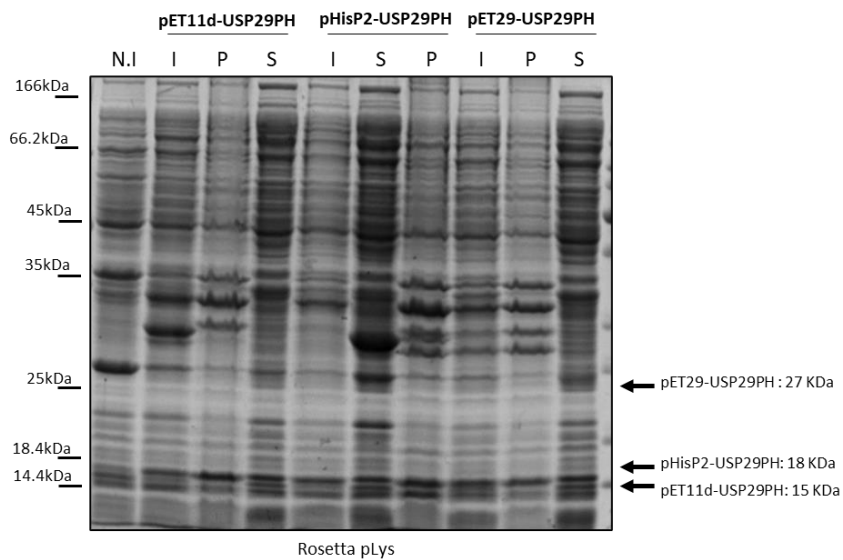


Figure R32: Glycine betaine and D-sorbitol do not favour USP29PH expression in bacterial cells. A Tris-glycine 12 % SDS-PAGE was loaded with a non-induced (N.I) sample from a previous expression test as a negative control, as well as the induced (I), pellet (P) and supernatant (S) of each construct. The molecular weights of each clone are indicated at the right side of the figure.

3.1.3 Expression and purification of USP29 in mammalian cells

Since the main problem in the purification of USP29 and USP29PH in *E. coli* was that the proteins were insoluble, mammalian cells (HEK293FT) were used to express the full-length USP29 as well as the PH domain.

Two different expression vectors (pOPINE and pOPING) were used to express and purify USP29 in HEK293FT cells. The two vectors express the protein under the control of the β -actin promoter with a Cytomegalovirus enhancer. Moreover, the expression vector pOPING contains a secretion signal peptide.

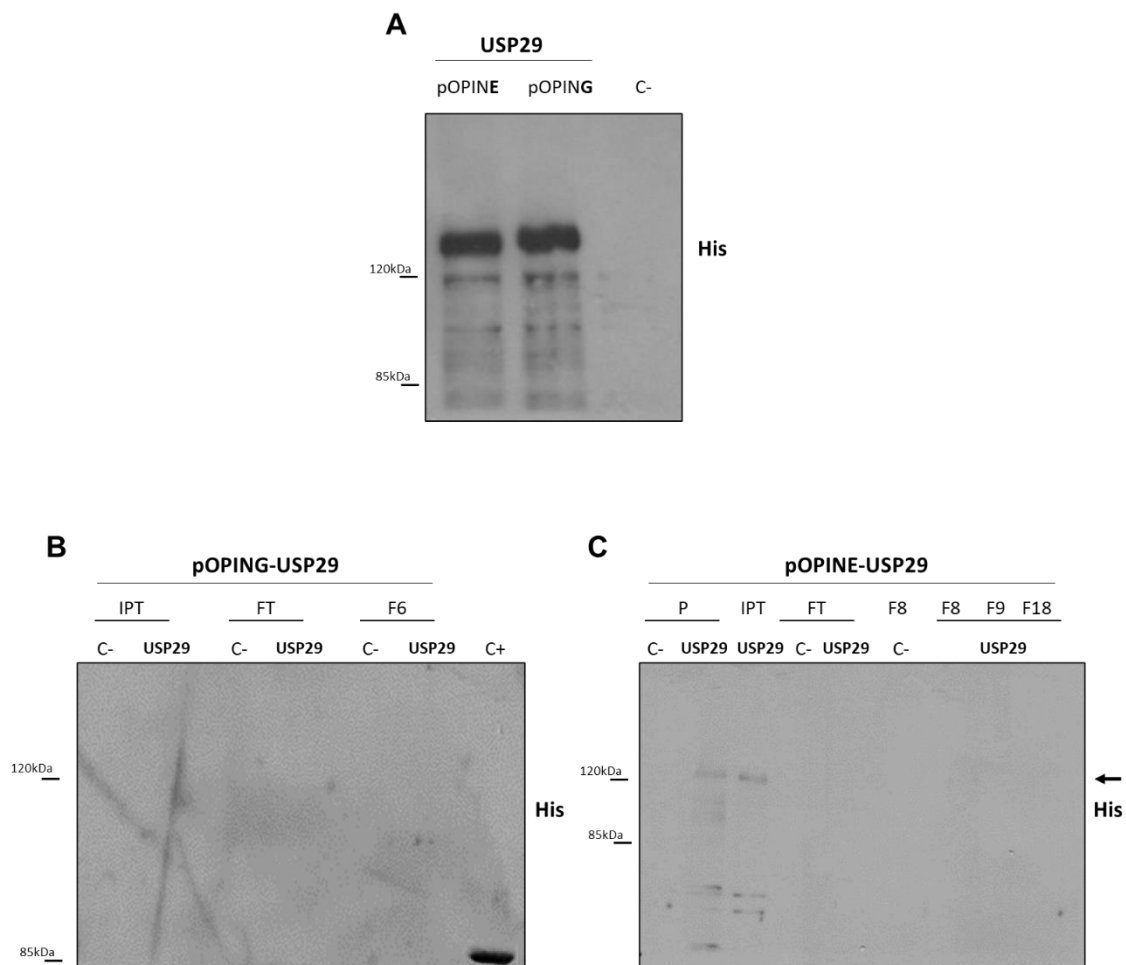


Figure R33: USP29 is expressed in HEK293FT cells. (A) Cells were transfected with pOPINE-USP29, pOPING-USP29 or an empty vector as a negative control, lysed 48 h post-transfection and the whole cell extracts were subjected to SDS-PAGE followed by WB against the His-tag. (B) The culture medium of pOPING-USP29 and the empty vector (C-) were run in a HisTrap column and the input (IPT), the flow-through (FT) and the fraction with the highest intensity in the chromatogram (as well as a positive control for the anti-His antibody), were subjected to SDS-PAGE followed by WB against the His-tag. (C) After cell harvesting and lysis, the supernatant of the HEK293FT cells transfected with pOPINE-USP29 or the empty vector were run in a HisTrap column. The pellet (P), the input (IPT), the flow-through (FT) and the fraction corresponding to the highest peak in the chromatogram, as well as a positive control for the anti-His antibody, were subjected to SDS-PAGE followed by immunoblotting with anti-His tag. The band corresponding to the molecular weight of USP29-His₆ (105 kDa) is indicated with an arrow in the input and F8 fraction samples.

The USP29 protein is expressed using both expression vectors in small scale cultures (2.5 mL), as shown in Figure R33A. USP29 expressed from the pOPING vector was not secreted into the culture media (Figure R33B). pOPINE-USP29 construct did express the protein, and after sonication and ultracentrifugation, the soluble fraction was purified by Ni²⁺ affinity chromatography with a very low yield (Figure R33C).

A scale-up of the expression of pOPINE-USP29 construct was performed in 1 L of cell culture. After 48 h of transfection the expression level of USP29 was very low as observed by WB (Figure R34A). The culture was homogenized and ultracentrifuged, the soluble fraction was loaded on a Ni²⁺ affinity column, but no protein was detected in the elution by Coomassie staining (Figure R34B). An additional cell culture grown for one week did not improve the expression level of USP29 (Figure R35) and purification was not attempted.

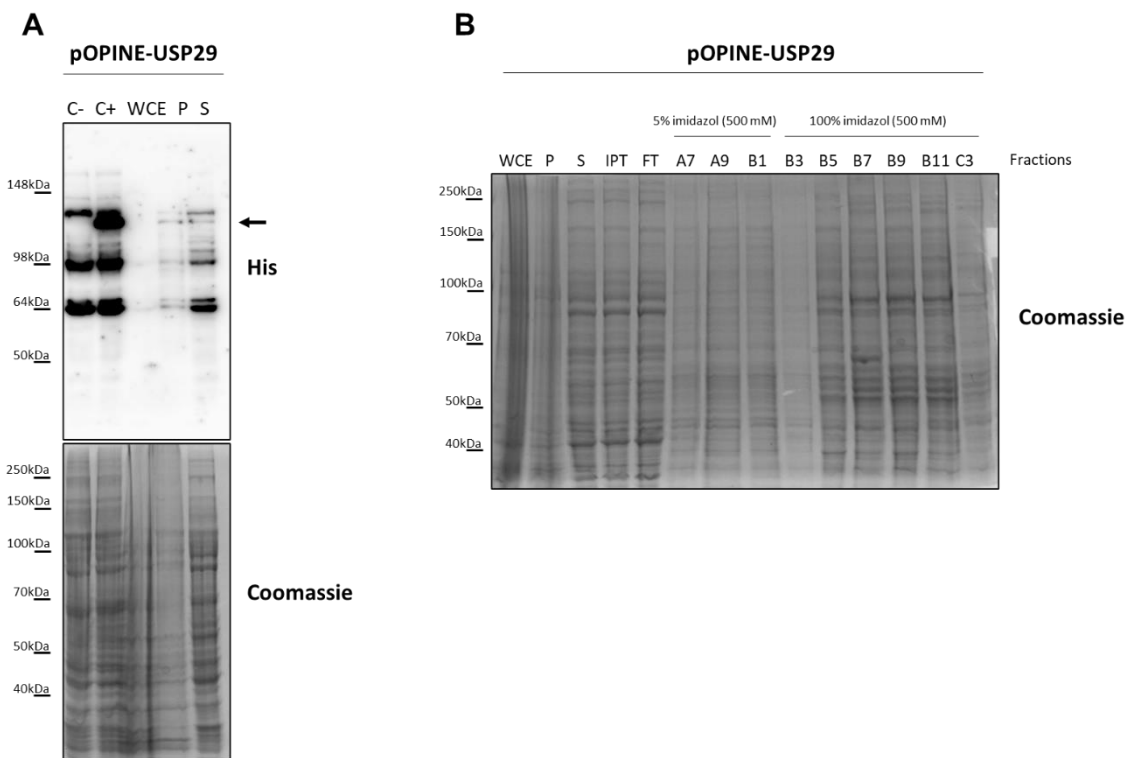


Figure R34: USP29 expression levels are low in HEK293FT . (A) HEK293FT cells were transfected with pOPINE-USP29 in 1 L of cell culture, lysed 48 h post-transfection, homogenized, centrifuged and separated into pellet (P) and supernatant (S), then subjected to SDS-PAGE (two different gels) followed by WB against His tag or staining with Coomassie brilliant blue. As a negative and positive control, the samples of the empty vector and pOPINE-USP29 from the small scale expression test were used, respectively. **(B)** A Tris-glycine 8 % SDS-PAGE was loaded with the whole cell extract (WCE), P and S samples from the lysed cells as well as with the input (IPT), which is the soluble fraction (S), the flow-through (FT) of the HisTrap column run and the eluted fractions at different concentrations of imidazol.

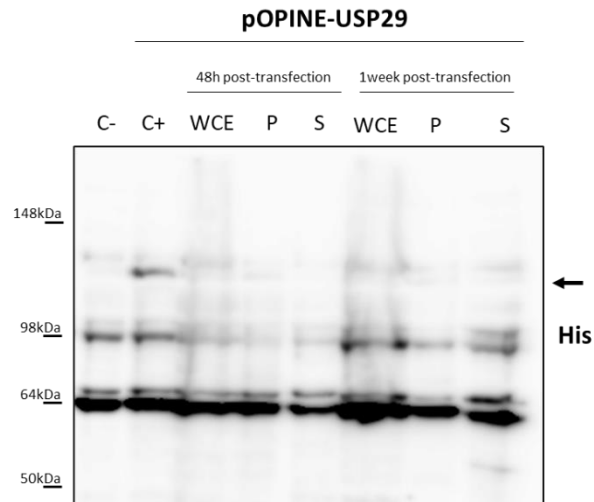


Figure R35: USP29 expression after one week of growth in HEK293FT is very low. (A) HEK293FT cells were transfected with pOPINE-USP29 and lysed 48h post-transfection and 1-week post-transfection, then separated into pellet (P) and supernatant (S) respectively and subjected to SDS-PAGE followed by WB against His tag. As a negative and positive control, the samples of the empty vector and pOPINE-USP29 from the small scale expression test were used.

3.1.4 Expression and purification of USP29PH in mammalian cells

Similarly, to full-length USP29, new constructs (pOPINE-USP29PH and pOPING-USP29PH) were generated to express the PH domain of USP29 in HEK293FT cells. While expressed protein was detected in the total cell extracts from small scale cultures (Figure R36A), no protein was detected after Ni²⁺ affinity chromatography (Figure R36B and Figure R36C). These results indicate that in the case of pOPING-USP29PH, the protein was not secreted into the culture media, and in the case of pOPINE-USP29PH, the protein was not present in the soluble fraction. Further trials with large scale cultures were not attempted.

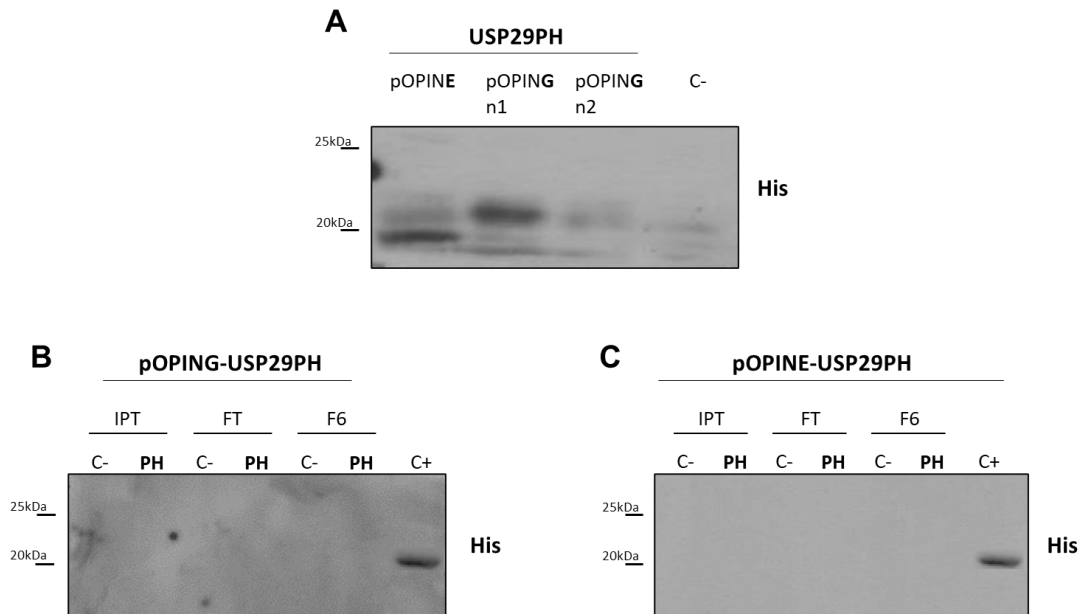


Figure R36: USP29PH expressed in HEK293FT cells is not detected after Ni²⁺ affinity chromatography. (A) HEK293FT cells were transfected with pOPINE-USP29PH, pOPING-USP29PH and an empty vector as a negative control and lysed 48 h post-transfection. (B) The culture medium of the cells transfected with pOPING-USP29PH and the empty vector (C-) were run in a HisTrap column and the input (IPT), the flow-through (FT) and the fraction with the highest peak in the chromatogram, as well as a positive control for the His antibody, were subjected to SDS-PAGE followed by WB against His tag. (C) The culture of HEK293FT cells transfected with pOPINE-USP29PH were lysed 48h post-transfection, homogenized and centrifuged. The supernatant obtained after the centrifugation and the empty vector were run in a HisTrap column. The input (IPT), the flow-through (FT) and the fraction corresponding to the highest peak in the chromatogram, as well as a positive control for the anti-His antibody were subjected to SDS-PAGE followed by immunoblotting against the His-tag.

3.2 Homology based model of USP29's structure

The purification trials of neither USP29 nor USP29PH were not successful and therefore, the experimental structural characterization could not be attempted. However, a model of the structure of USP29 was built (Figure R37) to gain insights on the structure-function relationship and possible interactions of USP29 with other proteins.

The PH domain of USP29 (residues 1 to 107) was modelled with the SWISS-MODEL SERVER (Waterhouse et al., 2018) using the crystal structure of the dimeric PH domain of USP37 (PDB 3u12) as template. The rest of the USP29 chain was modelled using the Protein Homology/analogY Recognition Engine V 2.0 (Phyre2) web server (Kelley et al., 2015).

From residue 108 to 280, the sequence was predicted as disordered (Figure R5) so it was modified manually from the Phyre2 model with Coot (Emsley et al., 2010), separating this disordered region from the rest of the protein.

The first part of the catalytic domain (residues 281 to 541) was modelled by Phyre2 based on six different templates: U4/U6.U5 tri-snRNP (PDB 3jcr), USP5 (PDB 3ihp), SAGA Ubp8/Sgf11/Sus1/Sgf73 DUB module (PDB 3mhs), USP7CD-UBL45 in complex with ubiquitin (PDB 5jtv), USP7 (PDB 2f1z) and the catalytic and three UBL domains of USP7 (PDB 5fwi). The region from residue 387 to 421 was a disordered one and was modelled as a loop. The zinc binding domain was created based on the Npl4 Zinc-Finger (PDB 1q5w) that binds ubiquitin. The potential zinc-finger ubiquitin-binding site was formed by 4 cysteines: C438, C441, C486 and C489.

From residue 542 to 706, a disordered region was predicted, but not as disordered as the 108-280 region (Figure R5). It was manually modelled using Coot, but two loops that were blocking the ubiquitin binding sites were manually moved. As this region locates between the two parts of the catalytic domain the ends of the fragment were forced to be close and therefore its structure is more compact than the other disordered regions.

The second part of the catalytic domain (residues 707 to 922) was modelled together with the first part. The 707-815 region was modelled on USP5, which includes 2 small α -helical domains (UBAs) that in the case of USP29 could be a disordered region. The C-terminal region of USP29 (886-922) was modelled on USP7.

Different parts of the model were put together by pdb-editing, some fragments were regularized with coot, and an energy minimization was done using Chimera (Pettersen et al., 2004). The USP29 dimer was built based on the dimeric PH domain of USP37.

The catalytic centre residues (C294, H840, N857), as expected, are close in space in the structure (Figure R37).

In the model structure, the canonical PIP motif of USP29 is part of an α -helix. In the context of the full-length molecule the model suggests that the interaction with PCNA will not occur through this region. The structures of PIP and PIP-like sequences bound to PCNA show a one-turn helix and flanking extended regions. Therefore, the longer helical structure of the region containing the PIP motif might

impair PCNA binding. However, the crystal structure of the yeast Replication Factor C shows the PIP motif as part of a long helix while bound to PCNA (Bowman et al., 2004).

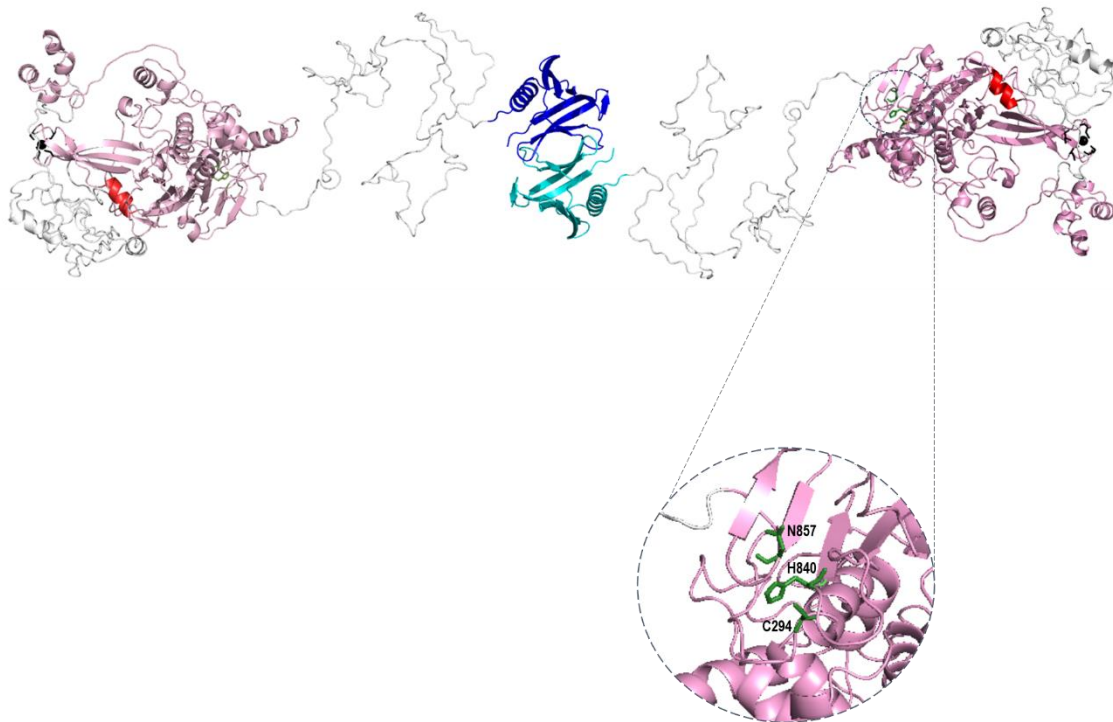


Figure R37. Homology based model of the structure of a homodimer of USP29. The oligomerization occurs via the PH domains (in blue and cyan). The catalytic domains (in pink) are in a flexible position due to the disordered regions (in grey). Within the catalytic domains, there is an α helix (in red) that contains the canonical PIP box of USP29. Catalytic centre residues (C294, H840, N857, in green), are located together in the structure as shown in the inset. The zn^{2+} (black sphere) binding site is formed by four cysteines: C438, C441, C486 and C489 (in black sticks).

4. Characterization of the interaction between p125 and PCNA

The interactions between PCNA and fragments from two of the four subunits of human Polymerase δ (p12 and p68) have been structurally characterized (Bruning & Shamo, 2004; Gonzalez-Magaña et al., 2019). However, the interaction between PCNA and the catalytic subunit of Pol δ (p125) had not been studied at the commencement of this thesis. After analysing the C-terminal sequence of p125, two potential non-canonical PIP-box sequences were found, which could be the potential interaction site with PCNA. Acharya and colleagues had discovered that yeast Pol δ showed less processivity during DNA synthesis after mutating one of the corresponding PIP-boxes in the p125 yeast homologue Pol3 (Acharya et al., 2011), suggesting this PIP-box as the potential PCNA binding site for p125. Very recently, this binding has been confirmed by the cryo-EM structure of human Pol δ bound to PCNA and DNA solved by Lancey and colleagues (Lancey et al., 2020).

This PIP-box motif of p125 was not predicted as disordered (Figure R38). Secondary structure prediction assigned a helical structure to the sequence.

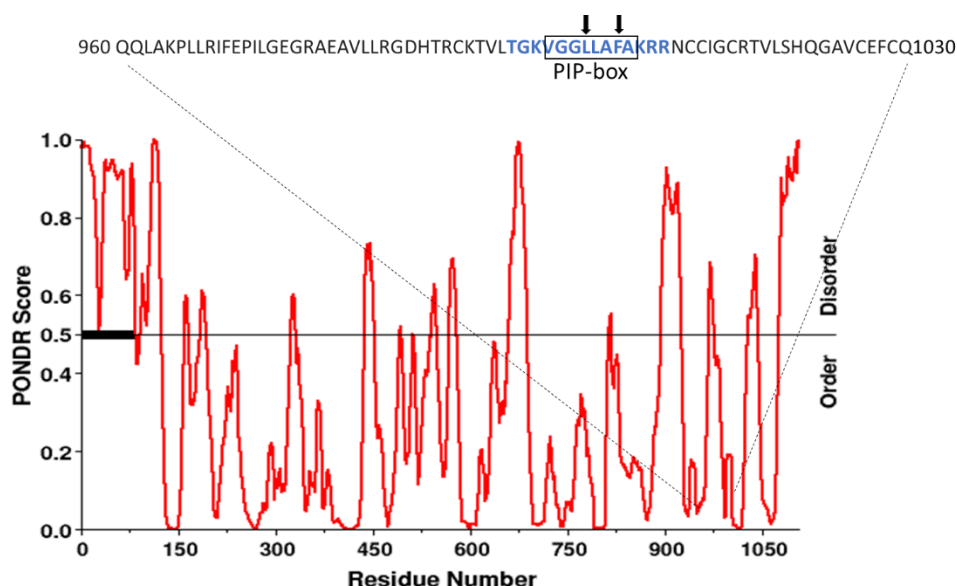


Figure R38: Disorder prediction for the p125 sequence. The red line shows the disorder prediction by the PONDR server (Predictor Of Naturally Disordered Regions, <http://www.pondr.com>), and the black line the threshold of 0.5. The sequence 960-1030 is shown above the graph. Residues encompassing the peptide used for biophysical characterization (p125⁹⁹⁶⁻¹⁰¹⁰) with PCNA are indicated in bold blue characters, those belonging to the non-canonical PCNA interacting motif are boxed. The consensus residues in the PIP-like motif are indicated by arrows

4.1 Binding reaction studied by calorimetry

The potential binding between PCNA and the p125⁹⁹⁶⁻¹⁰¹⁰ fragment was first analysed by isothermal titration calorimetry (ITC). The ITC measurements (Figure R39A) determined a dissociation constant of $250 \pm 40 \mu\text{M}$ at 25°C (Figure R39B). With this low affinity, the fitting of the data needed the assumption of a molar stoichiometry of binding of 1:1 (peptide:PCNA protomer). The binding is entropically driven as the enthalpic term is positive ($\Delta H = 7.51 \pm 1.15 \text{ kcal/mol}$) while the entropic term is negative ($-T\Delta S = -12.4 \pm 0.4 \text{ kcal/mol}$).

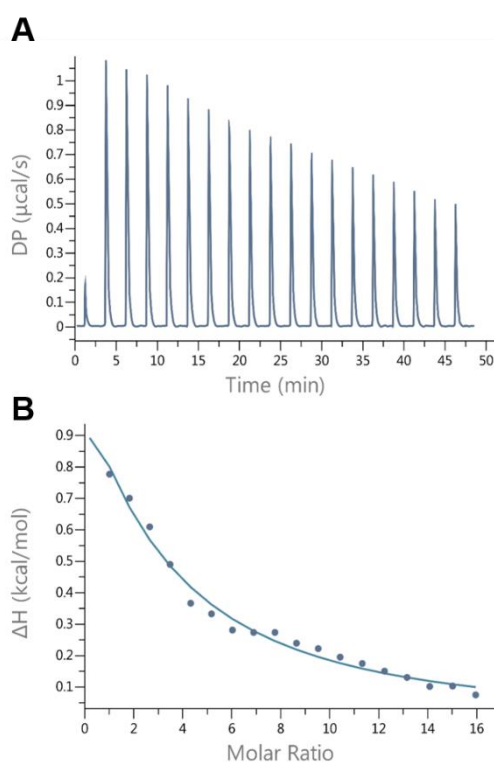


Figure R39: Isothermal calorimetric titration of PCNA with p125⁹⁹⁶⁻¹⁰¹⁰ PIP-box peptide. (A) Heat effect associated with the variable volume peptide injection. (B) Ligand concentration dependence of the heat released upon binding, after normalization and correction for the heat of dilution. The molar ratio is that of p125: PCNA protomer. The symbols correspond to the experimental data and the continuous line to the best fit to a model of one set of identical binding sites.

4.2 Binding site mapping by NMR

^2H - ^{13}C , ^{15}N -labeled PCNA was titrated with increasing amounts of unlabelled p125 peptide (Figure R40A and B). Along the titration, the NMR spectra of PCNA showed a single set of signals, indicating that three p125 peptides bind to the three equivalent PCNA protomers, confirming the 1:1 stoichiometry assumed for ITC data analysis. The dissociation constant (calculated as an average from the signals with chemical shift perturbation values higher than the average plus one standard deviation) is $103 \pm 14 \mu\text{M}$ at $35 \text{ }^\circ\text{C}$ (Figure R40C). This K_d is consistent with the result of the ITC, which shows that the binding between p125 and PCNA is an endothermic reaction (and thus, the dissociation constant is larger at a lower temperature). The pattern of the CSPs along the PCNA sequence (Figure R40D) is similar to the one observed for p21 binding to PCNA (De Biasio et al., 2012), indicating a similar mode of binding. Mapping the perturbed residues on the three-dimensional structure of PCNA (Figure R40E), shows that they cluster in the region where p21 binds PCNA, indicating that p125 also binds to the PIP-box site on the front face of PCNA.

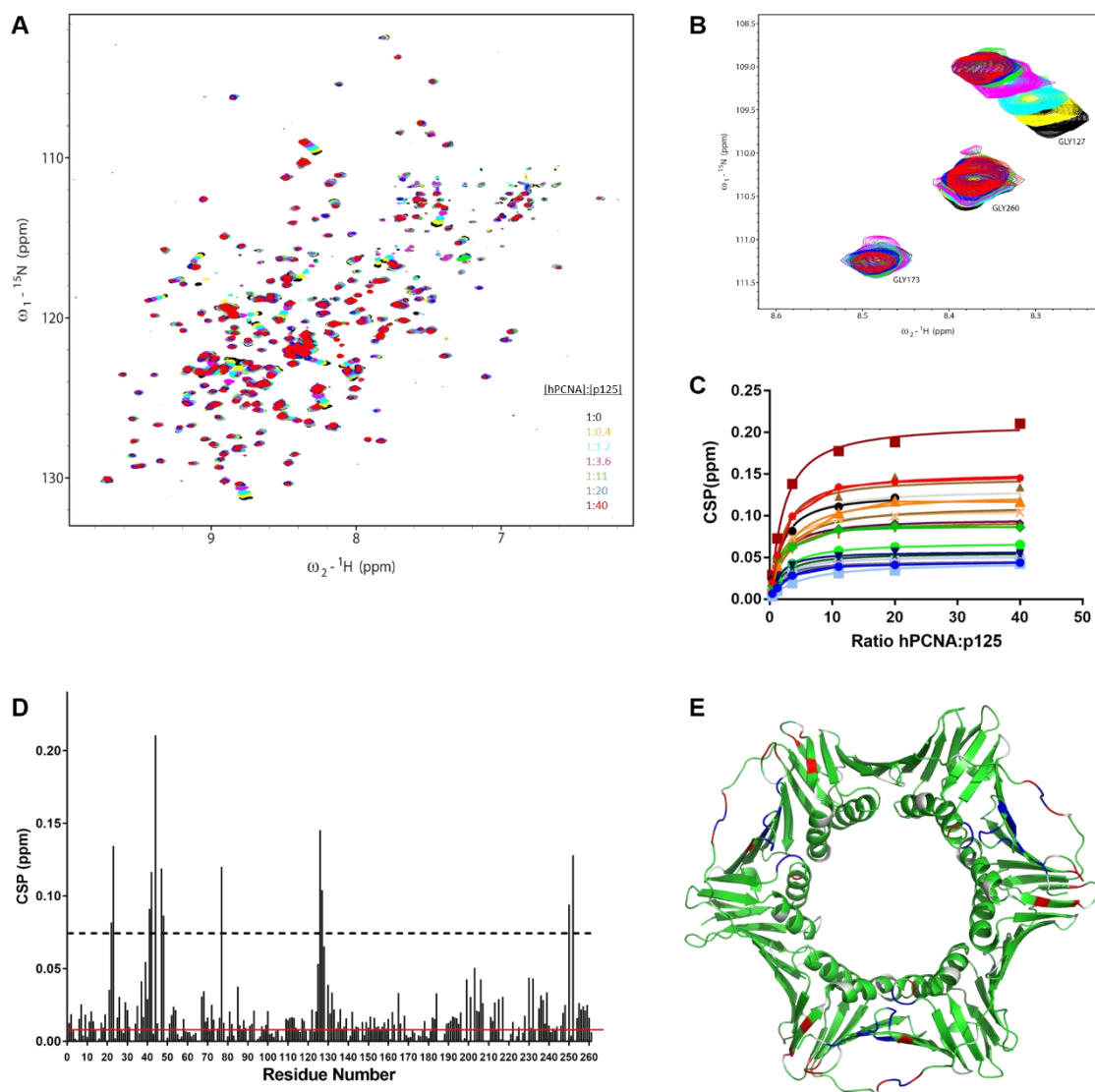


Figure R40: NMR analysis of the p125⁹⁹⁶⁻¹⁰¹⁰ interaction with PCNA. (A) Superposition of ${}^1\text{H}$ - ${}^{15}\text{N}$ TROSY spectra of 60 μM PCNA in the absence (black) and increasing concentrations (different colors) of p125⁹⁹⁶⁻¹⁰¹⁰ peptide. Spectra were acquired at 35°C in PBS pH 7.0. (B) Region of the NMR spectra displayed in A showing the shift of the G127 signal. (C) The CSP of residues with a combined ${}^1\text{H}$ and ${}^{15}\text{N}$ CSP of the backbone amide signal larger than the average plus one standard deviation is represented at different p125:PCNA ratios. The symbols correspond to the experimental data and the continuous line to the best fit to a model of one set of identical binding sites. (D) Bar plot of the measured CSPs along the PCNA sequence. The dashed line indicates the average plus one standard deviation. The red line indicates the estimated error in the calculated CSP (± 0.005 ppm). (E) Mapping of the CSPs on the three-dimensional structure of the complex formed by PCNA and the PIP-box peptide of p125.

Discussion

1. Characterization of the interaction between USP29 and PCNA

The DNA Damage Response comprises different pathways that have been extensively studied. However, when it comes to the DNA Damage Tolerance mechanisms the information becomes scarcer and sometimes contradictory.

Until now it has been reported that PCNA is polyubiquitinated by K63 chains upon the mono-ubiquitinated K164 of PCNA to activate an error-free tolerance pathway in mammals (Hoegge et al., 2002; Vujanovic et al., 2017). The E2/E3 ligases responsible for the poly-ubiquitination of PCNA have been identified (Kanao & Masutani, 2017; Motegi et al., 2008; Unk et al., 2010). PCNA poly-Ub seems to be a key factor in template switching (Chiu et al., 2006).

Nevertheless, some lines of thought differ in the relevance that ubiquitination has in the DDT mechanisms. In contrast to earlier work, there is new evidence suggesting that polymerase switching between Pol δ and Pol η , occurs independently of PCNA ubiquitination (Hedglin et al., 2016). Moreover, a study performed with PCNA-ubiquitin fusion proteins claimed that poly-Ub PCNA is not required to protect cells from genotoxic stress by DNA damage bypass (Gervai et al., 2017).

The template switching pathway remains to be fully understood. One of the unknowns is the protein or protein complex responsible for the de-poly-Ubiquitination of PCNA. USP1, the DUB responsible for de-mono-Ubiquitinating PCNA during TLS, has been proposed to de-poly-Ubiquitinate PCNA (Brun et al., 2010; Motegi et al., 2008). This study showed that when silencing USP1, both mono-Ub PCNA and poly-Ub PCNA decreased. However, it cannot be concluded that USP1 is negatively regulating both events since poly-Ub PCNA is most probably the consequence of mono-Ub PCNA Ub-chain extension.

In a screen overexpressing many human DUBs, USP29 was reported to reverse ubiquitination of PCNA (Mosbech et al., 2013), however no experimental data was shown in the publication. A later proteomics study in our laboratory identified USP29 as a PCNA interacting DUB, suggesting that PCNA was a target of USP29. The already known targets of USP29 have been reported to be protected from proteasomal degradation (Liu et al., 2011; Martín et al., 2015;

Mosbech et al., 2013; Schober et al., 2020). The results presented in this thesis, confirm the USP29-PCNA interaction (Figure R1) and a role of USP29 in PCNA de-poly-ubiquitination when over-expressing USP29 (Figure R2). However, no increasing in poly-Ub PCNA was detected when silencing USP29 (Figure R3). Upon genotoxic stress PCNA is poly-ubiquitinated, however, the silencing of USP29, as it happens when over-expressing catalytically inactive USP29 (Figure R2B), does not have to necessarily increase those poly-Ub levels. While the activity of USP29 can reduce poly-Ub PCNA, the silencing of USP29, hence its inactivity, could simply not affect poly-Ub PCNA. Further studies will be required to address the USP29/PCNA interaction in the cellular response to DNA damage.

Our initial hypothesis that the USP29 canonical PIP motif was the site of interaction with PCNA has not been confirmed. Our results show that fragments containing this sequence bind PCNA with an extremely low affinity, and the same happens with the two other non-canonical PIP motifs. Our co-immunoprecipitation experiments indicated that the PH domain of USP29 contains the site for interaction with PCNA. Indeed, the PH domains have been reported to play role in protein-protein interactions (Drugan et al., 2000). However, the PH domain does not have a recognisable PIP box motif, and further structural characterization of the USP29-PCNA interaction with PCNA was not possible because of the unsuccessful attempts to purify full-length USP29 or its isolated PH domain.

2. USP29 regulation

In this thesis it has been shown that USP29 oligomerizes inside cells via its PH domain (Figure R16), and that oligomerization is necessary for USP29's activity (Figure R20).

Since the structure of the isolated PH domain of the homologous USP37 shows a dimer, it is likely that the PH domain of USP29 also forms dimers.

USP29 is able to stabilize USP29PH by protecting it from proteasome-mediated degradation (Figure R19B & C). Thus, it is tempting to speculate that USP29PH domain contains ubiquitinated lysines. Since the PH domain lacks the catalytic centre, it can also be speculated that upon dimerization, USP29 suffers a conformational change that intramolecularly (in a cis-manner) activates the protomer. In contrast, USP29 protein levels decreased upon increasing amounts of ectopic USP29PH (Figure R20A). Moreover, the presence of USP29PH also decreased hypoxia-induced HIF1- α protein levels (Figure R20B). These results suggest that USP29 is catalytically active in an intermolecular way (in a trans-manner) and therefore, USP29PH acts as a dominant negative.

We propose that USP29 forms its catalytic centre intramolecularly, while deubiquitinates itself in a trans-manner (Figure D1). This model of the USP29 activity mechanism could also be postulated for the manner in which USP29 acts upon its substrates. Once USP29 is stable, USP29 could bind its target proteins via the PH domain, as it does in the case of PCNA (Figure R14) and deubiquitinate the proteins intermolecularly.

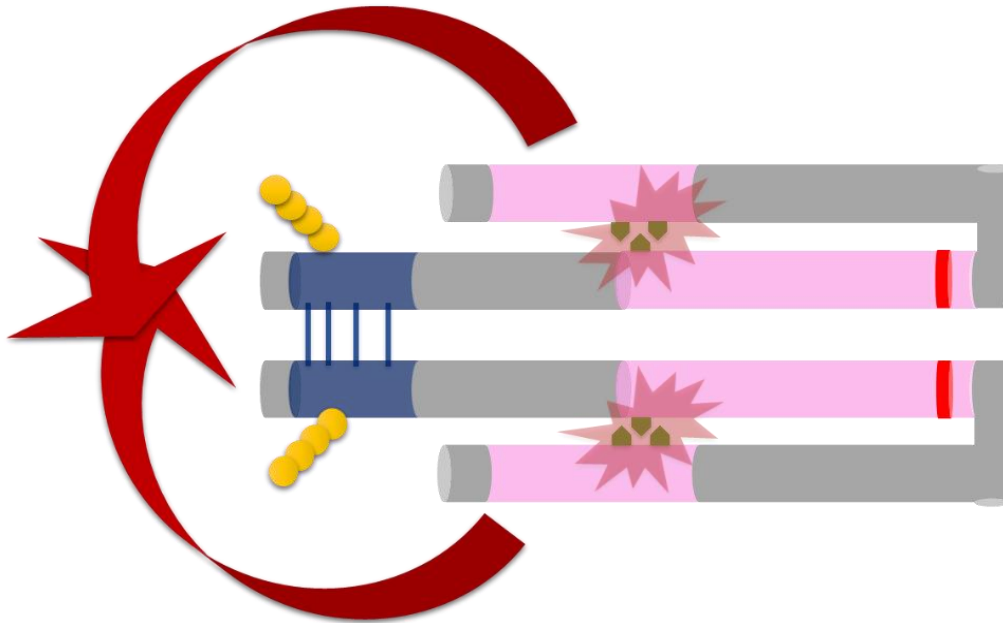


Figure D1: Model for USP29 activity mechanism. In blue the PH domains of two USP29 molecules are interacting (through unknown residues, the lines), forming a dimer. In pink the bipartite catalytic domain of USP29 is shown. Each monomer of USP29 forms its catalytic active site intramolecularly, building the catalytic triad (pink stars). Once each monomer is active, it deubiquitinates the other intermolecularly (red arrows), stabilizing the whole USP29 molecule.

This working model of USP29 activity is not unique among DUBs. Indeed, similarly to USP29, USP19 has been described to self-associate and remove its own poly-Ubiquitin chains to control protein stability (Mei, Hahn, Hu, & Yang, 2011). Another two DUBs have also shown auto-deubiquitination capacities: UCH-L1 and USP4. In these examples, however, the ubiquitination affects their activity and not their stability (Meray & Lansbury, 2007; Wijnhoven et al., 2015), as is the case of USP29, where ubiquitination affects the protein stability and consequently, its activity.

Although homology modelling based on USP37 PH domain suggests a dimerization site, this could not be experimentally confirmed. Mutation of three residues of the putative interface do not cause a loss of USP29 activity (Figure R18). Further mutagenesis experiments may be needed.

As USP29 dimer/oligomerization is required for USP29 activity and USP29 reduces poly-Ub PCNA (Figure R2B), which impairs the activation of a DNA

Damage Tolerance error-free pathway of for replicating cells, one approach to inhibit USP29 downstream effects could be the design of a specific peptide that could impede the interaction between USP29 molecules through their PH domains. This approach might be more specific than using drugs to target USP29's catalytic domain, since cysteine proteases are quite common. Nevertheless, a crystal structure of the USP29PH would be necessary to design such a peptide, and this needs the preparation of pure protein, which we have not been able to achieve.

3. Structural analysis of USP29

Different strategies have been used to express and purify the USP29 protein and its isolated PH domain, but, none of them were successful, because of non-detectable expression levels or expression as insoluble protein. Full length USP29 is a large protein, with multiple domains and long (predicted) disordered regions, and it was anticipated that expression and purification of this protein would be challenging.

The model structure of full-length USP29 (based on sequence homology with different domains of structurally characterised proteins and on disorder predictions) show a possible arrangement of two protomers dimerizing through the PH domains. While some features of the model are consistent with available experimental information on USP29 and other DUBs (for instance, the spatial disposition of the residues involved in the catalytic centre), other features have not been experimentally confirmed (like the dimerization site). The model also fails to offer insights on the regulation of USP29 enzymatic activity by the PH domain.

The USP29 fragment corresponding to the PH domain is a small polypeptide that was expressed at high levels in bacterial cells but could only be solubilised in very harsh denaturant conditions and could not be refolded. This result was not that expected because PH domains of many different proteins have already been prepared for structural studies, including the PH domain of USP37. Our results indicate that the PH domain of USP29, as defined by sequence homology, is not an autonomously folding unit. Perhaps additional residues at the C-terminal end should be included. Alternatively, it may be that it is stable only in association with subcellular structures, like chromatin or membranes.

Apart from mediating protein-protein interactions, the PH domain has also been extensively described as a binding domain for the polar heads of membrane lipids, and many of the proteins that contain a PH domain have to interact with membranes for their function (Riddihough, 1994). Based on our dimeric USP29PH model and the available data (Harlan et al., 1994; Riddihough, 1994), different phosphoinositide binding pockets within our model structure have been

predicted. In Figure D2 different phospholipids are shown in the potential phospholipid binding pocket of USP29PH. In this region USP29PH has four positive charged residues (K21, K23, K46 and R49) similarly to PEPP1 (Phosphoinositol 3-phosphate binding protein-1, PDB 1upr) PH domain (Yamamoto et al., 2016). There is a second potential phosphoinositol binding pocket where USP29PH has 5 positively charged residues (K21, K23, K66, K67 and R68), similar to the β -spectrin PH domain (PDB 1btn) phosphoinositol binding pocket.

A potential phosphotyrosine-binding (PTB) site in the model structure of USP29PH has also been predicted (Figure D2). The PTB site has been described to mediate protein-protein interactions in signal transduction (Zhou & Fesik, 1995), and some PH domains have a relevant role in intracellular signal transduction (Yingyao Zhou & Abagyan, 1998).

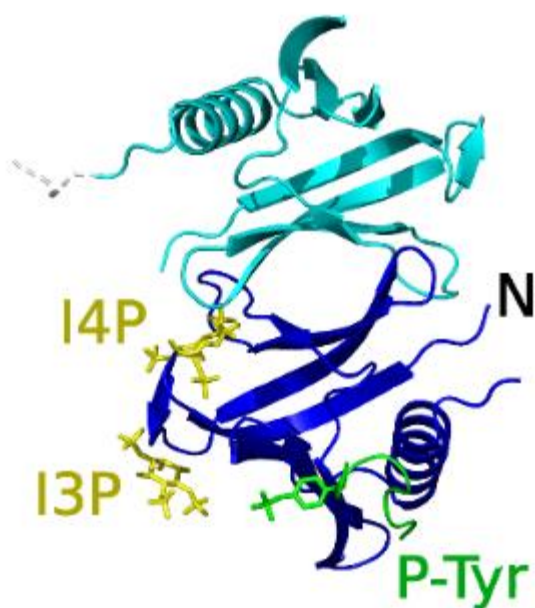


Figure D2: Representation of phospholipid pockets that could be present in the PH domain of USP29. A model of a PH dimer is used to show where the different phosphoinositides could be bound. In yellow Phosphoinositol 3-phosphate and Phosphoinositol 4-phosphate. In green the possible phosphotyrosine containing peptide, taken from Dok7 (docking protein 7, PDB 3ml4).

4. Characterization of the interaction between p125 and PCNA

Mammalian Pol δ was identified forty years ago (Byrnes et al., 1976). However, the architecture of this essential enzyme remained poorly understood until very recently, limiting our understanding of how Pol δ achieves processivity in DNA synthesis and how it interacts with PCNA. Early studies reported a direct interaction between p125 and PCNA (Zhang et al., 1995, 1999), but the p125-PCNA complex has low processivity *in vitro* (Yajing Zhou et al., 2012), suggesting that the interaction is weak. Our results using the p125⁹⁹⁶⁻¹⁰¹⁰ fragment show that p125 recognizes PCNA through a divergent PIP-box located at the flexible C-terminus of the catalytic domain with a dissociation constant of $103 \pm 14 \mu\text{M}$ at 35 °C and a 1:1 stoichiometry (peptide:PCNA protomer). This affinity is much lower than the affinity of the Pol δ complex for PCNA encircling DNA (dissociation constant $<10 \text{ nM}$) (Hedglin et al., 2016). The affinity of PCNA for fragments of other Pol δ subunits is also much lower than the global one. The affinity measured for a p12 is $38 \pm 4 \mu\text{M}$ at 25 °C (Gonzalez-Magaña et al., 2019) and $1.5 \mu\text{M}$ for p68 at 30 °C (Bruning & Shamo, 2004). These results suggest that besides the PIP boxes, other regions of the subunits of Pol δ may be involved in the interaction with PCNA. However, the direct interaction of Pol δ with the DNA will also contribute to the overall binding affinity.

A possible reason for the low affinity between p125 with PCNA compared with the binding affinities between PCNA and other Pol δ subunits could be the TLS mechanism in which the dissociation capacity of p125 from Pol δ plays a key role. After the replication fork stall upon DNA damage, the catalytic subunit p125 of Pol δ has to be replaced in a quick manner by the subunits Rev3-Rev7 of Pol ζ , promoting the effective switch from a DNA replication polymerase to a TLS polymerase (Leung et al., 2019).

Very recently the cryoEM structure of the Pol δ bound to PCNA and DNA at 3.0 Å resolution has been published (Lancey et al., 2020). In this structure Pol δ interacts with only one of the PCNA protomers through two regions of the p125 subunit: the divergent PIP-box contained in the p125⁹⁹⁶⁻¹⁰¹⁰ fragment (bound to the PIP-box site on the PCNA front face), and a short β -sheet spanning residues 991 to 995. The PIP-boxes of the p68 and p12 subunits, located at the extreme

C-terminus and N-terminus, respectively, are both in flexible regions invisible in the cryo-EM map. However, it can be speculated that both PIP-boxes possess a capture radius able to reach one of the unoccupied PCNA sites. Primer extension assays on p125 PIP-box mutants showed a severe activity reduction, while a minimal effect occurred when mutating the PIP-boxes of p68 and p12. Polymerase processivity assays on PIP-box mutants showed a severe defect in the case of p125 followed by p12 and no detectable effect in p68. The binding of Pol δ to only one PIP-box site of PCNA during synthesis may explain the dynamic processivity of the replisome, where the polymerase from solution can exchange the replisome-associated Pol δ (Lewis et al., 2020).

The p125⁹⁹⁶⁻¹⁰¹⁰ fragment binds to the same PCNA site as does the corresponding region of p125 in the context of Pol δ holoenzyme, but with a different affinity and stoichiometry. These observations point to the limitations of protein-protein interaction studies using small peptides.

Conclusions

1. USP29 interacts with both native (*in cellulo*) and recombinantly produced PCNA.
2. The ectopic expression of USP29 decreases PCNA poly-Ubiquitination upon a replication stress. Moreover, PCNA de-ubiquitination depends on the catalytic activity of USP29.
3. USP29 Pleckstrin Homology domain mediates the interaction between USP29 and PCNA.
4. USP29 forms dimers/oligomers via its Pleckstrin Homology domain, which is necessary and sufficient for such dimerization.
5. USP29 dimerization is required for its activity as the ectopic expression of USP29PH acts as a dominant negative mutant.
6. The C-terminal fragment of the catalytic subunit of the human polymerase δ (p125⁹⁹⁶⁻¹⁰⁰⁹) binds the PIP-box site on the PCNA front face through a divergent PIP box motif and with a dissociation constant of $103 \pm 14 \mu\text{M}$ at 35°C .

Bibliography

- Acharya, N., Klassen, R., Johnson, R. E., Prakash, L., & Prakash, S. (2011). PCNA binding domains in all three subunits of yeast DNA polymerase δ modulate its function in DNA replication. *Proceedings of the National Academy of Sciences*, *108*(44), 17927–17932. <https://doi.org/10.1073/PNAS.1109981108>
- Aguilera, A., & García-Muse, T. (2013). Causes of Genome Instability. *Annual Review of Genetics*, *47*(1), 1–32. <https://doi.org/10.1146/annurev-genet-111212-133232>
- Akutsu, M., Dikic, I., & Bremm, A. (2016). Ubiquitin chain diversity at a glance. *Journal of Cell Science*, *129*(5), 875–880. <https://doi.org/10.1242/jcs.183954>
- Baranovskiy, A. G., Duong, V. N., Babayeva, N. D., Zhang, Y., Pavlov, Y. I., Anderson, K. S., & Tahirov, T. H. (2018). Activity and fidelity of human DNA polymerase depend on primer structure. *Journal of Biological Chemistry*, *293*(18), 6824–6843. <https://doi.org/10.1074/jbc.RA117.001074>
- Bell, S. P., & Labib, K. (2016). Chromosome duplication in *Saccharomyces cerevisiae*. *Genetics*, *203*(3), 1027–1067. <https://doi.org/10.1534/genetics.115.186452>
- Bi, X., Barkley, L. R., Slater, D. M., Tateishi, S., Yamaizumi, M., Ohmori, H., & Vaziri, C. (2006). Rad18 Regulates DNA Polymerase and Is Required for Recovery from S-Phase Checkpoint-Mediated Arrest. *Molecular and Cellular Biology*, *26*(9), 3527–3540. <https://doi.org/10.1128/mcb.26.9.3527-3540.2006>
- Bi, Xin. (2015). Mechanism of DNA damage tolerance. *World Journal of Biological Chemistry*, *6*(3), 48. <https://doi.org/10.4331/wjbc.v6.i3.48>
- Bienko, M., Green, catherine M., Crosetto, N., Rudolf, F., Zapart, G., Coull, B., ... Dikic, I. (2005). Ubiquitin-binding domains in Y-family polymerases regulate translesion synthesis. *Science*, *310*(5755), 1821–1824. <https://doi.org/10.1210/jcem-10-10-1361>
- Branzei, D., & Foiani, M. (2008). Regulation of DNA repair throughout the cell cycle. *Nature Reviews Molecular Cell Biology*, *9*(4), 297–308. <https://doi.org/10.1038/nrm2351>
- Branzei, D., & Psakhye, I. (2016). DNA damage tolerance. *Current Opinion in Cell Biology*, *40*, 137–144. <https://doi.org/10.1016/j.ceb.2016.03.015>
- Branzei, D., & Szakal, B. (2016). DNA damage tolerance by recombination: Molecular pathways and DNA structures. *DNA Repair*, *44*, 68–75. <https://doi.org/10.1016/j.dnarep.2016.05.008>
- Bravo, R., & Celis, J. E. (1980). A search for differential polypeptide synthesis throughout the cell cycle of HeLa cells. *The Journal of Cell Biology*, *84*(3), 795–802.
- Brown, S., Niimi, A., & Lehmann, A. R. (2009). Ubiquitination and deubiquitination of PCNA in response to stalling of the replication fork. *Cell*

- Cycle*, 8(5), 689–692. <https://doi.org/10.4161/cc.8.5.7707>
- Bruck, I., Perez-Arnaiz, P., Colbert, M. K., & Kaplan, D. L. (2015). Insights into the initiation of eukaryotic DNA replication. *Nucleus*, 6(6), 449–454. <https://doi.org/10.1080/19491034.2015.1115938>
- Brun, J., Chiu, R. K., Wouters, B. G., & Gray, D. A. (2010). Regulation of PCNA polyubiquitination in human cells. *BMC Research Notes*, 3, 2–7. <https://doi.org/10.1186/1756-0500-3-85>
- Bruning, J. B., & Shamoo, Y. (2004). Structural and thermodynamic analysis of human PCNA with peptides derived from DNA polymerase- δ p66 subunit and flap endonuclease-1. *Structure*, 12(12), 2209–2219. <https://doi.org/10.1016/j.str.2004.09.018>
- Burkovics, P., Dome, L., Juhasz, S., Altmannova, V., Sebesta, M., Pacesa, M., ... Krejci, L. (2016). The PCNA-associated protein PARI negatively regulates homologous recombination via the inhibition of DNA repair synthesis. *Nucleic Acids Research*, 44(7), 3176–3189. <https://doi.org/10.1093/nar/gkw024>
- Byrnes, J. J., Downey, K. M., Black, V. L., & So, A. G. (1976). A New Mammalian DNA Polymerase with 3' to 5' Exonuclease Activity: DNA Polymerase δ . *Biochemistry*, 15(13), 2817–2823. <https://doi.org/10.1021/bi00658a018>
- Cazzalini, O., Sommatitis, S., Tillhon, M., Dutto, I., Bachi, A., Rapp, A., ... Prosperi, E. (2014). CBP and p300 acetylate PCNA to link its degradation with nucleotide excision repair synthesis. *Nucleic Acids Research*, 42(13), 8433–8448. <https://doi.org/10.1093/nar/gku533>
- Chang, D. J., & Cimprich, K. A. (2009). DNA damage tolerance: When it's OK to make mistakes. *Nature Chemical Biology*, 5(2), 82–90. <https://doi.org/10.1038/nchembio.139>
- Chang, D. J., Lupardus, P. J., & Cimprich, K. A. (2006). Monoubiquitination of proliferating cell nuclear antigen induced by stalled replication requires uncoupling of DNA polymerase and mini-chromosome maintenance helicase activities. *Journal of Biological Chemistry*, 281(43), 32081–32088. <https://doi.org/10.1074/jbc.M606799200>
- Chau, V., Tobias, J. W., Bachmair, A., Marriotr, D., Ecker, D. J., Gonda, D. K., & Varshavsky, A. (1989). Targeted to Specific Protein UX-E. *Science*, 243(1982), 1576–1583.
- Chiu, R. K., Brun, J., Ramaekers, C., Theys, J., Weng, L., Lambin, P., ... Wouters, B. G. (2006). Lysine 63-polyubiquitination guards against translesion synthesis-induced mutations. *PLoS Genetics*, 2(7), 1070–1083. <https://doi.org/10.1371/journal.pgen.0020116>
- Clague, M. J., Barsukov, I., Coulson, J. M., Liu, H., Rigden, D. J., & Urbé, S. (2013). Deubiquitylases from genes to organism. *Physiological Reviews*, 93(3), 1289–1315. <https://doi.org/10.1152/physrev.00002.2013>
- Clague, M. J., Urbé, S., & Komander, D. (2019). Breaking the chains:

deubiquitylating enzyme specificity begets function. *Nature Reviews Molecular Cell Biology*, 20(6), 338–352. <https://doi.org/10.1038/s41580-019-0099-1>

- Cohn, M. A., Kowal, P., Yang, K., Haas, W., Huang, T. T., Gygi, S. P., & D'Andrea, A. D. (2007). A UAF1-Containing Multisubunit Protein Complex Regulates the Fanconi Anemia Pathway. *Molecular Cell*, 28(5), 786–797. <https://doi.org/10.1016/j.molcel.2007.09.031>
- De Biasio, A., & Blanco, F. J. (2013). Proliferating cell nuclear antigen structure and interactions: Too many partners for one dancer? In *Advances in Protein Chemistry and Structural Biology* (1st ed., Vol. 91). <https://doi.org/10.1016/B978-0-12-411637-5.00001-9>
- De Biasio, A., Campos-Olivas, R., Sánchez, R., López-Alonso, J. P., Pantoja-Uceda, D., Merino, N., ... Blanco, F. J. (2012). Proliferating cell nuclear antigen (PCNA) interactions in solution studied by NMR. *PLoS One*, 7(11). <https://doi.org/10.1371/journal.pone.0048390>
- De Biasio, A., De Opakua, A. I., Mortuza, G. B., Molina, R., Cordeiro, T. N., Castillo, F., ... Blanco, F. J. (2015). Structure of p15PAF-PCNA complex and implications for clamp sliding during DNA replication and repair. *Nature Communications*, 6. <https://doi.org/10.1038/ncomms7439>
- de Biasio, A., Sánchez, R., Prieto, J., Villate, M., Campos-Olivas, R., & Blanco, F. J. (2011). Reduced stability and increased dynamics in the human Proliferating Cell Nuclear Antigen (PCNA) relative to the yeast homolog. *PLoS ONE*, 6(2). <https://doi.org/10.1371/journal.pone.0016600>
- De March, M., Merino, N., Barrera-Vilarmau, S., Crehuet, R., Onesti, S., Blanco, F. J., & De Biasio, A. (2017). Structural basis of human PCNA sliding on DNA. *Nature Communications*, 8. <https://doi.org/10.1038/ncomms13935>
- Downing, A. K., Driscoll, P. C., Gout, I., Salim, K., Zvelebil, M. J., & Waterfield, M. D. (1994). Three-dimensional solution structure of the pleckstrin homology domain from dynamin. *Current Biology*, 4(10), 884–891. [https://doi.org/10.1016/S0960-9822\(00\)00197-4](https://doi.org/10.1016/S0960-9822(00)00197-4)
- Drugan, J. K., Rogers-Graham, K., Gilmer, T., Campbell, S., & Clark, G. J. (2000). The Ras/p120 GTPase-activating protein (GAP) interaction is regulated by the p120 GAP pleckstrin homology domain. *Journal of Biological Chemistry*, 275(45), 35021–35027. <https://doi.org/10.1074/jbc.M004386200>
- Edmunds, C. E., Simpson, L. J., & Sale, J. E. (2008). PCNA Ubiquitination and REV1 Define Temporally Distinct Mechanisms for Controlling Translesion Synthesis in the Avian Cell Line DT40. *Molecular Cell*, 30(4), 519–529. <https://doi.org/10.1016/j.molcel.2008.03.024>
- Elia, A. E. H., Boardman, A. P., Wang, D. C., Huttlin, E. L., Everley, R. A., Dephoure, N., ... Elledge, S. J. (2015). Quantitative Proteomic Atlas of Ubiquitination and Acetylation in the DNA Damage Response. *Molecular Cell*, 59(5), 867–881. <https://doi.org/10.1016/j.molcel.2015.05.006>
- Emsley, P., Lohkamp, B., Scott, W. G., & Cowtan, K. (2010). Features and

development of Coot. *Acta Crystallographica Section D: Biological Crystallography*, 66(4), 486–501.
<https://doi.org/10.1107/S0907444910007493>

- Evrin, C., Fernández-Cid, A., Riera, A., Zech, J., Clarke, P., Herrera, M. C., ... Speck, C. (2014). The ORC/Cdc6/MCM2-7 complex facilitates MCM2-7 dimerization during prereplicative complex formation. *Nucleic Acids Research*, 42(4), 2257–2269. <https://doi.org/10.1093/nar/gkt1148>
- Fan, J., Otterlei, M., Wong, H. K., Tomkinson, A. E., & Wilson, D. M. (2004). XRCC1 co-localizes and physically interacts with PCNA. *Nucleic Acids Research*, 32(7), 2193–2201. <https://doi.org/10.1093/nar/gkh556>
- Finger, D., Atack, J. M., Tsutakawa, S., Classen, S., Tainer, T., Grasby, J., & Shen, B. (2012). The Wonders of Flap Endonucleases: Structure, Function, Mechanism and Regulation. *Subcellular Biochemistry*, 62, 301–326. <https://doi.org/10.1007/978-94-007-4572-8>
- Finley, D., Ulrich, H. D., Sommer, T., & Kaiser, P. (2012). The ubiquitin-proteasome system of *Saccharomyces cerevisiae*. *Genetics*, 192(2), 319–360. <https://doi.org/10.1534/genetics.112.140467>
- Freudenthal, B. D., Gakhar, L., Ramaswamy, S., & Washington, M. T. (2009). A charged residue at the subunit interface of PCNA promotes trimer formation by destabilizing alternate subunit interactions. *Acta Crystallographica Section D: Biological Crystallography*, 65(6), 560–566. <https://doi.org/10.1107/S0907444909011329>
- Friedberg, E. C. (2005). Suffering in silence: The tolerance of DNA damage. *Nature Reviews Molecular Cell Biology*, 6(12), 943–953. <https://doi.org/10.1038/nrm1781>
- Gali, H., Juhasz, S., Morocz, M., Hajdu, I., Fatyol, K., Szukacsov, V., ... Haracska, L. (2012). Role of SUMO modification of human PCNA at stalled replication fork. *Nucleic Acids Research*, 40(13), 6049–6059. <https://doi.org/10.1093/nar/gks256>
- Gary, R., Ludwig, D. L., Cornelius, H. L., MacInnes, M. A., & Park, M. S. (1997). The DNA repair endonuclease XPG binds to proliferating cell nuclear antigen (PCNA) and shares sequence elements with the PCNA-binding regions of FEN-1 and cyclin-dependent kinase inhibitor p21. *Journal of Biological Chemistry*, 272(39), 24522–24529. <https://doi.org/10.1074/jbc.272.39.24522>
- Gasteiger, E., Gattiker, A., Hoogland, C., Ivanyi, I., Appel, R. D., & Bairoch, A. (2003). ExPASy: The proteomics server for in-depth protein knowledge and analysis. *Nucleic Acids Research*, 31(13), 3784–3788. <https://doi.org/10.1093/nar/gkg563>
- Gervai, J. Z., Gálicza, J., Szeltner, Z., Zámorszky, J., & Szüts, D. (2017). A genetic study based on PCNA-ubiquitin fusions reveals no requirement for PCNA polyubiquitylation in DNA damage tolerance. *DNA Repair*, 54, 46–54. <https://doi.org/10.1016/j.dnarep.2017.04.003>
- Gilljam, K. M., Feyzi, E., Aas, P. A., Sousa, M. M. L., Müller, R., Vågbo, C. B.,

- ... Otterlei, M. (2009). Identification of a novel, widespread, and functionally important PCNA-binding motif. *Journal of Cell Biology*, 186(5), 645–654. <https://doi.org/10.1083/jcb.200903138>
- Gonzalez-Magaña, A., De Opakua, A. I., Romano-Moreno, M., Murciano-Calles, J., Merino, N., Luque, I., ... De Biasio, A. (2019). The p12 subunit of human polymerase uses an atypical PIP box for molecular recognition of proliferating cell nuclear antigen (PCNA). *Journal of Biological Chemistry*, 294(11), 3947–3956. <https://doi.org/10.1074/jbc.RA118.006391>
- Gulbis, J. M., Kelman, Z., Hurwitz, J., O'Donnell, M., & Kuriyan, J. (1996). Structure of the C-terminal region of p21(WAF1/CIP1) complexed with human PCNA. *Cell*, 87(2), 297–306. [https://doi.org/10.1016/S0092-8674\(00\)81347-1](https://doi.org/10.1016/S0092-8674(00)81347-1)
- Guzzo, C. M., & Matunis, M. J. (2013). Expanding SUMO and ubiquitin-mediated signaling through hybrid SUMO-ubiquitin chains and their receptors. *Cell Cycle*, 12(7), 1015–1017. <https://doi.org/10.4161/cc.24332>
- Haglund, K., Sigismund, S., Polo, S., Szymkiewicz, I., Di Fiore, P. P., & Dikic, I. (2003). Multiple monoubiquitination of RTKs is sufficient for their endocytosis and degradation. *Nature Cell Biology*, 5(5), 461–466. <https://doi.org/10.1038/ncb983>
- Harlan, J. E., Hajduk, P. J., Yoon, H. S., & Fesik, S. W. (1994). Pleckstrin homology domains bind to phosphatidylinositol-4,5-bisphosphate. *Nature*, Vol. 371, pp. 168–170. <https://doi.org/10.1038/371168a0>
- Havens, C. G., & Walter, J. C. (2009). Docking of a Specialized PIP Box onto Chromatin-Bound PCNA Creates a Degron for the Ubiquitin Ligase CRL4Cdt2. *Molecular Cell*, 35(1), 93–104. <https://doi.org/10.1016/j.molcel.2009.05.012>
- He, H., & Kim, J. (2014). Regulation and Function of the Peg3 Imprinted Domain. *Genomics & Informatics*, 12(3), 105. <https://doi.org/10.5808/gi.2014.12.3.105>
- He, H., Ye, A., & Kim, J. (2016). Transcriptional truncation of the long coding imprinted gene Usp29. *PLoS ONE*, 11(6), 1–14. <https://doi.org/10.1371/journal.pone.0158004>
- Hedglin, M., & Benkovic, S. J. (2015). Regulation of Rad6/Rad18 Activity During DNA Damage Tolerance. *Annual Review of Biophysics*, 44(1), 207–228. <https://doi.org/10.1146/annurev-biophys-060414-033841>
- Hedglin, M., & Benkovic, S. J. (2017). Replication Protein A Prohibits Diffusion of the PCNA Sliding Clamp along Single-Stranded DNA. *Biochemistry*, 56(13), 1824–1835. <https://doi.org/10.1021/acs.biochem.6b01213>
- Hedglin, M., Pandey, B., & Benkovic, S. J. (2016). Characterization of human translesion DNA synthesis across a UV-induced DNA lesion. *ELife*, 5(OCTOBER2016), 1–18. <https://doi.org/10.7554/eLife.19788>
- Hershko, A., Heller, H., Elias, S., & Ciechanover, A. (1983). Components of ubiquitin-protein ligase system. Resolution, affinity purification, and role in

- protein breakdown. *Journal of Biological Chemistry*, 258(13), 8206–8214.
- Hicke, L. (2001). Protein regulation by monoubiquitin. *Nature Reviews Molecular Cell Biology*, 2(3), 195–201. <https://doi.org/10.1038/35056583>
- Hishiki, A., Hashimoto, H., Hanafusa, T., Kamei, K., Ohashi, E., Shimizu, T., ... Sato, M. (2009). Structural basis for novel interactions between human translesion synthesis polymerases and proliferating cell nuclear antigen. *Journal of Biological Chemistry*, 284(16), 10552–10560. <https://doi.org/10.1074/jbc.M809745200>
- Hoegel, C., Pfander, B., Moldovan, G. L., Pyrowolakis, G., & Jentsch, S. (2002). RAD6-dependent DNA repair is linked to modification of PCNA by ubiquitin and SUMO. *Nature*, 419(6903), 135–141. <https://doi.org/10.1038/nature00991>
- Hofmann, K., & Falquet, L. (2001). A ubiquitin-interacting motif conserved in components of the proteasomal and lysosomal protein degradation systems. *Trends in Biochemical Sciences*, 26(6), 347–350. [https://doi.org/10.1016/S0968-0004\(01\)01835-7](https://doi.org/10.1016/S0968-0004(01)01835-7)
- Hu, M., Li, P., Li, M., Li, W., Yao, T., Wu, J. W., ... Shi, Y. (2002). Crystal structure of a UBP-family deubiquitinating enzyme in isolation and in complex with ubiquitin aldehyde. *Cell*, 111(7), 1041–1054. [https://doi.org/10.1016/S0092-8674\(02\)01199-6](https://doi.org/10.1016/S0092-8674(02)01199-6)
- Huang, T. T., Nijman, S. M. B., Mirchandani, K. D., Galardy, P. J., Cohn, M. A., Haas, W., ... D'Andrea, A. D. (2006). Regulation of monoubiquitinated PCNA by DUB autocleavage. *Nature Cell Biology*, 8(4), 339–347. <https://doi.org/10.1038/ncb1378>
- Jo, A., Lee, Y., Park, C., & Shin, J. (2020). *Deubiquitinase USP29 Governs MYBBP1A in the Brains of Parkinson ' s Disease Patients*. 1, 1–11.
- Kahli, M., Osmundson, J. S., Yeung, R., & Smith, D. J. (2019). Processing of eukaryotic Okazaki fragments by redundant nucleases can be uncoupled from ongoing DNA replication in vivo. *Nucleic Acids Research*, 47(4), 1814–1822. <https://doi.org/10.1093/nar/gky1242>
- Kanao, R., & Masutani, C. (2017). Regulation of DNA damage tolerance in mammalian cells by post-translational modifications of PCNA. *Mutation Research - Fundamental and Molecular Mechanisms of Mutagenesis*, 803–805, 82–88. <https://doi.org/10.1016/j.mrfmmm.2017.06.004>
- Kashiwaba, S. ichiro, Kanao, R., Masuda, Y., Kusumoto-Matsuo, R., Hanaoka, F., & Masutani, C. (2015). USP7 Is a Suppressor of PCNA Ubiquitination and Oxidative-Stress-Induced Mutagenesis in Human Cells. *Cell Reports*, 13(10), 2072–2080. <https://doi.org/10.1016/j.celrep.2015.11.014>
- Kelley, L. A., Mezulis, S., Yates, C. M., Wass, M. N., & Sternberg, M. J. E. (2015). The Phyre2 web portal for protein modeling, prediction and analysis. *Nature Protocols*, 10(6), 845–858. <https://doi.org/10.1038/nprot.2015.053>
- Kelman, Z., & O'donnell, M. (1995). Structural and functional similarities of

- prokaryotic and eukaryotic DNA polymerase sliding clamps. *Nucleic Acids Research*, 23(23), 4938. <https://doi.org/10.1093/nar/23.23.4938>
- Kim, J., Noskov, V. N., Lu, X., Bergmann, A., Ren, X., Warth, T., ... Stubbs, L. (2000). Discovery of a novel, paternally expressed ubiquitin-specific processing protease gene through comparative analysis of an imprinted region of mouse chromosome 7 and human chromosome 19q13.4. *Genome Research*, 10(8), 1138–1147. <https://doi.org/10.1101/gr.10.8.1138>
- Kleczkowska, H. E., Marra, G., Lettieri, T., & Jiricny, J. (2001). hMSH3 and hMSH6 interact with PCNA and colocalize with it to replication foci. *Genes and Development*, 15(6), 724–736. <https://doi.org/10.1101/gad.191201>
- Kontopidis, G., Wu, S. Y., Zheleva, D. I., Taylor, P., McInnes, C., Lane, D. P., ... Walkinshaw, M. D. (2005). Structural and biochemical studies of human proliferating cell nuclear antigen complexes provide a rationale for cyclin association and inhibitor design. *Proceedings of the National Academy of Sciences of the United States of America*, 102(6), 1871–1876. <https://doi.org/10.1073/pnas.0406540102>
- Krishna, T. S. R., Kong, X. P., Gary, S., Burgers, P. M., & Kuriyan, J. (1994). Crystal structure of the eukaryotic DNA polymerase processivity factor PCNA. *Cell*, 79(7), 1233–1243. [https://doi.org/10.1016/0092-8674\(94\)90014-0](https://doi.org/10.1016/0092-8674(94)90014-0)
- Lancey, C., Tehseen, M., Raducanu, V., Rashid, F., Merino, N., Ragan, T. J., ... Biasio, A. De. (2020). Structure of the processive human Pol delta holoenzyme. *Nature Communications*, 11(1109). <https://doi.org/10.1038/s41467-020-14898-6>
- Lee, K. Y., Yang, K., Cohn, M. A., Sikdar, N., D'Andrea, A. D., & Myung, K. (2010). Human ELG1 regulates the level of ubiquitinated proliferating cell nuclear antigen (PCNA) through its interactions with PCNA and USP1. *Journal of Biological Chemistry*, 285(14), 10362–10369. <https://doi.org/10.1074/jbc.M109.092544>
- Lee, M. Y. W. T., Wang, X., Zhang, S., Zhang, Z., & Lee, E. Y. C. (2017). Regulation and modulation of human dna polymerase δ activity and function. *Genes*, 8(7), 1–30. <https://doi.org/10.3390/genes8070190>
- Leung, W., Baxley, R. M., Moldovan, G. L., & Bielinsky, A. K. (2019). Mechanisms of DNA damage tolerance: post-translational regulation of PCNA. *Genes*, 10(1). <https://doi.org/10.3390/genes10010010>
- Li, Hao, Xie, B., Zhou, Y., Rahmeh, A., Trusa, S., Zhang, S., ... Lee, M. Y. W. T. (2006). Functional Roles of p12, the Fourth Subunit of Human DNA Polymerase δ^* . 281(21), 14748–14755. <https://doi.org/10.1074/jbc.M600322200>
- Li, Hubert, Sandhu, M., Malkas, L. H., Hickey, R. J., & Vaidehi, N. (2017). How Does the Proliferating Cell Nuclear Antigen Modulate Binding Specificity to Multiple Partner Proteins? *Journal of Chemical Information and Modeling*, 57(12), 3011–3021. <https://doi.org/10.1021/acs.jcim.7b00171>
- Li, Huilin, & Stillman, B. (2012). The origin recognition complex: a biochemical

and structural view. *Subcellular Biochemistry*, 62, 37–58.
<https://doi.org/10.1007/978-94-007-4572-8>

- Liu, J., Chung, H. J., Vogt, M., Jin, Y., Malide, D., He, L., ... Levens, D. (2011). JTV1 co-activates FBP to induce USP29 transcription and stabilize p53 in response to oxidative stress. *EMBO Journal*, 30(5), 846–858.
<https://doi.org/10.1038/emboj.2011.11>
- Lo, Y. H., Ho, P. C., & Wang, S. C. (2012). Epidermal growth factor receptor protects proliferating cell nuclear antigen from cullin 4A protein-mediated proteolysis. *Journal of Biological Chemistry*, 287(32), 27148–27157.
<https://doi.org/10.1074/jbc.M112.388843>
- Macias, M. J., Musacchio, A., Ponstingl, H., Nilges, M., Saraste, M., & Oschkinat, H. (1994). Structure of the pleckstrin homology domain from β -spectrin. *Nature*, 369(6482), 675–677. <https://doi.org/10.1038/369675a0>
- Maga, G., & Hübscher, U. (2003). Proliferating cell nuclear antigen (PCNA): A dancer with many partners. *Journal of Cell Science*, 116(15), 3051–3060.
<https://doi.org/10.1242/jcs.00653>
- Martín, Y., Cabrera, E., Amoedo, H., Hernández-Pérez, S., Domínguez-Kelly, R., & Freire, R. (2015). USP29 controls the stability of checkpoint adaptor Claspin by deubiquitination. *Oncogene*, 34(8), 1058–1063.
<https://doi.org/10.1038/onc.2014.38>
- Masuda, Y., Kanao, R., Kaji, K., Ohmori, H., Hanaoka, F., & Masutani, C. (2015). Different types of interaction between PCNA and PIP boxes contribute to distinct cellular functions of Y-family DNA polymerases. *Nucleic Acids Research*, 43(16), 7898–7910.
<https://doi.org/10.1093/nar/gkv712>
- Masuda, Y., & Masutani, C. (2019). Spatiotemporal regulation of PCNA ubiquitination in damage tolerance pathways. *Critical Reviews in Biochemistry and Molecular Biology*, 54(5), 418–442.
<https://doi.org/10.1080/10409238.2019.1687420>
- Mathews, M. B., Bernstein, R. M., Franza, B. R., & Garrels, J. I. (1984). Identity of the proliferating cell nuclear antigen and cyclin. *Nature*, 309(5966), 374–376. <https://doi.org/10.1038/309374a0>
- Matsumoto, M. L., Wickliffe, K. E., Dong, K. C., Yu, C., Bosanac, I., Bustos, D., ... Dixit, V. M. (2010). K11-linked polyubiquitination in cell cycle control revealed by a K11 linkage-specific antibody. *Molecular Cell*, 39(3), 477–484. <https://doi.org/10.1016/j.molcel.2010.07.001>
- McClellan, A. J., Laugesen, S. H., & Ellgaard, L. (2019). Cellular functions and molecular mechanisms of non-lysine ubiquitination. *Open Biology*, 9(9).
<https://doi.org/10.1098/rsob190147>
- Mei, Y., Hahn, A. A., Hu, S., & Yang, X. (2011). The USP19 deubiquitinase regulates the stability of c-IAP1 and c-IAP2. *Journal of Biological Chemistry*, 286(41), 35380–35387.
<https://doi.org/10.1074/jbc.M111.282020>

- Meray, R. K., & Lansbury, P. T. (2007). Reversible monoubiquitination regulates the Parkinson disease-associated ubiquitin hydrolase UCH-L1. *Journal of Biological Chemistry*, 282(14), 10567–10575. <https://doi.org/10.1074/jbc.M611153200>
- Mjelle, R., Hegre, S. A., Aas, P. A., Slupphaug, G., Drabløs, F., Sætrom, P., & Krokan, H. E. (2015). Cell cycle regulation of human DNA repair and chromatin remodeling genes. *DNA Repair*, 30, 53–67. <https://doi.org/10.1016/j.dnarep.2015.03.007>
- Moldovan, G. L., Pfander, B., & Jentsch, S. (2007a). PCNA, the Maestro of the Replication Fork. *Cell*, 129(4), 665–679. <https://doi.org/10.1016/j.cell.2007.05.003>
- Moldovan, G. L., Pfander, B., & Jentsch, S. (2007b). PCNA, the Maestro of the Replication Fork. *Cell*, 129(4), 665–679. <https://doi.org/10.1016/j.cell.2007.05.003>
- Montecucco, A., Rossi, R., Levin, D. S., Gary, R., Park, M. S., Motycka, T. A., ... Tomkinson, A. E. (1998). DNA ligase I is recruited to sites of DNA replication by an interaction with proliferating cell nuclear antigen: Identification of a common targeting mechanism for the assembly of replication factories. *EMBO Journal*, 17(13), 3786–3795. <https://doi.org/10.1093/emboj/17.13.3786>
- Mosbech, A., Lukas, C., Bekker-Jensen, S., & Mailand, N. (2013). The deubiquitylating enzyme USP44 counteracts the DNA double-strand break response mediated by the RNF8 and RNF168 ubiquitin ligases. *Journal of Biological Chemistry*, 288(23), 16579–16587. <https://doi.org/10.1074/jbc.M113.459917>
- Motegi, A., Liaw, H. J., Lee, K. Y., Roest, H. P., Maas, A., Wu, X., ... Myung, K. (2008). Polyubiquitination of proliferating cell nuclear antigen by HLTF and SHPRH prevents genomic instability from stalled replication forks. *Proceedings of the National Academy of Sciences of the United States of America*, 105(34), 12411–12416. <https://doi.org/10.1073/pnas.0805685105>
- Motegi, A., Sood, R., Moinova, H., Markowitz, S. D., Liu, P. P., & Myung, K. (2006). Human SHPRH suppresses genomic instability through proliferating cell nuclear antigen polyubiquitination. *Journal of Cell Biology*, 175(5), 703–708. <https://doi.org/10.1083/jcb.200606145>
- Musacchio, A., Gibson, T., Rice, P., Thompson, J., & Saraste, M. (1993). The PH domain: a common piece in the structural patchwork of signalling proteins. *Trends in Biochemical Sciences*, 18(9), 343–348. [https://doi.org/10.1016/0968-0004\(93\)90071-T](https://doi.org/10.1016/0968-0004(93)90071-T)
- Naryzhny, S. N., & Lee, H. (2004). The post-translational modifications of proliferating cell nuclear antigen: Acetylation, not phosphorylation, plays an important role in the regulation of its function. *Journal of Biological Chemistry*, 279(19), 20194–20199. <https://doi.org/10.1074/jbc.M312850200>
- Neelsen, K. J., & Lopes, M. (2015). Replication fork reversal in eukaryotes: From dead end to dynamic response. *Nature Reviews Molecular Cell*

- Biology*, 16(4), 207–220. <https://doi.org/10.1038/nrm3935>
- Oganesyanyan, N., Ankoudinova, I., Kim, S. H., & Kim, R. (2007). Effect of osmotic stress and heat shock in recombinant protein overexpression and crystallization. *Protein Expression and Purification*, 52(2), 280–285. <https://doi.org/10.1016/j.pep.2006.09.015>
- Okazaki, R., Okazaki, T., Sakabe, K., Sugimoto, K., & Sugino, A. (1968). Mechanism of DNA chain growth. I. Possible discontinuity and unusual secondary structure of newly synthesized chains. *Proceedings of the National Academy of Sciences of the United States of America*, 59(2), 598–605. <https://doi.org/10.1073/pnas.59.2.598>
- Ortega, J., Li, J. Y., Lee, S., Tong, D., Gu, L., & Li, G. M. (2015). Phosphorylation of PCNA by EGFR inhibits mismatch repair and promotes misincorporation during DNA synthesis. *Proceedings of the National Academy of Sciences of the United States of America*, 112(18), 5667–5672. <https://doi.org/10.1073/pnas.1417711112>
- Park, J. M., Yang, S. W., Yu, K. R., Ka, S. H., Lee, S. W., Seol, J. H., ... Chung, C. H. (2014). Modification of PCNA by ISG15 Plays a Crucial Role in Termination of Error-Prone Translesion DNA Synthesis. *Molecular Cell*, 54(4), 626–638. <https://doi.org/10.1016/j.molcel.2014.03.031>
- Park, S. Y., Jeong, M. S., Han, C. W., Yu, H. S., & Jang, S. B. (2016). Structural and functional insight into proliferating cell nuclear antigen. *Journal of Microbiology and Biotechnology*, 26(4), 637–647. <https://doi.org/10.4014/jmb.1509.09051>
- Peng, A., Xu, X., Wang, C., Yang, J., Wang, S., Dai, J., & Ye, L. (2018). EZH2 promotes DNA replication by stabilizing interaction of POL δ and PCNA via methylation-mediated PCNA trimerization. *Epigenetics and Chromatin*, 11(1), 1–14. <https://doi.org/10.1186/s13072-018-0213-1>
- Petroski, M. D., & Deshaies, R. J. (2005). Function and regulation of cullin–RING ubiquitin ligases. *Nature Reviews Molecular Cell Biology*, 6(1), 9–20. <https://doi.org/10.1038/nrm1547>
- Pettersen, E. F., Goddard, T. D., Huang, C. C., Couch, G. S., Greenblatt, D. M., Meng, E. C., & Ferrin, T. E. (2004). UCSF Chimera - A visualization system for exploratory research and analysis. *Journal of Computational Chemistry*, 25(13), 1605–1612. <https://doi.org/10.1002/jcc.20084>
- Pickart, C. M. (2001). Mechanisms underlying ubiquitination. *Annual Review of Biochemistry*, 70, 503–533.
- Pickart, C. M., & Fushman, D. (2004). Polyubiquitin chains: polymeric protein signals. *Current Opinion in Chemical Biology*, 8(6), 610–616. <https://doi.org/10.1016/j.cbpa.2004.09.009>
- Pierce, M. M., Raman, C. S., & Nall, B. T. (1999). <Isothermal Titration Calorimetry of Protein–Protein.pdf>. 221, 213–221.
- Prakash, S., Johnson, R. E., & Prakash, L. (2005). EUKARYOTIC TRANSLESION SYNTHESIS DNA POLYMERASES: Specificity of

- Structure and Function. *Annual Review of Biochemistry*, 74(1), 317–353. <https://doi.org/10.1146/annurev.biochem.74.082803.133250>
- Prestel, A., Wichmann, N., Martins, J. M., Marabini, R., Kassem, N., Broendum, S. S., ... Kragelund, B. B. (2019a). The PCNA interaction motifs revisited: thinking outside the PIP-box. In *Cellular and Molecular Life Sciences* (Vol. 76). <https://doi.org/10.1007/s00018-019-03150-0>
- Prestel, A., Wichmann, N., Martins, J. M., Marabini, R., Kassem, N., Broendum, S. S., ... Kragelund, B. B. (2019b). The PCNA interaction motifs revisited: thinking outside the PIP-box. *Cellular and Molecular Life Sciences*, 76(24), 4923–4943. <https://doi.org/10.1007/s00018-019-03150-0>
- Qian, J., Pentz, K., Zhu, Q., Wang, Q., He, J., Srivastava, A. K., & Wani, A. A. (2015). USP7 modulates UV-induced PCNA monoubiquitination by regulating DNA polymerase eta stability. *Oncogene*, 34(36), 4791–4796. <https://doi.org/10.1038/onc.2014.394>
- Rahmeh, A. A., Zhou, Y., Xie, B., Li, H., Lee, E. Y. C., & Lee, M. Y. W. T. (2012). Phosphorylation of the p68 subunit of pol δ acts as a molecular switch to regulate its interaction with PCNA. *Biochemistry*, 51(1), 416–424. <https://doi.org/10.1021/bi201638e>
- Riddihough, G. (1994). More meanders and sandwiches. *Nature Structural Biology*, 1(11), 755–757. <https://doi.org/10.1038/nsb1194-755>
- Rougeulle, C., Cardoso, C., Fontés, M., Colleaux, L., & Lalande, M. (1998). An imprinted antisense RNA overlaps UBE3A and a second maternally expressed transcript. *Nature Genetics*, 19(1), 15–16. <https://doi.org/10.1038/ng0598-51>
- Sancar, A., Lindsey-Boltz, L. A., Ünsal-Kaçmaz, K., & Linn, S. (2004). Molecular Mechanisms of Mammalian DNA Repair and the DNA Damage Checkpoints. *Annual Review of Biochemistry*, 73(1), 39–85. <https://doi.org/10.1146/annurev.biochem.73.011303.073723>
- Sánchez, R., Torres, D., Prieto, J., Blanco, F. J., & Campos-Olivas, R. (2007). Backbone assignment of human proliferating cell nuclear antigen. *Biomolecular NMR Assignments*, 1(2), 245–247. <https://doi.org/10.1007/s12104-007-9068-2>
- Schober, A. S., Martin-Barros, I., Martin-Mateos, T., Perez-Andres, E., Carlevaris, O., Pozo, S., ... Berra, E. (2020). USP29 is a novel non-canonical Hypoxia Inducible Factor- α activator. *BioRxiv Cell Biology*. <https://doi.org/10.1101/2020.02.20.957688>
- Schwartzman, J. B. (1984). *The Effects of Different Thymidine Concentrations DNA Replication in Pea-root Cells Synchronized Protracted 5-Fluorodeoxyuridine Treatment on by a precursor pools does not remain constant throughout the cell cycle . Pool sizes increase continuously as cel.* 150, 379–389.
- Stodola, J. L., & Burgers, P. M. (2017). Mechanism of lagging-strand DNA replication in eukaryotes. *Advances in Experimental Medicine and Biology*, 1042, 117–133. https://doi.org/10.1007/978-981-10-6955-0_6

- Strzalka, W., & Ziemienowicz, A. (2011). Proliferating cell nuclear antigen (PCNA): A key factor in DNA replication and cell cycle regulation. *Annals of Botany*, 107(7), 1127–1140. <https://doi.org/10.1093/aob/mcq243>
- Studier, F. W. (2005). Protein production by auto-induction in high density shaking cultures. *Protein Expression and Purification*, 41(1), 207–234. <https://doi.org/10.1016/j.pep.2005.01.016>
- Swatek, K. N., & Komander, D. (2016). Ubiquitin modifications. *Cell Research*, 26(4), 399–422. <https://doi.org/10.1038/cr.2016.39>
- Takawa, M., Cho, H. S., Hayami, S., Toyokawa, G., Kogure, M., Yamane, Y., ... Hamamoto, R. (2012). Histone lysine methyltransferase setd8 promotes carcinogenesis by deregulating PCNA expression. *Cancer Research*, 72(13), 3217–3227. <https://doi.org/10.1158/0008-5472.CAN-11-3701>
- Tanaka, S., Tak, Y. S., & Araki, H. (2007). The role of CDK in the initiation step of DNA replication in eukaryotes. *Cell Division*, 2, 1–6. <https://doi.org/10.1186/1747-1028-2-16>
- Tanno, H., Shigematsu, T., Nishikawa, S., Hayakawa, A., Denda, K., Tanaka, T., & Komada, M. (2014). Ubiquitin-interacting motifs confer full catalytic activity, but not ubiquitin chain substrate specificity, to deubiquitinating enzyme USP37. *Journal of Biological Chemistry*, 289(4), 2415–2423. <https://doi.org/10.1074/jbc.M113.528372>
- Thiaville, M. M., Kim, H., Frey, W. D., & Kim, J. (2013). Identification of an Evolutionarily Conserved Cis-Regulatory Element Controlling the Peg3 Imprinted Domain. *PLoS ONE*, 8(9), 1–12. <https://doi.org/10.1371/journal.pone.0075417>
- Thomas, D. B., & Lingwood, C. A. (1975). A model of cell cycle control: Effects of thymidine on synchronous cell cultures. *Cell*, 5(1), 37–44. [https://doi.org/10.1016/0092-8674\(75\)90089-6](https://doi.org/10.1016/0092-8674(75)90089-6)
- Tognetti, S., Riera, A., & Speck, C. (2015). Switch on the engine: how the eukaryotic replicative helicase MCM2–7 becomes activated. *Chromosoma*, 124(1), 13–26. <https://doi.org/10.1007/s00412-014-0489-2>
- Tsurimoto, T., & Stillman, B. (1991). Replication factors required for SV40 DNA replication in vitro. I. DNA structure-specific recognition of a primer-template junction by eukaryotic DNA polymerases and their accessory proteins. *Journal of Biological Chemistry*, 266(3), 1950–1960.
- Unk, I., Hajdú, I., Blastyák, A., & Haracska, L. (2010). Role of yeast Rad5 and its human orthologs, HLTf and SHPRH in DNA damage tolerance. *DNA Repair*, 9(3), 257–267. <https://doi.org/10.1016/j.dnarep.2009.12.013>
- Vujanovic, M., Krietsch, J., Raso, M. C., Terraneo, N., Zellweger, R., Schmid, J. A., ... Lopes, M. (2017). Replication Fork Slowing and Reversal upon DNA Damage Require PCNA Polyubiquitination and ZRANB3 DNA Translocase Activity. *Molecular Cell*, 67(5), 882–890.e5. <https://doi.org/10.1016/j.molcel.2017.08.010>
- Wang, D. S., & Shaw, G. (1995). The Association of the C-Terminal Region of

- β 1 Σ II Spectrin to Brain Membranes Is Mediated by a pH Domain, Does Not Require Membrane Proteins, and Coincides with a Inositol-1,4,5 Triphosphate Binding Site. *Biochemical and Biophysical Research Communications*, Vol. 217, pp. 608–615. <https://doi.org/10.1006/bbrc.1995.2818>
- Wang, Deng Shun, Shaw, R., Winkelmann, J. C., & Shaw, G. (1994). Binding of PH domains of β -adrenergic receptor kinase and β -spectrin to WD40/ β -transducin repeat containing regions of the β -subunit of trimeric G-proteins. *Biochemical and Biophysical Research Communications*, Vol. 203, pp. 29–35. <https://doi.org/10.1006/bbrc.1994.2144>
- Wang, S. C., Nakajima, Y., Yu, Y. L., Xia, W., Chen, C. Te, Yang, C. C., ... Hung, M. C. (2006). Tyrosine phosphorylation controls PCNA function through protein stability. *Nature Cell Biology*, 8(12), 1359–1368. <https://doi.org/10.1038/ncb1501>
- Warbrick, E., Heatherington, W., Lane, D. P., & Glover, D. M. (1998). PCNA binding proteins in *Drosophila melanogaster*: the analysis of a conserved PCNA binding domain. *Nucleic Acids Research*, 26(17), 3925–3932. <https://doi.org/10.1093/nar/26.17.3925>
- Watanabe, K., Tateishi, S., Kawasuji, M., Tsurimoto, T., Inoue, H., & Yamaizumi, M. (2004). Rad18 guides pol η to replication stalling sites through physical interaction and PCNA monoubiquitination. *EMBO Journal*, 23(19), 3886–3896. <https://doi.org/10.1038/sj.emboj.7600383>
- Waterhouse, A., Bertoni, M., Bienert, S., Studer, G., Tauriello, G., Gumienny, R., ... Schwede, T. (2018). SWISS-MODEL: Homology modelling of protein structures and complexes. *Nucleic Acids Research*, 46(W1), W296–W303. <https://doi.org/10.1093/nar/gky427>
- Whitfield, M. L., Sherlock, G., Saldanha, A. J., Murray, J. I., Ball, C. A., Alexander, K. E., ... Carolina, N. (2002). Human Cell Cycle and Their Expression in Tumors. *Molecular Biology of the Cell*, 13(June), 1977–2000. <https://doi.org/10.1091/mbc.02>
- Wijnhoven, P., Konietzny, R., Blackford, A. N., Travers, J., Kessler, B. M., Nishi, R., & Jackson, S. P. (2015). USP4 Auto-Deubiquitylation Promotes Homologous Recombination. *Molecular Cell*, 60(3), 362–373. <https://doi.org/10.1016/j.molcel.2015.09.019>
- Wong, E., & Cuervo, A. M. (2010). Integration of Clearance Mechanisms: The Proteasome and Autophagy. *Cold Spring Harbor Perspectives in Biology*, 2(12), a006734–a006734. <https://doi.org/10.1101/cshperspect.a006734>
- Xie, B., Mazloun, N., Liu, L., Rahmeh, A., Li, H., & Lee, M. Y. W. T. (2002). Reconstitution and characterization of the human DNA polymerase delta four-subunit holoenzyme. *Biochemistry*, 41(44), 13133–13142. <https://doi.org/10.1021/bi0262707>
- Yamamoto, E., Kalli, A. C., Yasuoka, K., & Sansom, M. S. P. (2016). Interactions of Pleckstrin Homology Domains with Membranes: Adding Back the Bilayer via High-Throughput Molecular Dynamics. *Structure*,

24(8), 1421–1431. <https://doi.org/10.1016/j.str.2016.06.002>

- Yao, L., Kawakami, Y., & Kawakami, T. (1994). The pleckstrin homology domain of Bruton tyrosine kinase interacts with protein kinase C. *Proceedings of the National Academy of Sciences of the United States of America*, 91(19), 9175–9179. <https://doi.org/10.1073/pnas.91.19.9175>
- Yau, R., & Rape, M. (2016). The increasing complexity of the ubiquitin code. *Nature Cell Biology*, 18(6), 579–586. <https://doi.org/10.1038/ncb3358>
- Ye, Y., Scheel, H., Hofmann, K., & Komander, D. (2009). Dissection of USP catalytic domains reveals five common insertion points. *Molecular BioSystems*, 5(12), 1797. <https://doi.org/10.1039/b907669g>
- Yeeles, J. T. P., Janska, A., Early, A., & Diffley, J. F. X. (2017). How the Eukaryotic Replisome Achieves Rapid and Efficient DNA Replication. *Molecular Cell*, 65(1), 105–116. <https://doi.org/10.1016/j.molcel.2016.11.017>
- Yoon, H. S., Hajduk, P. J., Petros, A. M., Olejniczak, E. T., Meadows, R. P., & Fesik, S. W. (1994). Solution structure of a pleckstrin-homology domain. *Nature*, 369(6482), 672–675. <https://doi.org/10.1038/369672a0>
- Young, P., Deveraux, Q., Beal, R. E., Pickart, C. M., & Rechsteiner, M. (1998). Characterization of two polyubiquitin binding sites in the 26 S protease subunit 5a. *Journal of Biological Chemistry*, 273(10), 5461–5467. <https://doi.org/10.1074/jbc.273.10.5461>
- Yu, C., Gan, H., & Zhang, Z. (2017). Both DNA Polymerases α and β Contact Active and Stalled Replication Forks Differently. *American Society for Microbiology*, 37(21), 1–14.
- Yu, Y., Cai, J. P., Tu, B., Wu, L., Zhao, Y., Liu, X., ... Zhu, W. G. (2009). Proliferating cell nuclear antigen is protected from degradation by forming a complex with MutT homolog2. *Journal of Biological Chemistry*, 284(29), 19310–19320. <https://doi.org/10.1074/jbc.M109.015289>
- Zhang, P., Mo, J. Y., Perez, A., Leon, A., Liu, L., Mazloum, N., ... Lee, M. Y. W. T. (1999). Direct interaction of proliferating cell nuclear antigen with the p125 catalytic subunit of Mammalian DNA polymerase δ . *Journal of Biological Chemistry*, 274(38), 26647–26653. <https://doi.org/10.1074/jbc.M200065200>
- Zhang, P., Zeng, X.-R., Zhang, P., Toomey, N. L., Chuang, R.-Y., Chang, L.-S., & Lee, M. Y. W. T. (1995). A conserved region in the amino terminus of DNA Polymerase δ is involved in Proliferating Cell Nuclear Antigen Binding (pp. 7988–7992). pp. 7988–7992.
- Zheleva, D. I., Zhelev, N. Z., Fischer, P. M., Duff, S. V., Warbrick, E., Blake, D. G., & Lane, D. P. (2000). A quantitative study of the in vitro binding of the C-terminal domain of p21 to PCNA: Affinity, stoichiometry, and thermodynamics. *Biochemistry*, 39(25), 7388–7397. <https://doi.org/10.1021/bi992498r>
- Zhou, M. M., & Fesik, S. W. (1995). Structure and function of the

phosphotyrosine binding (PTB) domain. *Progress in Biophysics and Molecular Biology*, 64(2–3), 221–235. [https://doi.org/10.1016/S0079-6107\(96\)00005-3](https://doi.org/10.1016/S0079-6107(96)00005-3)

- Zhou, Yajing, Meng, X., Zhang, S., Lee, E. Y. C., & Lee, M. Y. W. T. (2012). Characterization of human DNA polymerase delta and its subassemblies reconstituted by expression in the multibac system. *PLoS ONE*, 7(6), 1–12. <https://doi.org/10.1371/journal.pone.0039156>
- Zhou, Yingyao, & Abagyan, R. (1998). How and why phosphotyrosine-containing peptides bind to the SH2 and PTB domains. *Folding and Design*, 3(6), 513–522. [https://doi.org/10.1016/S1359-0278\(98\)00067-4](https://doi.org/10.1016/S1359-0278(98)00067-4)
- Zlatanou, A., Sabbioneda, S., Miller, E. S., Greenwalt, A., Aggathangelou, A., Maurice, M. M., ... Stewart, G. S. (2016). USP7 is essential for maintaining Rad18 stability and DNA damage tolerance. *Oncogene*, 35(8), 965–976. <https://doi.org/10.1038/onc.2015.149>
- Zou, Y., Liu, Y., Wu, X., & Shell, S. M. (2006). Functions of Human Replication Protein A (RPA): From DNA Replication to DNA Damage and Stress Responses. *Journal Cellular Physiology*, 208, 267–273. <https://doi.org/10.1002/JCP>

Appendix: Posters presented during the thesis

CICbioGUNE
CENTRO DE INVESTACIONES BIOMÉDICAS DEL PASADIZO

Red de UPOK
BFD2016-76872-R
SAF2017-90794-REDT
CTQ2017-83810-R

Exploring the relevance of USP29 and PCNA interaction

Inés Martín-Barros, Teresa Martín-Mateos, Oinaitza Carlevaris, Nekane Merino, Francisco J. Blanco & Eduarne Berra

CIC bioGUNE, Derio, ES

Red de UPOK
BFD2016-76872-R
SAF2017-90794-REDT
CTQ2017-83810-R

INTRODUCTION

The family of De/Ubiquitinating enzymes (DUBs) removes mono- and poly-ubiquitin from the target proteins [1]. Because of DUBs' direct or indirect impact on multiple biological processes, including DNA replication, and because of their potential druggability, DUBs have become of increasing interest in recent years. USP29 is a poorly characterized member of the large family of DUBs. USP29 has been suggested as a potential oncogene as it is involved in the regulation of p53, caspase and more recently HIF- α . Furthermore, USP29 expression levels correlate with the Gleason score in prostate cancer patients [2]. Our MS data show that USP29 interacts with the DNA sliding clamp Proliferating Cell Nuclear Antigen (PCNA). PCNA is a trimeric protein, which has a ring-shape structure that encircles the DNA duplex and slide bidirectionally along it, providing a molecular platform that facilitates multiple protein-protein and protein-DNA interactions at the replication fork [3]. Many of the proteins that interact with PCNA contain a conserved sequence known as the PIP-box (PCNA Interacting Protein-Box). The pattern of the PIP-box sequence is QXXIXXaa, where 'X' is an aliphatic hydrophobic residue and 'I' is an aromatic hydrophobic residue and it is an aromatic hydrophobic residue and it is an aromatic hydrophobic residue and it is an aromatic hydrophobic residue. We hypothesized a role for USP29 in the cellular response to replication stress through the deubiquitination of PCNA.

HYPOTHESIS

PCNA has a role in the cellular response to replication stress through the deubiquitination of PCNA by USP29¹

USP29 canonical PIP box peptide binds with nM affinity to PCNA

USP29 canonical PIP box peptide sequence: 68H₁QKTRPTPLS₁Q₂Q₃Q₄Q₅Q₆Q₇Q₈Q₉Q₁₀Q₁₁Q₁₂Q₁₃Q₁₄Q₁₅Q₁₆Q₁₇Q₁₈Q₁₉Q₂₀Q₂₁Q₂₂Q₂₃Q₂₄Q₂₅Q₂₆Q₂₇Q₂₈Q₂₉Q₃₀Q₃₁Q₃₂Q₃₃Q₃₄Q₃₅Q₃₆Q₃₇Q₃₈Q₃₉Q₄₀Q₄₁Q₄₂Q₄₃Q₄₄Q₄₅Q₄₆Q₄₇Q₄₈Q₄₉Q₅₀Q₅₁Q₅₂Q₅₃Q₅₄Q₅₅Q₅₆Q₅₇Q₅₈Q₅₉Q₆₀Q₆₁Q₆₂Q₆₃Q₆₄Q₆₅Q₆₆Q₆₇Q₆₈Q₆₉Q₇₀Q₇₁Q₇₂Q₇₃Q₇₄Q₇₅Q₇₆Q₇₇Q₇₈Q₇₉Q₈₀Q₈₁Q₈₂Q₈₃Q₈₄Q₈₅Q₈₆Q₈₇Q₈₈Q₈₉Q₉₀Q₉₁Q₉₂Q₉₃Q₉₄Q₉₅Q₉₆Q₉₇Q₉₈Q₉₉Q₁₀₀Q₁₀₁Q₁₀₂Q₁₀₃Q₁₀₄Q₁₀₅Q₁₀₆Q₁₀₇Q₁₀₈Q₁₀₉Q₁₁₀Q₁₁₁Q₁₁₂Q₁₁₃Q₁₁₄Q₁₁₅Q₁₁₆Q₁₁₇Q₁₁₈Q₁₁₉Q₁₂₀Q₁₂₁Q₁₂₂Q₁₂₃Q₁₂₄Q₁₂₅Q₁₂₆Q₁₂₇Q₁₂₈Q₁₂₉Q₁₃₀Q₁₃₁Q₁₃₂Q₁₃₃Q₁₃₄Q₁₃₅Q₁₃₆Q₁₃₇Q₁₃₈Q₁₃₉Q₁₄₀Q₁₄₁Q₁₄₂Q₁₄₃Q₁₄₄Q₁₄₅Q₁₄₆Q₁₄₇Q₁₄₈Q₁₄₉Q₁₅₀Q₁₅₁Q₁₅₂Q₁₅₃Q₁₅₄Q₁₅₅Q₁₅₆Q₁₅₇Q₁₅₈Q₁₅₉Q₁₆₀Q₁₆₁Q₁₆₂Q₁₆₃Q₁₆₄Q₁₆₅Q₁₆₆Q₁₆₇Q₁₆₈Q₁₆₉Q₁₇₀Q₁₇₁Q₁₇₂Q₁₇₃Q₁₇₄Q₁₇₅Q₁₇₆Q₁₇₇Q₁₇₈Q₁₇₉Q₁₈₀Q₁₈₁Q₁₈₂Q₁₈₃Q₁₈₄Q₁₈₅Q₁₈₆Q₁₈₇Q₁₈₈Q₁₈₉Q₁₉₀Q₁₉₁Q₁₉₂Q₁₉₃Q₁₉₄Q₁₉₅Q₁₉₆Q₁₉₇Q₁₉₈Q₁₉₉Q₂₀₀Q₂₀₁Q₂₀₂Q₂₀₃Q₂₀₄Q₂₀₅Q₂₀₆Q₂₀₇Q₂₀₈Q₂₀₉Q₂₁₀Q₂₁₁Q₂₁₂Q₂₁₃Q₂₁₄Q₂₁₅Q₂₁₆Q₂₁₇Q₂₁₈Q₂₁₉Q₂₂₀Q₂₂₁Q₂₂₂Q₂₂₃Q₂₂₄Q₂₂₅Q₂₂₆Q₂₂₇Q₂₂₈Q₂₂₉Q₂₃₀Q₂₃₁Q₂₃₂Q₂₃₃Q₂₃₄Q₂₃₅Q₂₃₆Q₂₃₇Q₂₃₈Q₂₃₉Q₂₄₀Q₂₄₁Q₂₄₂Q₂₄₃Q₂₄₄Q₂₄₅Q₂₄₆Q₂₄₇Q₂₄₈Q₂₄₉Q₂₅₀Q₂₅₁Q₂₅₂Q₂₅₃Q₂₅₄Q₂₅₅Q₂₅₆Q₂₅₇Q₂₅₈Q₂₅₉Q₂₆₀Q₂₆₁Q₂₆₂Q₂₆₃Q₂₆₄Q₂₆₅Q₂₆₆Q₂₆₇Q₂₆₈Q₂₆₉Q₂₇₀Q₂₇₁Q₂₇₂Q₂₇₃Q₂₇₄Q₂₇₅Q₂₇₆Q₂₇₇Q₂₇₈Q₂₇₉Q₂₈₀Q₂₈₁Q₂₈₂Q₂₈₃Q₂₈₄Q₂₈₅Q₂₈₆Q₂₈₇Q₂₈₈Q₂₈₉Q₂₉₀Q₂₉₁Q₂₉₂Q₂₉₃Q₂₉₄Q₂₉₅Q₂₉₆Q₂₉₇Q₂₉₈Q₂₉₉Q₃₀₀Q₃₀₁Q₃₀₂Q₃₀₃Q₃₀₄Q₃₀₅Q₃₀₆Q₃₀₇Q₃₀₈Q₃₀₉Q₃₁₀Q₃₁₁Q₃₁₂Q₃₁₃Q₃₁₄Q₃₁₅Q₃₁₆Q₃₁₇Q₃₁₈Q₃₁₉Q₃₂₀Q₃₂₁Q₃₂₂Q₃₂₃Q₃₂₄Q₃₂₅Q₃₂₆Q₃₂₇Q₃₂₈Q₃₂₉Q₃₃₀Q₃₃₁Q₃₃₂Q₃₃₃Q₃₃₄Q₃₃₅Q₃₃₆Q₃₃₇Q₃₃₈Q₃₃₉Q₃₄₀Q₃₄₁Q₃₄₂Q₃₄₃Q₃₄₄Q₃₄₅Q₃₄₆Q₃₄₇Q₃₄₈Q₃₄₉Q₃₅₀Q₃₅₁Q₃₅₂Q₃₅₃Q₃₅₄Q₃₅₅Q₃₅₆Q₃₅₇Q₃₅₈Q₃₅₉Q₃₆₀Q₃₆₁Q₃₆₂Q₃₆₃Q₃₆₄Q₃₆₅Q₃₆₆Q₃₆₇Q₃₆₈Q₃₆₉Q₃₇₀Q₃₇₁Q₃₇₂Q₃₇₃Q₃₇₄Q₃₇₅Q₃₇₆Q₃₇₇Q₃₇₈Q₃₇₉Q₃₈₀Q₃₈₁Q₃₈₂Q₃₈₃Q₃₈₄Q₃₈₅Q₃₈₆Q₃₈₇Q₃₈₈Q₃₈₉Q₃₉₀Q₃₉₁Q₃₉₂Q₃₉₃Q₃₉₄Q₃₉₅Q₃₉₆Q₃₉₇Q₃₉₈Q₃₉₉Q₄₀₀Q₄₀₁Q₄₀₂Q₄₀₃Q₄₀₄Q₄₀₅Q₄₀₆Q₄₀₇Q₄₀₈Q₄₀₉Q₄₁₀Q₄₁₁Q₄₁₂Q₄₁₃Q₄₁₄Q₄₁₅Q₄₁₆Q₄₁₇Q₄₁₈Q₄₁₉Q₄₂₀Q₄₂₁Q₄₂₂Q₄₂₃Q₄₂₄Q₄₂₅Q₄₂₆Q₄₂₇Q₄₂₈Q₄₂₉Q₄₃₀Q₄₃₁Q₄₃₂Q₄₃₃Q₄₃₄Q₄₃₅Q₄₃₆Q₄₃₇Q₄₃₈Q₄₃₉Q₄₄₀Q₄₄₁Q₄₄₂Q₄₄₃Q₄₄₄Q₄₄₅Q₄₄₆Q₄₄₇Q₄₄₈Q₄₄₉Q₄₅₀Q₄₅₁Q₄₅₂Q₄₅₃Q₄₅₄Q₄₅₅Q₄₅₆Q₄₅₇Q₄₅₈Q₄₅₉Q₄₆₀Q₄₆₁Q₄₆₂Q₄₆₃Q₄₆₄Q₄₆₅Q₄₆₆Q₄₆₇Q₄₆₈Q₄₆₉Q₄₇₀Q₄₇₁Q₄₇₂Q₄₇₃Q₄₇₄Q₄₇₅Q₄₇₆Q₄₇₇Q₄₇₈Q₄₇₉Q₄₈₀Q₄₈₁Q₄₈₂Q₄₈₃Q₄₈₄Q₄₈₅Q₄₈₆Q₄₈₇Q₄₈₈Q₄₈₉Q₄₉₀Q₄₉₁Q₄₉₂Q₄₉₃Q₄₉₄Q₄₉₅Q₄₉₆Q₄₉₇Q₄₉₈Q₄₉₉Q₅₀₀Q₅₀₁Q₅₀₂Q₅₀₃Q₅₀₄Q₅₀₅Q₅₀₆Q₅₀₇Q₅₀₈Q₅₀₉Q₅₁₀Q₅₁₁Q₅₁₂Q₅₁₃Q₅₁₄Q₅₁₅Q₅₁₆Q₅₁₇Q₅₁₈Q₅₁₉Q₅₂₀Q₅₂₁Q₅₂₂Q₅₂₃Q₅₂₄Q₅₂₅Q₅₂₆Q₅₂₇Q₅₂₈Q₅₂₉Q₅₃₀Q₅₃₁Q₅₃₂Q₅₃₃Q₅₃₄Q₅₃₅Q₅₃₆Q₅₃₇Q₅₃₈Q₅₃₉Q₅₄₀Q₅₄₁Q₅₄₂Q₅₄₃Q₅₄₄Q₅₄₅Q₅₄₆Q₅₄₇Q₅₄₈Q₅₄₉Q₅₅₀Q₅₅₁Q₅₅₂Q₅₅₃Q₅₅₄Q₅₅₅Q₅₅₆Q₅₅₇Q₅₅₈Q₅₅₉Q₅₆₀Q₅₆₁Q₅₆₂Q₅₆₃Q₅₆₄Q₅₆₅Q₅₆₆Q₅₆₇Q₅₆₈Q₅₆₉Q₅₇₀Q₅₇₁Q₅₇₂Q₅₇₃Q₅₇₄Q₅₇₅Q₅₇₆Q₅₇₇Q₅₇₈Q₅₇₉Q₅₈₀Q₅₈₁Q₅₈₂Q₅₈₃Q₅₈₄Q₅₈₅Q₅₈₆Q₅₈₇Q₅₈₈Q₅₈₉Q₅₉₀Q₅₉₁Q₅₉₂Q₅₉₃Q₅₉₄Q₅₉₅Q₅₉₆Q₅₉₇Q₅₉₈Q₅₉₉Q₆₀₀Q₆₀₁Q₆₀₂Q₆₀₃Q₆₀₄Q₆₀₅Q₆₀₆Q₆₀₇Q₆₀₈Q₆₀₉Q₆₁₀Q₆₁₁Q₆₁₂Q₆₁₃Q₆₁₄Q₆₁₅Q₆₁₆Q₆₁₇Q₆₁₈Q₆₁₉Q₆₂₀Q₆₂₁Q₆₂₂Q₆₂₃Q₆₂₄Q₆₂₅Q₆₂₆Q₆₂₇Q₆₂₈Q₆₂₉Q₆₃₀Q₆₃₁Q₆₃₂Q₆₃₃Q₆₃₄Q₆₃₅Q₆₃₆Q₆₃₇Q₆₃₈Q₆₃₉Q₆₄₀Q₆₄₁Q₆₄₂Q₆₄₃Q₆₄₄Q₆₄₅Q₆₄₆Q₆₄₇Q₆₄₈Q₆₄₉Q₆₅₀Q₆₅₁Q₆₅₂Q₆₅₃Q₆₅₄Q₆₅₅Q₆₅₆Q₆₅₇Q₆₅₈Q₆₅₉Q₆₆₀Q₆₆₁Q₆₆₂Q₆₆₃Q₆₆₄Q₆₆₅Q₆₆₆Q₆₆₇Q₆₆₈Q₆₆₉Q₆₇₀Q₆₇₁Q₆₇₂Q₆₇₃Q₆₇₄Q₆₇₅Q₆₇₆Q₆₇₇Q₆₇₈Q₆₇₉Q₆₈₀Q₆₈₁Q₆₈₂Q₆₈₃Q₆₈₄Q₆₈₅Q₆₈₆Q₆₈₇Q₆₈₈Q₆₈₉Q₆₉₀Q₆₉₁Q₆₉₂Q₆₉₃Q₆₉₄Q₆₉₅Q₆₉₆Q₆₉₇Q₆₉₈Q₆₉₉Q₇₀₀Q₇₀₁Q₇₀₂Q₇₀₃Q₇₀₄Q₇₀₅Q₇₀₆Q₇₀₇Q₇₀₈Q₇₀₉Q₇₁₀Q₇₁₁Q₇₁₂Q₇₁₃Q₇₁₄Q₇₁₅Q₇₁₆Q₇₁₇Q₇₁₈Q₇₁₉Q₇₂₀Q₇₂₁Q₇₂₂Q₇₂₃Q₇₂₄Q₇₂₅Q₇₂₆Q₇₂₇Q₇₂₈Q₇₂₉Q₇₃₀Q₇₃₁Q₇₃₂Q₇₃₃Q₇₃₄Q₇₃₅Q₇₃₆Q₇₃₇Q₇₃₈Q₇₃₉Q₇₄₀Q₇₄₁Q₇₄₂Q₇₄₃Q₇₄₄Q₇₄₅Q₇₄₆Q₇₄₇Q₇₄₈Q₇₄₉Q₇₅₀Q₇₅₁Q₇₅₂Q₇₅₃Q₇₅₄Q₇₅₅Q₇₅₆Q₇₅₇Q₇₅₈Q₇₅₉Q₇₆₀Q₇₆₁Q₇₆₂Q₇₆₃Q₇₆₄Q₇₆₅Q₇₆₆Q₇₆₇Q₇₆₈Q₇₆₉Q₇₇₀Q₇₇₁Q₇₇₂Q₇₇₃Q₇₇₄Q₇₇₅Q₇₇₆Q₇₇₇Q₇₇₈Q₇₇₉Q₇₈₀Q₇₈₁Q₇₈₂Q₇₈₃Q₇₈₄Q₇₈₅Q₇₈₆Q₇₈₇Q₇₈₈Q₇₈₉Q₇₉₀Q₇₉₁Q₇₉₂Q₇₉₃Q₇₉₄Q₇₉₅Q₇₉₆Q₇₉₇Q₇₉₈Q₇₉₉Q₈₀₀Q₈₀₁Q₈₀₂Q₈₀₃Q₈₀₄Q₈₀₅Q₈₀₆Q₈₀₇Q₈₀₈Q₈₀₉Q₈₁₀Q₈₁₁Q₈₁₂Q₈₁₃Q₈₁₄Q₈₁₅Q₈₁₆Q₈₁₇Q₈₁₈Q₈₁₉Q₈₂₀Q₈₂₁Q₈₂₂Q₈₂₃Q₈₂₄Q₈₂₅Q₈₂₆Q₈₂₇Q₈₂₈Q₈₂₉Q₈₃₀Q₈₃₁Q₈₃₂Q₈₃₃Q₈₃₄Q₈₃₅Q₈₃₆Q₈₃₇Q₈₃₈Q₈₃₉Q₈₄₀Q₈₄₁Q₈₄₂Q₈₄₃Q₈₄₄Q₈₄₅Q₈₄₆Q₈₄₇Q₈₄₈Q₈₄₉Q₈₅₀Q₈₅₁Q₈₅₂Q₈₅₃Q₈₅₄Q₈₅₅Q₈₅₆Q₈₅₇Q₈₅₈Q₈₅₉Q₈₆₀Q₈₆₁Q₈₆₂Q₈₆₃Q₈₆₄Q₈₆₅Q₈₆₆Q₈₆₇Q₈₆₈Q₈₆₉Q₈₇₀Q₈₇₁Q₈₇₂Q₈₇₃Q₈₇₄Q₈₇₅Q₈₇₆Q₈₇₇Q₈₇₈Q₈₇₉Q₈₈₀Q₈₈₁Q₈₈₂Q₈₈₃Q₈₈₄Q₈₈₅Q₈₈₆Q₈₈₇Q₈₈₈Q₈₈₉Q₈₉₀Q₈₉₁Q₈₉₂Q₈₉₃Q₈₉₄Q₈₉₅Q₈₉₆Q₈₉₇Q₈₉₈Q₈₉₉Q₉₀₀Q₉₀₁Q₉₀₂Q₉₀₃Q₉₀₄Q₉₀₅Q₉₀₆Q₉₀₇Q₉₀₈Q₉₀₉Q₉₁₀Q₉₁₁Q₉₁₂Q₉₁₃Q₉₁₄Q₉₁₅Q₉₁₆Q₉₁₇Q₉₁₈Q₉₁₉Q₉₂₀Q₉₂₁Q₉₂₂Q₉₂₃Q₉₂₄Q₉₂₅Q₉₂₆Q₉₂₇Q₉₂₈Q₉₂₉Q₉₃₀Q₉₃₁Q₉₃₂Q₉₃₃Q₉₃₄Q₉₃₅Q₉₃₆Q₉₃₇Q₉₃₈Q₉₃₉Q₉₄₀Q₉₄₁Q₉₄₂Q₉₄₃Q₉₄₄Q₉₄₅Q₉₄₆Q₉₄₇Q₉₄₈Q₉₄₉Q₉₅₀Q₉₅₁Q₉₅₂Q₉₅₃Q₉₅₄Q₉₅₅Q₉₅₆Q₉₅₇Q₉₅₈Q₉₅₉Q₉₆₀Q₉₆₁Q₉₆₂Q₉₆₃Q₉₆₄Q₉₆₅Q₉₆₆Q₉₆₇Q₉₆₈Q₉₆₉Q₉₇₀Q₉₇₁Q₉₇₂Q₉₇₃Q₉₇₄Q₉₇₅Q₉₇₆Q₉₇₇Q₉₇₈Q₉₇₉Q₉₈₀Q₉₈₁Q₉₈₂Q₉₈₃Q₉₈₄Q₉₈₅Q₉₈₆Q₉₈₇Q₉₈₈Q₉₈₉Q₉₉₀Q₉₉₁Q₉₉₂Q₉₉₃Q₉₉₄Q₉₉₅Q₉₉₆Q₉₉₇Q₉₉₈Q₉₉₉Q₁₀₀₀Q₁₀₀₁Q₁₀₀₂Q₁₀₀₃Q₁₀₀₄Q₁₀₀₅Q₁₀₀₆Q₁₀₀₇Q₁₀₀₈Q₁₀₀₉Q₁₀₁₀Q₁₀₁₁Q₁₀₁₂Q₁₀₁₃Q₁₀₁₄Q₁₀₁₅Q₁₀₁₆Q₁₀₁₇Q₁₀₁₈Q₁₀₁₉Q₁₀₂₀Q₁₀₂₁Q₁₀₂₂Q₁₀₂₃Q₁₀₂₄Q₁₀₂₅Q₁₀₂₆Q₁₀₂₇Q₁₀₂₈Q₁₀₂₉Q₁₀₃₀Q₁₀₃₁Q₁₀₃₂Q₁₀₃₃Q₁₀₃₄Q₁₀₃₅Q₁₀₃₆Q₁₀₃₇Q₁₀₃₈Q₁₀₃₉Q₁₀₄₀Q₁₀₄₁Q₁₀₄₂Q₁₀₄₃Q₁₀₄₄Q₁₀₄₅Q₁₀₄₆Q₁₀₄₇Q₁₀₄₈Q₁₀₄₉Q₁₀₅₀Q₁₀₅₁Q₁₀₅₂Q₁₀₅₃Q₁₀₅₄Q₁₀₅₅Q₁₀₅₆Q₁₀₅₇Q₁₀₅₈Q₁₀₅₉Q₁₀₆₀Q₁₀₆₁Q₁₀₆₂Q₁₀₆₃Q₁₀₆₄Q₁₀₆₅Q₁₀₆₆Q₁₀₆₇Q₁₀₆₈Q₁₀₆₉Q₁₀₇₀Q₁₀₇₁Q₁₀₇₂Q₁₀₇₃Q₁₀₇₄Q₁₀₇₅Q₁₀₇₆Q₁₀₇₇Q₁₀₇₈Q₁₀₇₉Q₁₀₈₀Q₁₀₈₁Q₁₀₈₂Q₁₀₈₃Q₁₀₈₄Q₁₀₈₅Q₁₀₈₆Q₁₀₈₇Q₁₀₈₈Q₁₀₈₉Q₁₀₉₀Q₁₀₉₁Q₁₀₉₂Q₁₀₉₃Q₁₀₉₄Q₁₀₉₅Q₁₀₉₆Q₁₀₉₇Q₁₀₉₈Q₁₀₉₉Q₁₁₀₀Q₁₁₀₁Q₁₁₀₂Q₁₁₀₃Q₁₁₀₄Q₁₁₀₅Q₁₁₀₆Q₁₁₀₇Q₁₁₀₈Q₁₁₀₉Q₁₁₁₀Q₁₁₁₁Q₁₁₁₂Q₁₁₁₃Q₁₁₁₄Q₁₁₁₅Q₁₁₁₆Q₁₁₁₇Q₁₁₁₈Q₁₁₁₉Q₁₁₂₀Q₁₁₂₁Q₁₁₂₂Q₁₁₂₃Q₁₁₂₄Q₁₁₂₅Q₁₁₂₆Q₁₁₂₇Q₁₁₂₈Q₁₁₂₉Q₁₁₃₀Q₁₁₃₁Q₁₁₃₂Q₁₁₃₃Q₁₁₃₄Q₁₁₃₅Q₁₁₃₆Q₁₁₃₇Q₁₁₃₈Q_{1139</}

USP29: a new potential interactor of PCNA

Inés Martín-Barros, Alain Ibáñez de Opakua, Teresa Martín-Mateos, Onintza Carlevaris, Nekane Merino, Francisco J. Blanco & Edurne Berra
CIC bioGUNE, Derio, ES

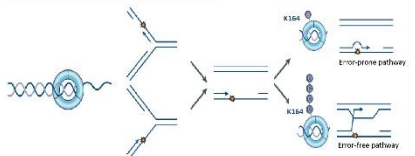


BACKGROUND

The family of DeUbiquitinating enzymes (DUBs) removes mono- and poly-ubiquitin from the target proteins [1]. Because of DUB's direct or indirect impact on multiple biological processes, including DNA replication, and because of their potential druggability, DUBs have become of increasing interest in recent years. USP29 is a poorly characterized member of the large family of DUBs. USP29 has been suggested as a potential oncogene as it is involved in the regulation of p53, claspin and more recently HIF- α . Furthermore, USP29 expression levels correlate with the Gleason score in prostate cancer patients [2]. Our MS data show that USP29 interacts with the DNA sliding clamp Proliferating Cell Nuclear Antigen (PCNA). PCNA is a homotrimer protein, which has a ring-shape structure that encircles the DNA duplex and slide bidirectionally along it, providing a molecular platform that facilitates multiple protein-protein and protein-DNA interactions at the replication fork [3]. Many of the proteins that interact with PCNA contain a conserved sequence known as the PIP-box (PCNA-Interacting Protein-box). The pattern of the PIP-box sequence is QXXhXXaa, where h is an aliphatic hydrophobic residue and a is an aromatic hydrophobic one (F, W, or Y). A bioinformatic analysis of the sequence of USP29 found that USP29 contains a potential canonical PIP-box (PCNA interacting protein-box) sequence. We hypothesized a role for USP29 in the cellular response to replication stress through the deubiquitination of PCNA. Mono-ubiquitination of PCNA on lysine 164 triggers the error prone pathway and therefore, genomic instability while polyubiquitination of PCNA activates the error free pathway.

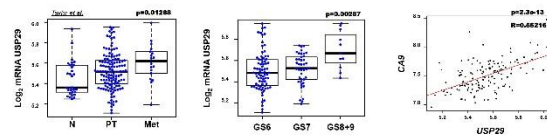
Aim: Characterize the interaction between human USP29 and PCNA

HYPOTHESIS



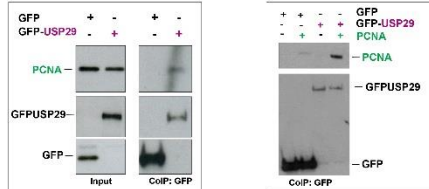
"PCNA/USP29 has a role in the cellular response to replication stress through the deubiquitination of PCNA by USP29"

USP29: oncogene in prostate cancer



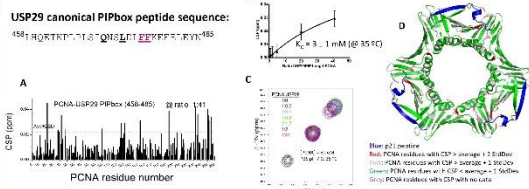
USP29 expression correlates with bad prognosis in prostate cancer. Left and middle panel: USP29 mRNA levels in prostate cancer samples. Samples were compared on the basis of their tissue origin (normal tissue (N), primary tumours (PT), metastatic tumours (Met)) or the Gleason score (GS) of the patient (Taylor et al., 2001), using CancerTool. Right panel: Correlation analysis between USP29 and CA9 mRNA levels in the aforementioned dataset of PT cancer samples.

USP29 interacts with endogenous and recombinant PCNA



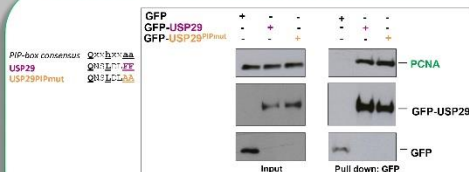
Endogenous as well as recombinant PCNA interacts with USP29 by CoIP. HEK293T cells were transfected with GFP or GFP-USP29 and lysed 24h post-transfection. GFP and GFP-fused proteins were pulled down in native conditions with GFP-traps[®] and eluates were subjected to SDS-PAGE followed by WB against endogenous PCNA protein (left panel). GFP or GFP-USP29 pulled down in native conditions with GFP-traps[®] were incubated in the presence of recombinant PCNA and analyzed by SDS-PAGE followed by WB against PCNA protein (right panel).

USP29PIPbox peptide binds with mM affinity to PCNA



PCNA and USP29 interaction by NMR. A. Chemical shift perturbations (CSP) caused by the USP29 PIP peptide in the NMR signals of PCNA. The dashed line corresponds to the average value plus one standard deviation. B. Fitting of the CSP of Gly127 to a model of one set of equivalent binding sites. C. Overlay of 800 MHz NMR spectra of PCNA in the presence of increasing amounts of the USP29 PIP peptide. The zoomed region shows the changes in the Gly127 signal. D. Mapping of the CSPs on the three dimensional structure of the complex formed by PCNA and the PIP peptide of USP29. The cluster of perturbed residues (red and pink) in the pocket where the short helix of p21 binds PCNA indicates that USP29 also binds to this pocket.

USP29PIPbox mutant interacts with PCNA



Mutation of the canonical PIPbox does not affect the interaction with endogenous PCNA. HEK293T cells were transfected with GFP or GFP-USP29 constructs and lysed 24h post-transfection. GFP and GFP-fused proteins were pulled down in native conditions with GFP-traps[®] and eluates were subjected to SDS-PAGE and WB against endogenous PCNA protein.

CONCLUSIONS

- Endogenous and recombinant PCNA interact with USP29.
- However, the interaction affinity, measured by NMR, between PCNA and the PIPbox sequence is extremely low.
- The canonical PIPbox of USP29 is not the PCNA binding site.

FUTURE PERSPECTIVES

- Study the interaction between USP29 and PCNA by NMR.
- Study the relevance of USP29 in PCNA polyUbiquitination.
- Structural analysis of USP29 by NMR and/or crystallography.

REFERENCES

- Schober AS, Berra E. DUBs, New Members in the Hypoxia Signaling cHub. *Front Oncol.* 2016;6:53.
- Schober et al., in revision
- De Blasio A, Bianco RJ. Proliferating Cell Nuclear Antigen (PCNA) Structure and Interactions. Too Many Partners for One Dancer? (2013) *Adv Protein Chem Struct Biol* 91, 1-36.

USP29: a new potential regulator of DNA Damage Tolerance through PCNA

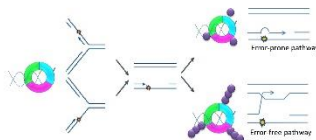
Inés Martín-Barros, Teresa Martín-Mateos, Alain Ibáñez de Opakua, Nekane Merino, Onintza Carlevaris, Francisco J. Blanco & Edurne Berra
CIC bioGUNE, Derio, ES

BACKGROUND

The family of DeUbiquitinating enzymes (DUBs) removes mono- and poly-ubiquitin from the target proteins [1]. Because of DUB's direct or indirect impact on multiple biological processes, including DNA replication, and because of their potential druggability, DUBs have become of increasing interest in recent years. USP29 is a poorly characterized member of the large family of DUBs. USP29 has been suggested as a potential oncogene as it is involved in the regulation of p53, claspin and more recently HIF- α . Furthermore, USP29 expression levels correlate with the Gleason score in prostate cancer patients [2]. Our MS data show that USP29 interacts with the DNA sliding clamp Proliferating Cell Nuclear Antigen (PCNA). PCNA is a homotrimer protein, which has a ring-shape structure that encircles the DNA duplex and slide bidirectionally along it, providing a molecular platform that facilitates multiple protein-protein and protein-DNA interactions at the replication fork [3]. Many of the proteins that interact with PCNA contain a conserved sequence known as the PIP-box (PCNA-Interacting Protein-box). The pattern of the PIP-box sequence is QXXhXXaa, where h is an aliphatic hydrophobic residue and a is an aromatic hydrophobic one (F, W, or Y). A bioinformatical analysis of the sequence of USP29 found that USP29 contains a potential canonical PIP-box (PCNA interacting protein-box) sequence. We hypothesized a role for USP29 in the cellular response to replication stress through the deubiquitination of PCNA. Mono-ubiquitination of PCNA on lysine 164 triggers the error prone pathway and therefore, genomic instability while polyubiquitination of PCNA activates the error free pathway.

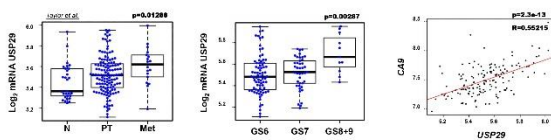
Aim: Characterize the interaction between human USP29 and PCNA

HYPOTHESIS



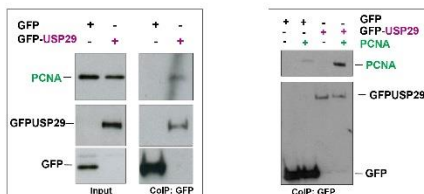
"PCNA/USP29 has a role in the cellular response to replication stress through the deubiquitination of PCNA by USP29"

USP29: oncogene in prostate cancer



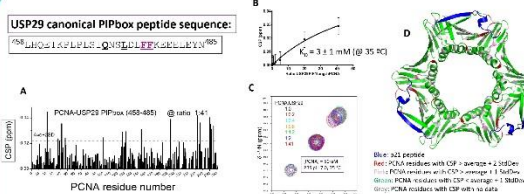
USP29 expression correlates with bad prognosis in prostate cancer. Left and middle panel: USP29 mRNA levels in prostate cancer samples. Samples were compared on the basis of their tissue origin (normal tissue (N), primary tumours (PT), metastatic tumours (Met)) or the Gleason score (GS) of the patient. (Taylor et al., 2001), using CancerTOOL. Right panel: USP29 and CA9 correlation analysis in the aforementioned dataset of PT cancer samples.

USP29 interacts with endogenous and recombinant PCNA



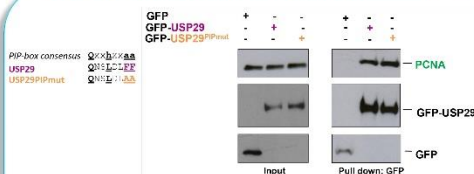
Endogenous as well as recombinant PCNA interacts with USP29 by CoIP. HEK293T cells were transfected with GFP or GFP-USP29 and lysed 24h post-transfection. GFP and GFP-fused proteins were pulled down in native conditions with GFP-traps[®] and eluates were subjected to SDS-PAGE followed by WB against endogenous PCNA protein (left panel). GFP or GFP-USP29 pulled down in native conditions with GFP-traps[®] were incubated in the presence of recombinant PCNA and analyzed by SDS-PAGE followed by WB against PCNA protein (right panel).

USP29PIPbox peptide binds to PCNA with mM affinity



PCNA and USP29 interaction by NMR. A. Chemical shift perturbations (CSP) caused by the PIP peptide of USP29 in the NMR signals of PCNA. The dashed line corresponds to the average value plus one standard deviation. B. Fitting of the CSP of Gly127 to a model of one set of equivalent binding sites. C. Overlay of 800 MHz NMR spectra of PCNA in the presence of increasing amounts of the USP29 PIP peptide. The zoomed region shows the changes in the Gly127 signal. D. Mapping of the CSPs on the three dimensional structure of the complex formed by PCNA and the PIP peptide of USP29. The cluster of perturbed residues (red and pink) in the pocket where the short helix of p21 binds PCNA indicates that USP29 also binds to this pocket.

USP29PIPbox mutant interacts with PCNA



Mutation of the canonical PIPbox does not affect the interaction with endogenous PCNA. HEK293T cells were transfected with GFP or GFP-USP29 constructs and lysed 24h post-transfection. GFP and GFP-fused proteins were pulled down in native conditions with GFP-traps[®] and eluates were subjected to SDS-PAGE and WB against endogenous PCNA protein.

CONCLUSIONS

- Endogenous and recombinant PCNA interact with USP29.
- However, the interaction affinity, measured by NMR, between PCNA and the PIPbox sequence is extremely low.
- The canonical PIPbox of USP29 is not the PCNA binding site.

FUTURE PERSPECTIVES

- Study the interaction between USP29 and PCNA by NMR.
- Study the relevance of USP29 in PCNA polyubiquitination.
- Structural analysis of USP29 by NMR and/or crystallography.

REFERENCES

- [1] Schober AS, Berra E. DUBs, New Members in the Hypoxia Signaling cUb. Front Oncol. 2016;6:53.
- [2] Schober et al., in revision
- [3] De Blasio A, Blanco FJ. Proliferating Cell Nuclear Antigen (PCNA) Structure and Interactions. Too Many Partners for One Dancer? (2013) Adv Protein Chem Struct Biol 91, 1-36.

